

3.4 Cooperative Phenomena in Complex Macroscopic Systems

Tensor-Network Renormalization-Group Study of Critical Phenomena

Naoki KAWASHIMA

Institute for Solid State Physics,

The University of Tokyo, Kashiwa-no-ha, Kashiwa, Chiba 277-8581

The objective of the project is to develop new methods for studying the critical phenomena, both classical and quantum, and apply them to strongly correlated systems. Especially, we aim at improving the real-space renormalization group (RSRG) method based on the tensor network representation with the hope for fuller understanding of the structure of the scaling dimensions of 2+1 or 3 dimensional fixed-point theories.

In [1], we proposed a method for obtaining an efficient low-rank approximation of a given tensor. This was motivated by the conventional RSRG methods such as the loop-TNR and entanglement filtering. In those methods, the crucial part is removal of redundancy in the tensor-network representation arising from loops. They can be regarded as a special form of low-rank approximation of a given tensor. It might then be useful also for more general class of tensors, e.g., the image data in the form of tensors. The proposed method successfully identified the redundant structure of the entanglement naturally formed in the process of the tensor renormalization group (TRG) calculation.

In [2], we studied the J-K- Γ model, a model that may represent some aspect of the compound α -RuCl₃, which is expected to be close to the Kitaev spin liquid and presents some features hinting a non-trivial topological structure of its state. We discovered that the chiral spin liquid phase proposed by a preceding study is realized in a narrower region than predicted. In addition, we discovered two more non-magnetic phases that our calculation suggested possesses also non-trivial topological structure.

In [3], we studied the spin-1 Kitaev model. This was motivated by the preceding work by Lee, Kaneko, Okubo and I on the conventional spin-1/2 case, in which we discovered relationship between the gapless Kitaev spin liquid and the classical loop gas model. In [3], in contrast to the S=1/2 case, we discovered the gapful spin liquid with Z_2 structure of the quasi-particles.

In [4], we improved the high-order tensor renormalization group (HOTRG), one of the conventional RSRG based on the tensor-network representation. In the HOTRG, we bind two parallel bonds together to form one

renormalized bond in much the same spirit as the Migdal-Kadanoff RG. In doing so, we need a projection operator for the rank reduction. In its simplest implementation of the HOTRG, only the local environment is taken into account in computing the projection operator, while it would obviously be better to optimize the projector in more global environment. Several methods for better optimization has been proposed at the cost of higher computational complexity. The method we proposed is based on the corner transfer-matrix technique and reduces the computational complexity without serious degrading of the accuracy.

In [5], we applied the method of variational uniform matrix-product-state (VUMPS), an MPS-based method for one-dimensional quantum systems to the 2-leg ladder system with four-body interaction, i.e., a one-dimensional analogue of the JQ model that shows a deconfined critical phenomena. While DMRG is known to be a very powerful numerical tool in investigating the one dimensional quantum systems, direct

characterization of the quantum critical phenomena has been a tough problem even for DMRG. In our study, we successfully characterize various phases including symmetry protected topological phases by the 2nd cohomology group represented by the resulting fixed-point tensors. Critical behaviors between the phases are also accurately characterized.

References

- [1] Hyun-Yong Lee, and Naoki Kawashima: J. Phys. Soc. Jpn. 89, 054003 (2020)
- [2] Hyun-Yong Lee, Ryui Kaneko, Li Ern Chern, Tsuyoshi Okubo, Youhei Yamaji, Naoki Kawashima and Yong Baek Kim: Nature Communications 11, 1639 (2020).
- [3] Hyun-Yong Lee, Naoki Kawashima and Yong Baek Kim: Phys. Rev. Res. 2, 033318 (2020).
- [4] Satoshi Morita and Naoki Kawashima: Phys. Rev. B103, 045131 (1-6) (2020)
- [5] Takuhiro Ogino, Ryui Kaneko, Satoshi Morita, Shunsuke Furukawa and Naoki Kawashima: Phys. Rev. B 103, 085117 (2021).

Molecular Dynamics Simulations of Bio-Inspired Materials

Wataru Shinoda

Department of Materials Chemistry, Nagoya University

Nagoya 464-8603

We have studied the surface hydrophobicity of self-assembled monolayers (SAM) [1] using massive parallel computer simulations. The surface hydrophobicity was investigated for a range chemically functionalized ($-\text{CF}_3$, $-\text{CH}_3$, $-\text{OCH}_3$, $-\text{OH}$) SAMs as illustrated in Fig. 1. These SAMs have many industrial and biological applications such as for making well-defined non-fouling surfaces, cell supports, receptors, sensors, microarrays, separation devices, and for surface reactions [1, 2]. A good understanding of surface properties of these SAMs can allow us to further modify and control them for the specific uses.

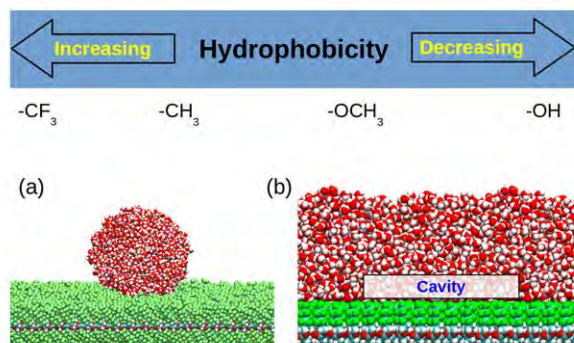


Figure 1: Surface hydrophobicity of chemically functionalized ($-\text{CF}_3$, $-\text{CH}_3$, $-\text{OCH}_3$, $-\text{OH}$) self-assembled monolayers. (a) Structure of a water droplet on the fluoroalkyl SAM surface (b) The formation of a cavity near the SAM-water interface.

The study was conducted with all-atom (AA) simulation model using the LAMMPS

molecular dynamics (MD) simulation package [3]. The systems were modeled using the optimized potentials for liquid simulation (OPLS) force field [4]. SPC/E rigid-body water model was used for the water molecules [5]. A wide range of packing densities and chain lengths were considered in the study to understand their effects on the surface hydrophobicity. Analyses of the MD trajectories were done using the in-house codes. The complete details of the computational method can be found in Ref. [6, 7].

The surface hydrophobicity was investigated by means of (1) the structure, (2) the contact angle of a water droplet on the surface, and (3) the cavity formation free energy. In the structure, we mainly focused on density distribution, hydrogen-bonding, chain flexibility via root mean square displacement (RMSD), and roughness of the SAM surfaces. The free energy of cavity formation was calculated from indirect umbrella sampling methods [6, 7], in which used massive parallel computing resource. The results were found quite consistent with experiments. Through these studies, we demonstrated a systematic path to examine the hydrophobicity of such synthetic surfaces. For the hydrophobic surfaces such as for the fluorinated chains, it was found that the surface hydrophobicity is mainly governed by packing density rather than the chain length. It increases on reducing the packing density of SAMs. The SAM flexibility causes an enhancement in the surface hydrophobicity inde-

pendent of chemical functional groups. These information would be certainly useful for the material design and modifying the surfaces.

Additionally, we developed a coarse-grained (CG) model for the semi-fluorocarbon diblocks and studied the hemimicelle formation of these chains at the air-water interface using ISSP supercomputer. These systems contain more than 100,000 particles even in the CG model. We showed a mechanism of micelle formation for these diblocks and successfully explained the non-coalescence behavior of micelles, which was a puzzle for the experimentalists [8]. It was found that an unique alternating P-phase forms in between the micelles, which has lateral and vertical dimensions of the nanoscale order (see Fig. 2). We believe that this P-phase could be reason for the non-coalescence behavior of micelles under strong compression.

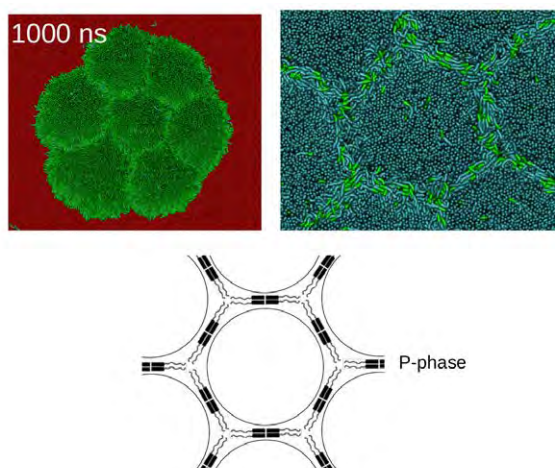


Figure 2: The hemimicelle formation of semi-fluorocarbons at the air-water interface and the structure of P-phase existing in between the hemimicelles.

More recently, we studied the amino acids and protein adsorption on the SAM surfaces (see Fig 3). We are in the process of summarizing results of these simulations for the publication. We found ISSP supercomputer really useful for conducting simulation of such large-scale complex systems. We are further looking to simulate protein adsorption on the polymers using a coarse-grained model to cover extensive

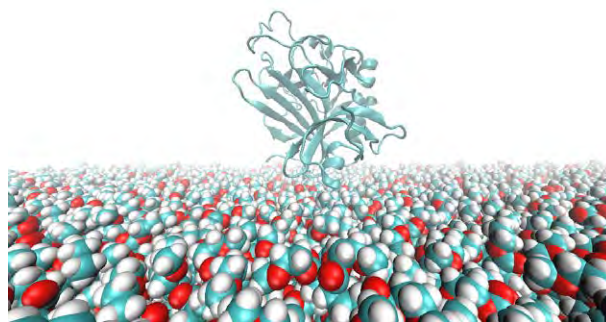


Figure 3: Adsorption of protein on synthetic SAM surfaces.

time scale. In this study, we will also consider the adsorption of more larger systems such as virus capsids and organelles.

References

- [1] J. C. Love, L. A. Estroff, J. K. Kriebel, R. G. Nuzzo, and G. M. Whitesides: *Chem. Rev.* 2005, **105** (2005) 1103.
- [2] J. E. Raynor, J. R. Capadona, D. M. Collard, T. A. Petrie, and A. J. Garcia: *Biointerphases* 4 (2009) FA3.
- [3] S. Plimpton: *J. Comput. Phys.* **117** (1995) 1-19.
- [4] W. L. Jorgensen, D. S. Maxwell, and J. Tirado-Rives: *J. Am. Chem. Soc.* **118** (1996) 11225.
- [5] H. J. C. Berendsen, J. R. Grigera, and T. P. Straatsma: *J. Phys. Chem. A* **91** (1987) 6269.
- [6] H. O. S. Yadav, A. -T. Kuo, S. Urata and W. Shinoda: *Langmuir* **35** (2019) 14316.
- [7] H. O. S. Yadav, A. -T. Kuo, S. Urata and W. Shinoda: *J. Phys. Chem. C* **124** (2020) 14237.
- [8] H. O. S. Yadav and S. Harada, A. -T. Kuo, S. Urata, and W. Shinoda: *Mol. Phys.* (2021) e1910355.

Construction of data assimilation in materials science

Munehisa MATSUMOTO

*Institute of Materials Structure Science, High Energy Accelerator Research Organization
Oho 1-1, Tsukuba 305-0801*

We have been developing methods to use both of experimental data and theoretical data to better characterize and predict good magnetic materials [1, 2]. Experimental data taken from actual materials and corresponding computational data constitute an integrated data model. The desired properties of materials are often well defined and it now looks as though it is getting more and more feasible to implement a scheme for rational materials design based on the integrated data among various experimental probes and *ab initio* materials data. However, during the course of our developments we are rather finding the relevance of stochastic aspects of the materials design.

The problem is caused by multiple requirements which are often simultaneously imposed on the target materials. For permanent magnets, a candidate compound should have strong magnetization, magnetic anisotropy, high Curie temperature, and sufficient structure stability. Unfortunately it is hardly the case that all of these can be maximized with a particular chemical composition. Trade-off's are encountered and we have to work with a good compromise. Besides, another problem is imposed by the multi-scale nature of materials. The material is put into practical use in a macroscopic world in non-equilibrium and at the moment it is hardly possible to keep all those extrinsic parameters under control in the modeling.

A starting point is to restrict the working parameter space and implement an optimization scheme therein referring to the given set of requirements for the target material [2]. An-

other solution which potentially has the flexibility to deal with the effect of the extrinsic parameters is a stochastic sampling over the landscape of the parameter space. A set of equivalently preferable parameter points can be sampled out and proposed as a set of candidate materials to meet the given needs. We note that the external needs can vary depending on social and economical trends. Even some unexpected requirements can pop up depending on how the material is used in practical applications. These are not predictable, which points to an unavoidable stochasticity in the materials design. Thus it seems to be a good idea to consider the materials design as a stochastic process working on the integrated data space constructed over various experimental probes and theoretical calculations. We adapt the data assimilation techniques in weather forecasts into the materials science. Developments are in progress and will be reported in detail elsewhere.

The author benefited from the online school for data assimilation in the autumn 2020 [3].

References

- [1] MM, T. Hawaii, K. Ono, Phys. Rev. Applied **13**, 064028 (2020).
- [2] Y. Harashima, K. Tamai *et al.*, Phys. Rev. Materials **5**, 013806 (2021).
- [3] http://www.data-assimilation.riken.jp/jp/events/riken_da_tr_2020/index.html

Data integration between experiments and calculations: the new stages

Munehisa MATSUMOTO

*Institute of Materials Structure Science, High Energy Accelerator Research Organization
Oho 1-1, Tsukuba 305-0801*

We have been working on magnetic materials made of transition metals and rare-earth elements. Since magnetism is a relatively low-energy phenomenon coexisting with high-energy properties of conducting electrons in the metallic parts, fundamental problems caused by the dichotomy between localized magnetic moments and delocalized electrons is already implied. On top of this, we encounter the multiple-scale problem where the intrinsic properties determined on the basis of atomic-scale structure is combined with extrinsic properties controlled by the microstructure to yield the macroscopic properties of magnetic materials. They both involve different layers of physics and we have accordingly used combined approaches such as LDA+DMFT [1] to address the magnetism of localized f -electrons embedded in the metallic environments. Here a quantum impurity problem is solved with quantum Monte Carlo method within the dynamical mean field theory (DMFT), and the realistic electronic structure is addressed with density functional theory based on local density approximation (LDA). In an analogous spirit, we have worked on a computational scheme where the electronic structure calculations for metallic ferromagnets and the input structure information taken from the Rietveld analysis of neutron diffraction data proceed via feedback to each other, which is tentatively termed “LDA+Rietveld” [2]. Here the experimental data play the role of an effective self-energy in the language of LDA+DMFT.

Both approaches can be considered as developments for data integration of different types. The LDA+DMFT was originally developed for the simulation of strongly correlated electron systems which may be considered as a prototype to bridge over multiple scales in the target systems, which is often encountered in physics and materials science. While the past fiscal year 2020 was dominated by the serious pandemic problem, remote working and on-line learning tools have significantly improved which helped us to import several techniques from experts outside of our conventional discipline. This included the data assimilation techniques in weather forecast where unpredictable phenomenon coming from nonlinear dynamics can be put under numerical control by combining a limited number of observatory data and relatively abundant simulation data. This methodology adapted into the materials science might help the upcoming materials design and discovery to be done in an accelerated and predictable way, prospectively including a more comprehensive data integration with sample-fabrication processes. Further developments are in progress.

References

- [1] MM, Phys. Rev. Materials **4**, 054401 (2020).
- [2] MM, T. Hawaii, K. Ono, Phys. Rev. Applied **13**, 064028 (2020).

Co-equivalent of Ce in $4f$ - $3d$ intermetallics

Munehisa MATSUMOTO

Rare-earth permanent magnets based on Nd-Fe-B alloys have been widely used and expected to be even more of the key material in the upcoming decades. The weak anisotropy field at high temperatures and the relatively low Curie temperature of the main-phase compound, $\text{Nd}_2\text{Fe}_{14}\text{B}$, sometimes require supplementary rare metals in order to put the material in practical use. Since such rare metals are expensive and not always straightforwardly available, we have been in urgent quest for good ferromagnets on which permanent magnets may be developed in a cost-effective, robust, and sustainable manner. In this regard, clarification of the potential utility of Ce can be of a help. Indeed from the viewpoint of solid state physics, many interesting phenomena associated with Ce, such as valence fluctuations, heavy fermions, and unconventional superconductivity, have been known. Some of the fundamental ideas can help in answering the problems posed from material science.

We have looked into the potential utility of Ce for most of the representative properties of a ferromagnet to qualify as a constituent of a permanent magnet, namely, magnetization, magnetic anisotropy [1], Curie temperature, and structure stability. Among all these properties, we have observed that the largest merits actually seem to originate in the valence fluctuations, in particular the contribution from Ce^{4+} states to the bulk properties. One of such aspects can be illustrated with an effect of Ce substitution in SmFe_{12} [2]: we can computationally get an analogue of the Slater-Pauling curve with the Ce-substituted ferromagnets. The magnetization of the Fe-based ferromagnet shows a peak as a function

of the concentration of dopants, typically Co. Remarkably, the same thing can happen even when the dopant is Ce.

Obviously it is hard to observe this phenomenon in real experiments. There seems to be a strict constraint on the inter-atomic distance between the rare-earth sublattice and the transition-metal sublattice in order for the delocalized $4f$ -electron to contribute to the bulk magnetization that is mostly made of $3d$ -electrons. Especially for $\text{Nd}_2\text{Fe}_{14}\text{B}$ with the relatively inflated lattice, extracting the merit of Ce with the Slater-Pauling analogue is not straightforward. Nevertheless there has been some actual observation [3] confirmed both experimentally and computationally. Several findings as exemplified by these cases point to some hope for promising ferromagnets with reduced costs. So far we identified and understood several singular cases. Systematic quest to pop up further candidates on the basis of data assimilation between theory and experiments are in progress.

Helpful discussions with K. Saito, T. Ueno, and H. Shishido through the JSPS KAKENHI 15K13525 project are gratefully acknowledged.

References

- [1] H. Shishido *et al.*, arXiv:2103.10202.
- [2] MM, T. Hawai, K. Ono, *Phys. Rev. Applied* **13**, 064028 (2020).
- [3] X. Tang *et al.*, *Acta Materialia* **175**, 1 (2019).

Finite temperature properties of frustrated systems

Tsuyoshi OKUBO

Department of Physics, The University of Tokyo
7-3-1 Hongo, Bunkyo-ku, Tokyo 113-0033

A variety of exciting phenomena, including non-collinear magnetic order, magnetization plateaus, and spin liquids, occur in the frustrated spin systems. Frustrated interactions often appear as geometrical frustrations based on the antiferromagnetic interaction on triangular units. Another origin of the frustration might be the competition of several interactions, such as the J_1 - J_2 model on the square lattice. The honeycomb lattice Kitaev model could be considered as an example of the latter frustration [1]. In the Kitaev model, the interactions are Ising type, $S_i^\gamma S_j^\gamma$, and the spin component $\gamma = x, y, z$ is determined from the direction to the neighboring site. The Kitaev model is exactly solvable, and its ground state is known to be a spin liquid without long-range magnetic order. Such Kitaev interaction could appear in the realistic situation through the strong spin-orbit interaction [2]. α -RuCl₃ is an example of such a Kitaev compound. In this compound, the ground state is not the spin liquid: it is a magnetically ordered state. However, when we apply a magnetic field, the compound looks show the spin-liquid-like behaviors. In particular, a half-integer thermal Hall conductivity was observed at finite temperature [3], indicating the appearance of Kitaev spin liquid.

In this year's project, we investigated finite temperature properties of the Kitaev model with off-diagonal interactions motivated by the recent experiments on a Kitaev compound. The model Hamiltonian is given as

$$\mathcal{H} = \sum_{\gamma \in x, y, z} \mathcal{H}_\gamma - \frac{h}{\sqrt{3}} \sum_i (S^x + S^y + S^z), \quad (1)$$

where for $\gamma = z$,

$$\begin{aligned} \mathcal{H}_z = \sum_{\langle i, j \rangle_z} [& K S_i^z S_j^z + \Gamma (S_i^x S_j^y + S_i^y S_j^x) \\ & + \Gamma' (S_i^z (S_j^x + S_j^y) + (S_i^x + S_i^y) S_j^z)]. \end{aligned} \quad (2)$$

In the cases of $\gamma = x, y$, we consider similar interaction with cyclic rotation of x, y, z components. To numerically calculate the physical quantities at a finite temperature, we represent the system's density matrix as a tensor network and optimize its elements.

Firstly, we considered pure ferromagnetic Kitaev model ($K = -1$, $\Gamma = \Gamma' = 0$ and $h = 0$) in the thermodynamic limit. In our previous calculation using the infinite tensor product operator (iTPO) tensor network, we have found that the accuracy at the low temperature is not sufficient; we could not quantitatively reproduce the low-temperature specific heat peak previously calculated by quantum Monte Carlo [4]. In this year, we considered a cluster optimization of the tensor to improve the accuracy. In the standard optimization based on the imaginary time evolution, we perform Suzuki-Trotter decomposition and only optimize two sites simultaneously (simple update). In the new cluster optimization, we consider the imaginary time evolution of six sites and optimize them simultaneously. In Fig. 1, we plot thus obtained specific heat for the Kitaev model in the thermodynamic limit. Although both the simple update and the cluster optimization reproduce two expected peak structures of the specific heat, the lower peak height is largely increased by using the cluster

optimization. Because the specific heat calculated by unbiased QMC shows a higher peak than the present data obtained by the cluster optimization, the accuracy is still not enough. However, we hope it will be improved when we consider larger bond dimensions in the future.

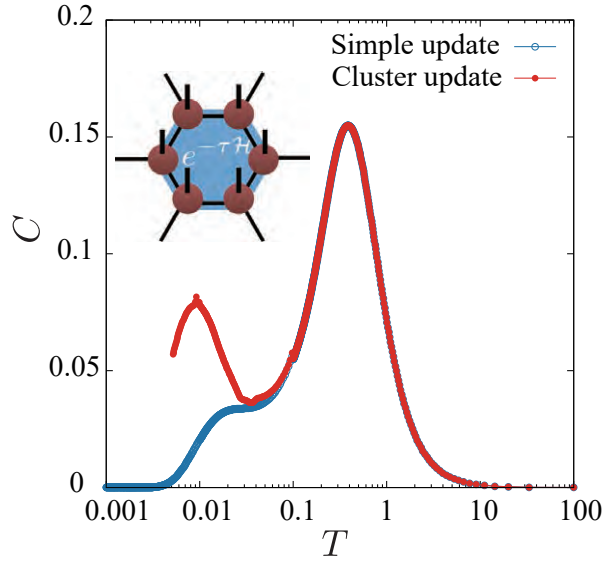


Figure 1: Specific heat of the infinite Kitaev model calculated by iTPO method. (open circle) Specific heat calculated by the standard simple update. (filled circle) Specific heat calculated by the new cluster optimization.

Secondary, we investigated the thermal Hall conductivity under a magnetic field. As we discussed, the accuracy of the infinite size simulation is still insufficient. Thus, we calculated the thermal Hall conductivity for the finite size cluster, and the density matrices are represented by matrix product operators (MPO) instead of iTPO. It has been demonstrated that by using such MPO representation, indeed, one can calculate finite temperature properties of the Kitaev model very accurately [5]. By using this MPO representation, we successfully calculated the thermal Hall conductivity under a magnetic field. For the pure Kitaev model, the thermal Hall conductivity has a peak at a finite temperature, and it overshoots the half quantized value; it is consistent with the exper-

imental observation [3]. We also investigated the effect of the weak Γ and Γ' terms, and we found that depending on the sign of Γ and Γ' , the thermal Hall conductivity is largely modified from that of the pure Kitaev model.

A part of this work has been done in collaboration with J. Nasu, T. Misawa and Y. Motome.

References

- [1] A. Kitaev: *Ann. Phys.* **321** (2006) 2.
- [2] G. Jackeli and G. Khaliullin, *Phys. Rev. Lett.* **102** (2009) 017205.
- [3] Y. Kasahara, T. Ohnishi, Y. Mizukami, *et al.*, *Nature* **559** (2018) 227.
- [4] J. Nasu, M. Udagawa, and Y. Motome: *Phys. Rev. B* **92** (2015) 115122.
- [5] H. Li, D.-W. Qu, H.-K. Zhang, *et al.* *Phys. Rev. Research* **2** (2020) 043015.

Conformation of ultra-long-chain fatty acid in lipid bilayer

Kazutomo KAWAGUCHI^a, Koh M. NAKAGAWA^b, Satoshi NAKAGAWA^a,
Hideo SHINDOU^c, Hidemi NAGAO^a, and Hiroshi NOGUCHI^b

^a *Institute of Science and Engineering, Kanazawa University,
Kanazawa, Ishikawa 920-1192, Japan*

^b *Institute for Solid State Physics, University of Tokyo, Kashiwa, Chiba 277-8581*

^c *Department of Lipid Signaling, National Center for Global Health and Medicine,
Shinjuku-ku, Tokyo 162-8655, Japan; Department of Lipid Science, Graduate School
of Medicine, University of Tokyo, Bunkyo-ku, Tokyo, 113-0033, Japan*

In living cells, the most abundant lipids are phospholipids, which have a polar head group and two hydrocarbon tails. Each tail typically contains between 14 and 22 carbon atoms. Around C22 fatty acids such as docosahexaenoic acid (C22:6, DHA) are called very long-chain fatty acids (VLCFAs). Moreover, much longer chains, called ultra-long-chain fatty acids (ULCFAs), with 32 to 36 carbons with 6 double bonds were found at the sn-1 position of phosphatidylcholine (PC) in photoreceptors, spermatoocytes, fibroblasts, and keratinocytes. However, the biosynthetic mechanisms and biological roles of ULCFAs have not understood yet. In this study, we examined the conformation of one of ULCFAs, dotriacontahexaenoic acid (C32:6) containing phosphatidylcholine (dTSPC, C32:6-C18:0), in phospholipid bilayers using all-atom molecular dynamics simulations [1].

One dTSPC is embedded in the lipid bilayer consisting of one of the following three lipids: Distearoyl PC (DSPC, C18:0-C18:0), Stearoyl-DHA PC (SDPC, C18:0-C22:6), and stearoyl-oleoyl PC (SOPC, C18:0-C18:1). Moreover, we examined the effects of the difference in lipid density between the two leaflets.

We found that the ultra-long tail of the ULCFA flips between two leaflets and fluctuates among an elongation into the opposite leaflet, lying between two leaflets, and turning back. The time scale of the conformational change between the elongated and turned shapes is \sim

10 ns, so that it is quite fast. The ratio of these three states depends on the lipid-density difference between the two leaflets. The sn-1 chain is located at the opposite leaflet more frequently, as the lipid density of the opposite leaflet relatively decreases. We have clarified the linear relationships between the position of the sn-1 terminal of dTSPC and the lipid-density difference in all three types of membranes.

The main difference among the three types of host lipids is the number of the double bonds, and clear effects appear in the order profiles. Nevertheless, the conformation of dTSPC exhibits no qualitative differences. A minor influence is found in the distribution of C₃₂ of dTSPC. Different shapes are obtained between SDPC and the others, whereas those of C₁₈ and C₃ are not. In the SDPC membrane, C₃₂ has a rounded triangular distribution. In contrast, a small peak or shoulder shape appears for the DSPC and SOPC membranes.

As described above, we revealed that ULCFA can sense and rapidly respond to the lipid-density difference to reduce such a difference. This behavior may be essential for the functions of ULCFAs in living cells.

References

- [1] K. Kawaguchi, K. M. Nakagawa, S. Nakagawa, H. Shindou, H. Nagao, and H. Noguchi: *J. Chem. Phys.* **15**, 165101 (2020).

Giant magnetic response of hidden SU(2) symmetric antiferromagnets induced by impurity disorder

Hidemaro SUWA

*Department of Physics, University of Tokyo
Hongo, Bunkyo, Tokyo 113-0033*

In the research area of antiferromagnetic (AFM) spintronics, one of the most fundamental and challenging subjects is the efficient manipulation of the AFM order parameter. The key to extreme susceptibility lies in two-dimensional (2D) systems with spin isotropy. Although the ground state typically has a long-range order, any continuous symmetry is not broken at finite temperature in a 2D system with short-range interactions, according to the Mermin-Wagner theorem. As a result, the magnetic susceptibility exhibits an exponential divergence in the low-temperature region. Here the strongest divergence is obtained in the presence of the spin isotropy.

To achieve a giant magnetic response, we have proposed exploiting the hidden SU(2) symmetry built in a spin-orbit system [1]. The large spin-orbit coupling of iridates gives rise to $J_{\text{eff}} = 1/2$ quantum states and pins the $J_{\text{eff}} = 1/2$ pseudo-spins on the IrO_6 octahedral network. The octahedral rotation around the axis perpendicular to the plane can lead to a canted in-plane magnetic order and a linear coupling to uniform magnetic fields without breaking the spin isotropy. This hidden SU(2) symmetry is revealed by a staggered rotation of the spin reference frame under the frustration-free condition of the Dzyaloshinskii-Moriya interaction. Nevertheless, real materials have other perturbations to the pure 2D spin isotropic system: in particular, spin anisotropy introduced by the mixing with the $J_{\text{eff}} = 3/2$ orbitals. For efficient manipulation of the AFM order, it is

crucial to make the perturbations smaller than the external fields we control.

We have shown that the AFM tunability can be systematically and significantly enhanced by introducing magnetic dilution and diminishing the spin anisotropy effect in the 2D antiferromagnets. We used ISSP System B and C in class C projects (ID: 2020-Ca-0097, 2020-Cb-0091) and calculated the large-scale quantum spin system consisting of more than one million spins using ALPS/looper (<http://github.com/wistaria/alps-looper>). Hybrid parallel computation was performed using up to 3,456 cores. We numerically showed that the non-magnetic substitution significantly suppresses the spin stiffness. Therefore, the perturbation of the controllable magnetic field, quantified by the ratio of the Zeeman energy to the intralayer spin stiffness, is significantly enhanced and dominant over the other perturbations. We have accomplished an extreme response of SU(2) symmetric AFM fluctuations in a diluted system close to the percolation threshold. The quasi-2D system of iridates thus represents a prototype of the magnetic dilution problem in 2D pseudo-spin-half antiferromagnets, leading to a tunability of effective spin anisotropy.

References

- [1] L. Hao, D. Meyers, H. Suwa, et al., *Nat. Phys.* **14**, 806 (2018)

Development of Thermal Functional Materials Using Materials Informatics

Junichiro SHIOMI

Department of Mechanical Engineering,

The University of Tokyo, 7-3-1, Hongo, Bunkyo-ku, Tokyo 113-8656

The ability to effectively reduce a material's thermal conductivity while keeping its electrical properties unchanged is the ultimate goal for thermoelectric materials. Due to the relative difference in the mean free paths (MFPs) of electrons and phonons, introducing nanostructures can effectively scatter phonon while affecting less to the electron transport. For example, the thermal conductivities of nanostructured materials like superlattice, nanowire, and nano-porous material are about one or two orders of magnitude lower than the bulk counterpart.

On the other hand, Silicon also has many allotropes other than the commonly seen diamond phase (referred to as Si-I phase) and has nature low thermal conductivity. Under high pressure, it can also form the body-centered cubic (BC8, referred to as Si-III) phase and rhombohedral (R8, referred to as Si-XII) phase as well as many other intermediate phases. How those multiphase nanostructure will affect the thermal conductivity remains unknown.

In this work, we utilized a multiscale modeling technique that including first-

principles lattice dynamics, the Monte Carlo ray-tracing method, and effective medium theory was used to understand the mechanism of phonon transport in multiphase nanostructured silicon as well as the weak temperature dependence. The thermal conductivity values as well as its temperature dependence are also verified by the experimental measurements.

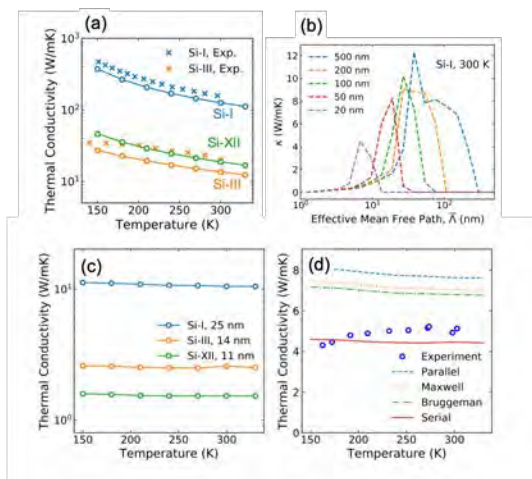


Figure 1(a) Bulk thermal conductivity of Si-I, Si-III, and Si-XII phases of silicon (b) The thermal conductivity spectrum as a function of effective mean free (c) The effective thermal conductivity of nanograin Si-I, Si-III, and Si-XII at different temperature. (d) The effective thermal conductivity of multiphase nanograin silicon as function of temperature.

The bulk phonon properties of the three phases are shown in Fig. 1(a), which are calculated from anharmonic lattice dynamics with interatomic force constants from first-principle calculations. The bulk phonon thermal conductivities of these three phases of silicon are quite high, which is unfavored for the thermoelectric energy conversion. Even for the Si-III phase, which has the lowest thermal conductivity among the three phases, the thermal conductivity is still above 10 W/mK at room temperature. Base on the Monte Carlo ray-tracing simulations, we found that introducing nanograin is an efficient way to reduce its lattice thermal conductivity. Taken the Si-phase as an example [Fig. 1(b)], we found that with the decreasing in the grain sizes, both the effective mean free path and the thermal conductivity will be shifted to low values. The effective thermal conductivity the nanograined silicon as a function of temperature is shown in Fig. 1(c), which shows

a temperature-independent behavior. This weak temperature dependence suggests that the phonon-boundary scattering, which is a temperature-independent process in the elastic regime, is the dominate process that limits the thermal transport. To further verify the simulation, we also compared the simulation results with the experiment measurements, and the results are shown in Fig. 1(d). The inputs parameters like the volume fractions and the averaged grain sizes are extracted from the samples, and the good agreement between the simulations and the experimental measurements suggests the prediction power of our multiscale modeling scheme.

References

- [1] C. Shao, K. Matsuda, S. Ju, Y. Ikoma, M. Kohno, & J. Shiomi, *Journal of Applied Physics*, 129(8), 085101 (2021)

Efficient Sampling Simulation of the Soft Modes Significantly Contribute to Protein Properties

K. TAKEMURA, D. TRAN, K. TAKABA, M.M. SOBEH, Y. MIYAZAWA, R. KIUCHI,
T.N. WIJAYA, T. OGAWA, Y. TAIRA, R. MISU, and A. KITAO
School of Life Science and Technology, Tokyo Institute of Technology
Ookayama, Meguro, Tokyo 152-8550

As an efficient conformation sampling method, we previously developed parallel cascade selection molecular dynamics (PaCS-MD) [1]. PaCS-MD consists of cycles of multiple independent short MD simulations. The initial structures of each cycle were selected as the closest structures to a target structure based on suitable properties such as root-mean-square-deviation (RMSD), center-of-mass distance. These selections increase the probability of rare event occurrences, and PaCS-MD enhances conformation sampling without external perturbations.

One problem in the original PaCS-MD is a requirement prior knowledge of the target structure. To address this issue, we proposed edge expansion PaCS-MD (eePaCS-MD) [2]. As illustrated in Fig. 1, eePaCS-MD requires only the initial structure (black cross). The initial structures of each cycle are randomly taken from the vertices (stars) of a multi-dimensional principal component subspace. The subspace consists of conformations

sampled during previous cycles of eePaCS-MD and solving the “convex hull problem” provide the edges and vertices.

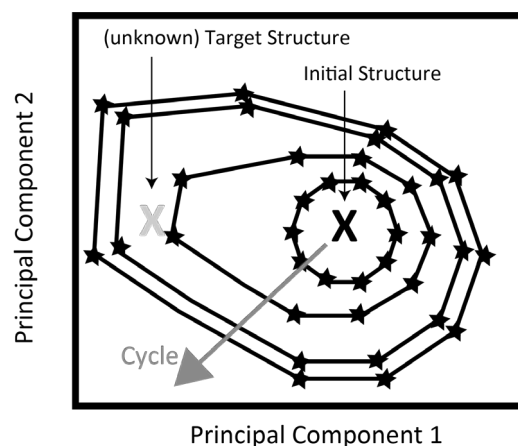


Fig. 1 Schematic illustration of the evolution of the vertices and edges in eePaCS-MD.

The sampling efficiency of the method can be examined by conducting eePaCS-MD from one state and examining whether the sampled conformations contain the target structures or not. For this purpose, we applied eePaCS-MD to open-close transitions (Fig.2) of glutamine binding protein (QBP), maltose/maltodextrin binding protein (MBP), adenylate kinase (ADK). We conducted

eePaCS-MD from both open and close states.

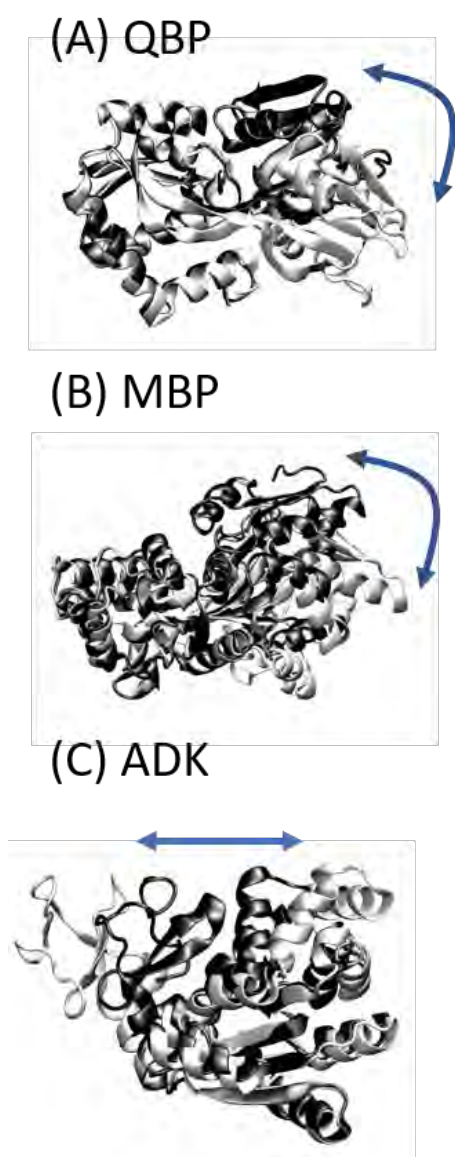


Fig. 2 Structures of target complexes. (A) Glutamine binding protein (QBP). (B) Maltose binding protein (MBP). (C) Adenylate kinase (ADK). Structures colored in black and white correspond to close and open states, respectively.

For all targets, eePaCS-MD efficiently sampled open-close transitions (generated conformations containing structures similar to

the close state when simulations started from the open state). For QBP and MBP, close-open transitions were also successfully sampled. We also showed that the combination of eePaCS-MD and accelerated MD (eePaCS-aMD) achieved a further improvement of sampling efficiency. Minimum RMSD (RMSD_{\min}), time to reach RMSD_{\min} (t_{\min}), and the total computational cost used to reach the opposite state for the first time ($T_{1\text{st}}$) of eePaCS-aMD are shown in Table 1. OC and CO represent open to close and close to open transition, respectively. As shown in Table 1, open to close transitions were observed within 10 ns, which is several orders of magnitude shorter simulation time than conventional MD. Thus, eePaCS-MD is a very efficient sampling method that does not require prior knowledge.

Table 1 Summary of results (eePaCS-aMD)

Target	RMSD_{\min} (Å)	t_{\min} (ns)	$T_{1\text{st}}$ (ns)
QBP (OC)	1.3	4.9	40.4
QBP (CO)	1.3	6.4	52.8
MBP (OC)	1.2	6.7	41.6
MBP (CO)	1.3	7.2	49.4
ADK (OC)	1.9	8.9	114
ADK (CO)	3.2	9.3	-

References

- [1] R. Harada and A. Kitao. J Chem Phys 139, 035103 (2013).
- [2] K. Takaba, D.P. Tran and A. Kitao. J Chem Phys 152, 225101 (2020).

Anderson-Kitaev spin liquid

Masahiko G. YAMADA and Satoshi FUJIMOTO

*Department of Materials Engineering Science, Osaka University
Toyonaka, 560-8531, Japan*

More than half a century, the Anderson localization has been investigated intensively on the low-dimensional electron systems or fermionic systems. Normal magnets with a long-range order does not have a fermionic excitation, and thus the randomness effect has been investigated in a different manner. On the other hand, in Kitaev spin liquids excitations are described by Majorana fermions, and the Anderson localization of Majorana fermions can be expected. We name this new localized state Anderson-Kitaev spin liquid. This state potentially explains the experimental observation in α -RuCl₃ or A₃LiIr₂O₆ with A = H, D, Ag.

We discovered Anderson-Kitaev spin liquid in the bond-disordered Kitaev model with a numerical simulation. In the presence of a magnetic field, we need to recompute the flux gap of the disordered Kitaev model in the third-order perturbation. We compute this quantity in two methods. One is the exact diagonalization of the Majorana one-body Hamiltonian, and the other is the kernel polynomial method. Especially, the kernel polynomial method is very much suitable for the parallel computing, and we implement a hybrid parallelization code for this algorithm for a large-scale simulation. We note in the small scale two methods agree well.

With a massive parallel computation, we succeed in computing the flux gap, and hence the thermal Hall conductivity up to a $O(10000)$ -site system for the bond-disordered Kitaev model. In the 100×100 honeycomb lattice, the thermal Hall conductivity shows

a rapid decay as the disorder strength grows. After the extrapolation, the region where the thermal Hall conductivity is quantized disappears when only 5% disorder is added. These results are published in npj Quantum Materials [1].

Overall we discover the new Anderson transition into an Anderson-Kitaev spin liquid thanks to the supercomputer in the Institute for Solid State Physics. The calculation has been done in the manner suitable for the supercomputer based on our newly established method.

References

- [1] M. G. Yamada: npj Quantum Mater. **5** (2020) 82.

Analyses on complex fluids using multiscale simulation platform

Yohei MORII and Toshihiro KAWAKATSU

Department of Physics, Tohoku University, Sendai, Miyagi 980-8578

We have been developing a simulation platform named Multiscale Simulation Platform for complex fluids (MSSP), with which one can simulate macroscopic complex flows coupled with microscopic molecular simulators. MSSP uses smoothed particle hydrodynamics (SPH) method, where each hydrodynamic particle contains microscopic molecular simulator or microscopic stress calculator.

In this project, we implemented moving boundary conditions into MSSP so that we can simulate moving and deforming objects such as floating filler particles and deformable vesicles [1].

Figure 1 shows several characteristic flow properties of a viscoelastic fluid passing by a rotating cylindrical obstacle. The viscoelastic fluid is modelled as a Newtonian fluid where many dumbbells, i.e. each consists of two particles connected by a finite extensible nonlinear elastic (FENE) spring, are immersed.

The obstacle is an elastic cylinder that rotates with a rotation rate (i.e. the speed at the surface of the obstacle/flow speed) 1.0, and the Reynolds number 40.0, and Weissenberg number 4.0, respectively. We used 230,000 SPH particles, each of which contains 1000 FENE dumbbells. As a result, total number of dumbbells are 230,000,000.

We can confirm that the rotation of the obstacle induces an asymmetric flow pattern around the obstacle, and that the dumbbells are strongly stretched at the obstacle surface, which is the origin of the nonlinear behavior of the viscoelastic fluid.

We also develop a simulation technique with which one can simulate an elastic membrane, i.e. a vesicle, in a channel flow. This is a preliminary work for simulating red blood cells in a blood vessel.

References

[1] Y.Morii and T.Kawakatsu, in preparation.

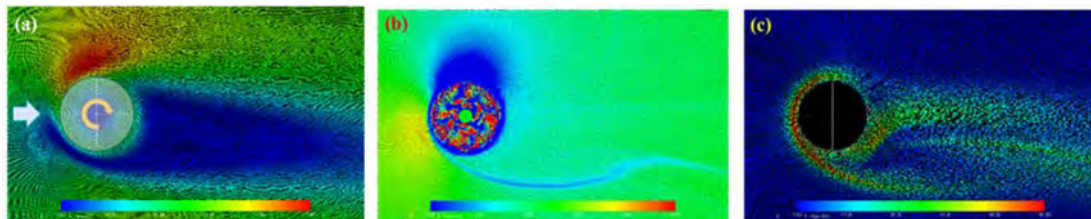


Figure 1: A FENE dumbbell flow around a rotating cylindrical obstacle. (a) Flow field, (b) pressure distribution, and (c) orientation distribution of FENE dumbbells.

Topological Order and Quantum Dynamics in Quantum Many-body Systems

Synge TODO

Department of Physics, University of Tokyo, Tokyo, 113-0033

Institute for Solid State Physics, University of Tokyo, Kashiwa, 277-8581

We have developed various novel numerical methods for quantum/classical many-body systems with strong correlations and performed large-scale simulations on ISSP supercomputer systems.

Rokhsar and Kivelson proposed the quantum dimer model in 1988 as a low-energy effective model for frustrated magnets. Although there is no negative sign problem in the Hamiltonian of the quantum dimer model, Monte Carlo simulations are challenging because of the strong geometrical restriction on the configuration of the dimers. With the help of efficient cluster update based on stochastic series expansion, we now extend our simulation to a more general class of models, including dimers and monomers and multiple interactions between them. It can include a larger Hilbert space based on the quantum dimer model, under the same framework of Monte Carlo simulation and update techniques, by which we can detect the deconfinement of monomers under the finite temperature phase transition (Fig. 1). We also implemented the exchange Monte Carlo method on the quantum dimer model to make a winding number-free simulation, with the kinetic terms to break a dimer into two monomers and still obtain the measurements for only dimer configurations.

In the meantime, the real-space renormalization group method using tensor networks has recently been widely used as a numerical method for many-body spin systems. The tensor network method can efficiently com-

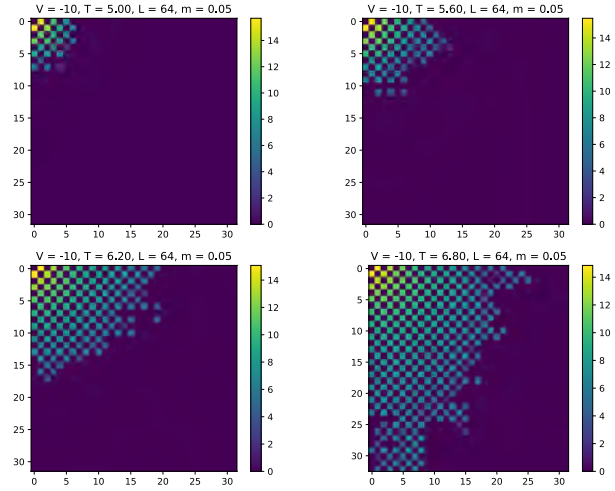


Figure 1: Deconfinement of monomers in quantum dimer model.

pute the physical quantities of large-scale classical and quantum systems. However, existing methods, such as TRG and HOTRG, have a problem that the computational complexity becomes enormous as the spatial dimension increases. Our proposed Anisotropic Tensor Renormalization Group can dramatically reduce the computational complexity of high-dimensional systems such as three-dimensional quantum systems. Furthermore, by extending the tensor network to include tensors not only on the vertices but also on the lines connecting the vertices, the accuracy of the real-space renormalization method can be increased by a factor of 100 compared to existing numerical methods that require a similar amount of computation time.

Confirmation of stress-overshoot phenomena under biaxial elongational flow of ring-linear mixtures

Katsumi HAGITA¹ and Takahiro MURASHIMA²

¹*Department of Applied Physics, National Defense Academy, Yokosuka 239-8686*

²*Department of Physics, Tohoku University, Sendai 980-8578*

Recently, we have studied (linear-rich) ring-linear mixtures [1,2] using Kremer-Grest (KG) [3] based coarse grained molecular dynamics (CGMD) simulations. To study linear-chain penetrations into rings, we performed topology analyses based on the Gauss linking number (GLN) for all pairs of linear and ring polymers. The probability distributions of the number of linear chain penetrations per ring (n_p) were evaluated. We have investigated the possibility of increase of n_p by some conditions in order to make rings to work as a movable cross-linkers.

In the preliminary simulations at the last year, we discovered the increase of n_p under biaxial elongational flows [4]. Here, we used our extended uniform extensional flow (UEF) method [5]. We also discovered the stress overshoot under the biaxial elongational flows. Although the stress overshoot under uniaxial elongational flows were reported, that under biaxial elongational flows had been not. Thus, we proposed the D-Class project to publish a paper as quickly as possible.

In the proposed D-Class project, we started systematic preparation of ring-linear blends. Here, we treated uncatenated rings and ring

complexes such as catenanes and bonded-rings consist of two or three rings per complex as shown in Fig. 1. We studied the cases with $(N_{\text{linear}}, N_{\text{ring}}) = (160,40), (160,80), (160,120), (160,160), (40,160), (10,160)$ and ring fraction was fixed to be about 0.1. Here, N_{linear} and N_{ring} denotes number of beads per a linear chain and a ring, respectively. To keep enough statistical precisions, we used large system sizes with approximate 0.7 M beads. As the initial relaxation run, we performed a run with 10^9 MD steps for each system. As the MD solvers, we used LAMMPS [5] for preparations at the ISSP supercomputer. At later we also used HooMD-bule [6] on the GPUs for continuous product runs.

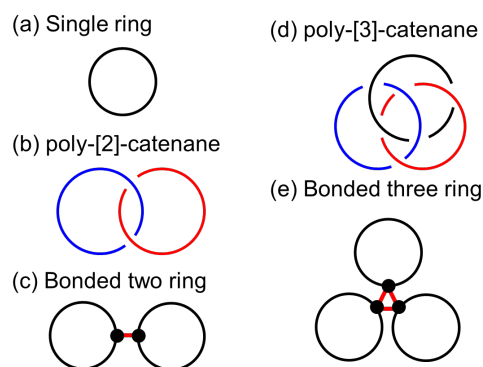


Fig. 1: Schematics of single ring, bonded-rings, poly-catenanes and ring-linear mixture.

In the present project, we developed a method to estimate n_p by using GLN. Here, the ends of linear chains are virtually connected to each other, but we prepared an extra linear chain and connected it to the original linear chain to form a cyclic chain as explained in our work [1,2]. For computation of GLN among cyclic chain and ring polymer, we used the Topoly Python package [7]. Figure 2 shows the probability distributions of linear chains penetrating into a single ring with $(N_{\text{linear}}, N_{\text{ring}}) = (160, 40), (160, 80), (160, 120), (160, 160)$.

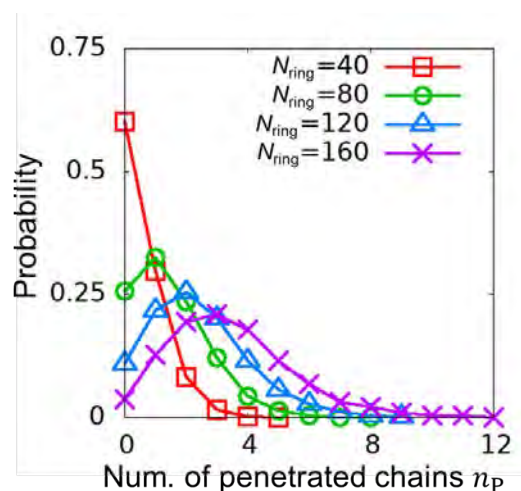


Fig. 2: Probability distributions of linear chains penetrating into a single ring with $(N_{\text{linear}}, N_{\text{ring}}) = (160, 40), (160, 80), (160, 120), (160, 160)$.

In this project, we also performed deformed simulations with the deformation rate of 0.001 in order to grab preliminary results. As results, we obtained the key result for biaxial elongational flows as shown in Fig. 3.

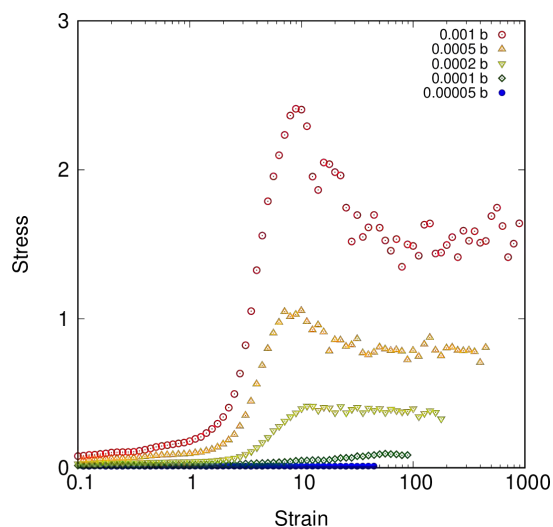


Fig. 3: Stress overshoot under biaxial elongational flows. $(N_{\text{linear}}, N_{\text{ring}}) = (160, 40)$

References

- [1] K. Hagita and T. Murashima: *Polymer* **218** (2021) 123493.
- [2] K. Hagita and T. Murashima: *Polymer* **223** (2021) 123705.
- [3] K. Kremer and G. S. Grest: *J. Chem. Phys.* **92** (1990) 5057.
- [4] T. Murashima, K. Hagita, and T. Kawakatsu: Under review in *Macromolecules*.
- [5] T. Murashima, K. Hagita, and T. Kawakatsu: *Nihon Reoroji Gakkaishi (J. Soc. Rheol. Jpn.)*, **46** (2018) 207.
- [6] S. Plimpton: *J. Comp. Phys.* **117** (1995) 117.
- [7] J. A. Anderson, et. al.: *Comput. Mat. Sci.* **173** (2020) 173, 109363
- [8] P. Dąbrowski-Tumański, et. al.: *Brief. Bionformatics* (2020) bbaa196.

Frustration-induced symmetric skyrmion lattices in three dimensions

K. MITSUMOTO¹, R. OSAMURA², K. AOYAMA² and H. KAWAMURA¹

¹ *Molecular Photoscience Research Center, Kobe University, Kobe 657-8501*

² *Graduate School of Science, Osaka University, Toyonaka 560-0043*

Considerable attention has recently been paid to “skyrmion”, a topologically stable nano-scale spin texture, both from fundamental interest of topology and also from possible application to spintronics. In the usual situation, skyrmion and “skyrmion lattice” are stabilized in the non-centrosymmetric magnets without the inversion center via the anti-symmetric Dzyaloshinskii-Moriya (DM) interaction, which energetically discriminates “right” and “left” spirals. Meanwhile, it was proposed in Ref.[1] that the symmetric skyrmion and skyrmion lattice might be stabilized in centrosymmetric magnets with the inversion center by the frustrated exchange interaction. Examples might be the J_1 - J_3 (J_1 - J_2) Heisenberg magnet on the two-dimensional (2D) triangular lattice under magnetic fields. In such frustrated magnets, in contrast to the DM case, “right” and “left” spirals are energetically equivalent, and the skyrmion with both signs of the scalar chirality (or the topological charge) is possible, giving rise to both the skyrmion and anti-skyrmion lattices. Interestingly, skyrmion and anti-skyrmion lead to the topological Hall effect of mutually opposite signs.

Real magnets are of course three-

dimensional (3D) with certain amount of interlayer coupling. In this year’s project, we investigate the properties of the possible skyrmion and skyrmion lattice in 3D, by performing extensive Monte Carlo simulations on the frustrated classical Heisenberg model on the 3D stacked-triangular lattice. We investigate by means of extensive Monte Carlo simulations both (i) the short-range interaction model mimicking insulators, i.e., J_1 - J_3 - J_{1c} Heisenberg model, and (ii) the long-range RKKY interaction (falling with $1/r^3$) model mimicking metals.

In the short-range model (i), the transition behavior of the 3D model turns out to be similar to that of the 2D model for the ferromagnetic interlayer coupling, exhibiting the skyrmion (anti-skyrmion)-lattice state, while, for the antiferromagnetic interlayer coupling, the nature of the skyrmion-lattice state changes somewhat. In the RKKY model (ii), we also find the skyrmion-lattice state, which, however, seems to accompany an exotic *replica-symmetry breaking (RSB)* unlike the short-range model.

[1] T. Okubo, S. Chung and H. Kawamura, Phys. Rev. Letters **108**, 017206 (2012).

Rotational dynamics of water molecules on the lipid membranes

Yuji HIGUCHI

*Institute for Solid State Physics, The University of Tokyo
Kashiwa-no-ha, Kashiwa, Chiba 277-8581*

We have studied the structures and properties of soft matter. We revealed the fracture processes of semicrystalline polymers [1] by coarse-grained molecular dynamics simulations. Understanding the mechanical properties is essential to improve the toughness of polymeric materials. This year, we study the water dynamics on the lipid membranes, which are considered as a model system for biological membranes. All atomic molecular dynamics (MD) simulations are performed on System B and C using the LAMMPS program [2] and DFTB+ software [3].

We calculate the rotational relaxation of water molecules on the lipid membranes with phosphatidylcholine (PC) and phosphatidylethanolamine (PE) head groups. The relaxation is faster in PE than that in PC (Fig. 1), which is consistent with the previous experiment [4]. To reveal the mechanism of the different relaxation, hydrogen bond (HB) networks among water molecules are analyzed. The number of HBs in PE is less than that in PC. The PE head group is strongly hydrated, which breaks the HB network. In contrast, the weaker hydration around the PC head group does not break the HB network. In DFTB-MD simulation, the head groups of PC and PE are modeled as $N(CH_3)_4^+$ and NH_4^+ , respectively. The rotational relaxation of water molecules and the number of HBs around ions are consistent with those on the lipid membranes, confirming the mechanism. Thus, we successfully reveal the atomistic mechanism of the different

water dynamics on the lipid membranes [5].

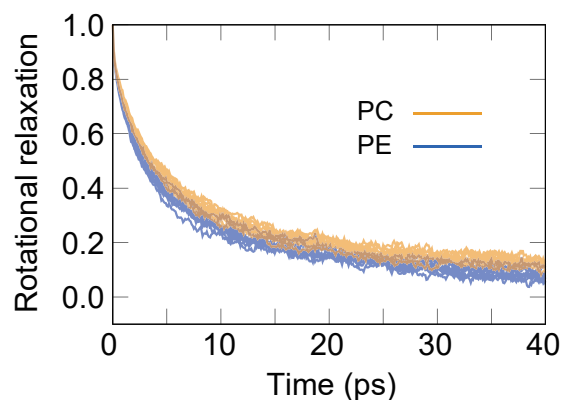


Figure 1: The rotational relaxation of water molecules just above the lipid membranes. Ten trajectories are shown, which confirms the significant difference.

References

- [1] Y. Higuchi: Phys. Rev. E **103** (2021) 042502.
- [2] S. Plimpton: J. Comput. Phys. **117** (1995) 1.
- [3] B. Hourahine, et al.: J. Chem. Phys. **152** (2020) 124101.
- [4] M. Hishida, K. Tanaka, Y. Yamamura, and K. Saito, J. Phys. Soc. Jpn. **83** (2014) 044801.
- [5] Y. Higuchi, Y. Asano, T. Kuwahara, and M. Hishida: Langmuir (2021). DOI: 10.1021/acs.langmuir.1c00417

FRG study on realization of the Kitaev quantum spin liquid in condensed matter physics

Kiyu FUKUI, Yukitoshi MOTOME, and Yusuke KATO

Department of Physics, The University of Tokyo, Bunkyo, Tokyo 113-0033

Department of Applied Physics, The University of Tokyo, Bunkyo, Tokyo 113-8656

Department of Basic Science, The University of Tokyo, Meguro, Tokyo 153-8902

Frustrated quantum spin systems have been studied intensively for very long time. In general, however, it is impossible to solve them exactly mathematically. Therefore, numerical approaches to investigate them are indispensable. Numerical approaches used widely to study them are, for example, exact diagonalization (ED), quantum Monte Carlo (QMC), density matrix renormalization group (DMRG). Each method has pros and cons, of course. Since 2010s, a new method called pseudo-fermion functional renormalization group (PFFRG or pf-FRG) has been used gradually [1]. Although PFFRG overestimates ordering tendencies to magnetic orders [2], it can treat large-size systems and strongly-frustrated systems and detect quantum paramagnetism due to strong frustration. We done two studies on the feasibility of the Kitaev quantum spin liquid by PFFRG [3].

The first one is the study on the feasibility of it in ultracold molecular systems trapped in the optical lattice rather than in solids. We define dipolar Kitaev model on the honeycomb lattice as

$$\begin{aligned} \mathcal{H} = & -\frac{1}{2} \sum_{i,j}^{i \neq j} \frac{1}{3r_{ij}^3} \\ & \times \{ J_x [1 - 2 \cos(2\Phi_{ij} - \frac{4\pi}{3})] S_i^x S_j^x \\ & + J_y [1 - 2 \cos(2\Phi_{ij} - \frac{2\pi}{3})] S_i^y S_j^y \\ & + J_z [1 - 2 \cos(2\Phi_{ij})] S_i^z S_j^z \}, \end{aligned} \quad (1)$$

based on the realization of Kitaev-type inter-

actions proposed in 2013 [4]. In the dipolar Kitaev model, the interactions between the nearest-neighboring sites are consistent with the Kitaev model, but those between sites farther than the nearest-neighbor are more complicated. We apply PFFRG to this model to investigate the ground state at each parameter. The results show that FM order and zigzag AFM order are realized in the FM and AFM dipolar Kitaev model, respectively, for all anisotropy parameters. Furthermore, in order to investigate the connection between the (nearest-neighbor) Kitaev model and the dipolar Kitaev model, we introduce an artificial range of interactions and calculate the susceptibility when approaching the dipolar Kitaev model with long-range interactions from the Kitaev model with only nearest-neighbor interactions. From this calculation, it is clarified that the spin liquid state realized in the Kitaev model is quickly collapses, as the range of interactions is extended. After the proposals of Kitaev-type interaction in ultracold polar molecular systems by microwave irradiation in 2013, the calculation based on these proposals has not been performed, and whether Kitaev quantum spin liquid state is actually realized has remained an open question. We address this issue with PFFRG and elucidated the above results for the first time.

The other is the study on the realization of the Kitaev quantum spin liquid in the high-spin materials. We calculate the phase dia-

gram of the spin- S Kitaev-Heisenberg model with $S = 1/2$ - $5/2$ and $S = 50$. Its Hamiltonian is

$$\mathcal{H} = A \sum_{\mu} \sum_{\langle i,j \rangle_{\mu}} [2 \sin(2\pi\xi) S_i^{\mu} S_j^{\mu} + \cos(2\pi\xi) \mathbf{S}_i \cdot \mathbf{S}_j]. \quad (3)$$

We apply the extension of PFFRG to treat spin- S systems proposed in 2017 [5]. The obtained phase diagrams of the Kitaev-Heisenberg model for $S = 1/2$ and $S = 1$ are in general good agreement with the previous studies by other numerical methods. The phase diagram for $S = 50$ is also in good agreement with the previous study on the classical Kitaev-Heisenberg model by Monte Carlo simulation, except for some special points. As a result of systematic calculations with different S , for $S \leq 3/2$, both the AFM and FM Kitaev spin liquid regions have a finite extent. For $S \geq 2$, no region showing Kitaev spin liquid state was found. Therefore, we believe that $S = 3/2$ gives an upper bound on the spins possessed by the candidate materials in which Kitaev quantum spin liquid is realized. The phase diagram calculation of the Kitaev-Heisenberg model with a systematic change of spin S , as we perform here, has not been done before. This is the first study of the application of spin- S PFFRG to the Kitaev-Heisenberg systems. The results we obtain here provide a guideline for the recent intensive search for candidate materials of $S > 1/2$ Kitaev quantum spin liquid.

References

- [1] J. Reuther and P. Wölfle, Phys. Rev. B **81**, 144410 (2010).
- [2] S. Göttel, S. Andergassen, C. Honerkamp, D. Schuricht, and S. Wessel, Phys. Rev. B **85**, 214406 (2012).
- [3] K. Fukui, Ph.D Thesis, The University of Tokyo (2021).
- [4] S. R. Manmana *et al.*, Phys. Rev. B **87**, 081106 (2013); A. V. Gorshkov, K. R. Hazzard, and A. M. Rey, Mol. Phys. **111**, 1908 (2013).
- [5] M. L. Baez and J. Reuther, Phys. Rev. B **96**, 045144 (2017).

Molecular dynamics simulations for assembly and disassembly of protein aggregates

Hisashi Okumura

*Exploratory Research Center on Life and Living Systems,
Institute for Molecular Science, Okazaki, Aichi 444-8585*

Proteins are normally folded correctly and perform functions that are necessary to sustain life. However, when the concentration of proteins increases due to aging or other reasons, they can aggregate and cause a variety of diseases. Alzheimer's disease, which is one type of dementia, is caused by amyloid- β ($A\beta$) peptides, which aggregate into spherical oligomers or amyloid fibrils. We are conducting theoretical studies on the aggregation and disaggregation of $A\beta$ peptides [1]. In this fiscal year, we investigated the destruction process of an $A\beta$ amyloid fibril by infrared free electron laser irradiation using molecular dynamics simulation.

In recent years, $A\beta$ aggregates have been irradiated with infrared free electron lasers and destroyed. We performed non-equilibrium molecular dynamics simulations of $A\beta$ amyloid fibrils under a time-varying electric field mimicking that of an infrared free electron laser to clarify the destruction process and the structure of amyloid fibrils after destruction.

As a result, we have discovered a new mechanism by which water molecules destroy the $A\beta$ amyloid fibril. Intermolecular hydrogen

bonds formed between C=O and N-H in the amyloid fibril are broken with each pulse of laser irradiation. In most cases, these bonds are reformed spontaneously after the irradiation. However, if a water molecule happens to enter the gap between C=O and N-H made by the laser irradiation, the reformation of the hydrogen bonds is inhibited. This role of water molecules is quite different from other known mechanisms. This new mechanism can explain recent experiments showing that amyloid fibrils are not destroyed by laser irradiation under dry conditions [2].

Furthermore, we found that more α -helix structures are formed after the laser-irradiated amyloid-fibril destruction. This is because the α -helix structure has a different resonance frequency from the β -sheet structure. Our findings provide a theoretical basis for the application of the laser to the future treatment of amyloidosis.

References

- [1] H. Okumura, S. G. Itoh, *J. Am. Chem. Soc.* **136** (2014) 10549-10552.
- [2] T. Kawasaki, et al. *Cellular and Molecular Neurobiology* **38** (2018) 1039-1049.

Study on Complex Systems by Generalized-Ensemble Algorithms

Takuya HAYASHI and Yuko OKAMOTO

Department of Physics, Graduate School of Science, Nagoya University

Furo-cho, Chikusa-ku, Nagoya, Aichi 464-8602

We had two projects regarding generalized-ensemble algorithms applied to complex systems.

The density of states (DOS) is one of the most important physical quantities in statistical mechanics. Recently, we proposed a simulation protocol, REWL-MUCAREM [1], in order to obtain the DOS with high accuracy in complex systems by combining the *Replica-Exchange Wang-Landau* (REWL) method [2] and the *Multicanonical Replica-Exchange Method* (MUCAREM) [3]. The effectiveness of REWL-MUCAREM was demonstrated by using the 2-dimensional Ising model in [1].

We also applied the REWL-MUCAREM protocol to the ice Ih system in order to estimate the residual entropy with high accuracy. The residual entropy of ice has become one of good examples to test the effectiveness of sampling algorithms.

Our latest estimate of residual entropy per one water molecule [4] is:

$$W_0 = 1.507472 \pm 0.000047$$

$$S_0 = k_B \ln W_0 \\ = 0.815615 \pm 0.000063 \text{ [cal/(mol K)]}.$$

This estimate is in good agreement with the results of several other research groups (see Fig. 1).

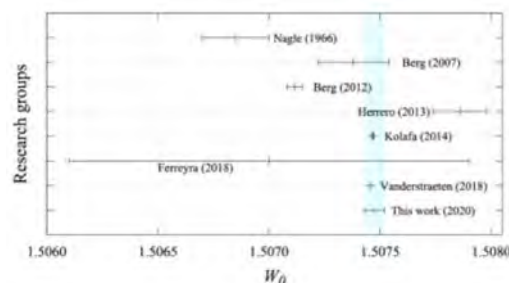


Figure 1: The estimates of residual entropy of ice Ih by several research groups.

However, our previous results disagreed with the above results [5]. We found that the discrepancy resulted from the choice of the random number generators [4]. The present

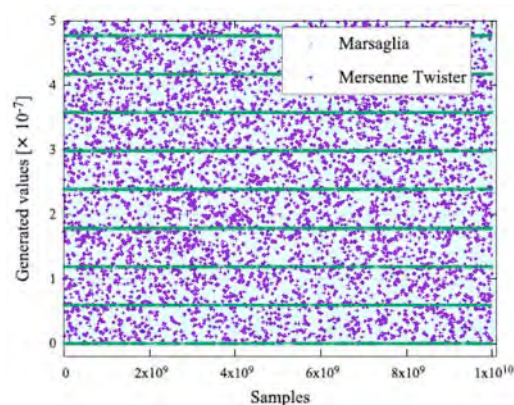


Figure 2: Generated random numbers by the Marsaglia generator (green) and Mersenne Twister generator (purple).

work used Mersenne Twister generator [6], while our previous work used Marsaglia generator [7]. In Fig. 2 we compare the two random number generators. Although the Mersenne Twister generator gives uniform distribution, Marsaglia takes on only nine values in this narrow range. We have reminded the reader that the choice of random number generators is very important.

In the second project, we studied the helix-coil transitions of homo-alanine polymers [8] based on the Microcanonical Inflection-Point Analysis (MIPA) Method [9]. Two lengths of homo-polymers were taken, $N=10$ and 20 , and two environment conditions (in vacuum and in water) were considered. We performed the REWL-MUCAREM simulations. In Fig. 3, we compare the specific heat.

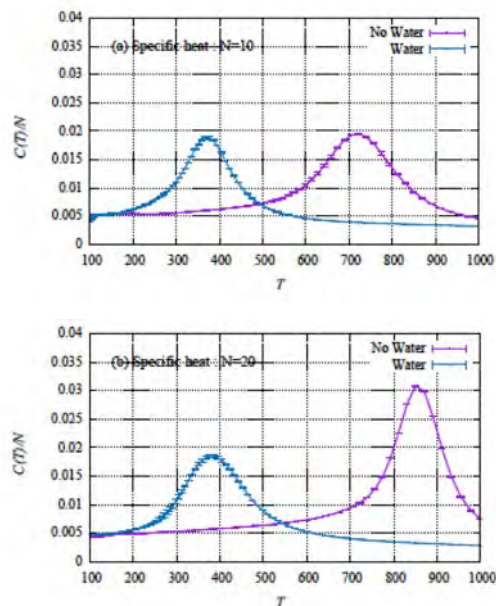


Figure 3: Specific heat as functions of temperature for $N=10$ and 20 .

We see that the helix-coil transition temperature is higher for $N=20$ than for $N=10$. It is also shown that this transition temperature is higher for in vacuum than in water.

By calculating the microcanonical entropy and its derivative with respect to energy, we found that the latter has an inflection point in vacuum but no inflection point in water. This suggests that the helix-coil transition is first-order-like in vacuum, but it is second-order-like in water [8].

References

- [1] T. Hayashi and Y. Okamoto, Phys. Rev. E. **100**, 043304 (2019).
- [2] T. Vogel, Y. W. Li, T. Wüst and D. P. Landau, Phys. Rev. Lett. **110**, 210603 (2013).
- [3] Y. Sugita and Y. Okamoto, Chem. Phys. Lett. **329**, 261 (2000).
- [4] T. Hayashi, C. Muguruma, and Y. Okamoto, J. Chem. Phys. **154**, 044503 (2021).
- [5] B. A. Berg, C. Muguruma, and Y. Okamoto, Mol. Sim. **38**, 856 (2012).
- [6] M. Matsumoto and T. Nishiura, ACM Trans. Modle. Comput. Simul. **8**, 3 (1998).
- [7] G. Marsaglia, A. Zaman, and W. W. Tsang, Stat. Probab. Lett. **9**, 35 (1990).
- [8] T. Hayashi, Y. Sakae, and Y. Okamoto, submitted for publication.
- [9] K. Qi and M. Bachmann, Phys. Rev. Lett. **120**, 180601 (2018).

Numerical Diagonalization Study on the Field-Induced Spin Nematic Liquid

Tôru SAKAI^{1,2}, Hiroki NAKANO¹, Rito FURUCHI¹, and Tokuro SHIMOKAWA³,

¹*Graduate School of Material Science, University of Hyogo,
Kouto, Kamigori, Hyogo 678-1297, Japan*

²*Synchrotron Radiation Research Center, Kansai Photon Science Institute,
Quantum Beam Science Research Directorate,
National Institute for Quantum and Radiological Science and Technology (QST)
SPring-8, Kouto, Sayo, Hyogo 679-5148, Japan*

³*Okinawa Institute of Science and Technology Graduate University, Onna,
Okinawa 904-0945, Japan*

The quantum spin nematic state has attracted a lot of interest in the field of the magnetism. It is a kind of state between the conventional long-range antiferromagnetic order and the quantum spin liquid. This state has been proposed as one of mechanisms of the hidden order which was observed in some strongly correlated electron systems. The spin nematic state was theoretically predicted to be realized in several frustrated systems; the square lattice model with the ferromagnetic nearest-neighbor and antiferromagnetic next-nearest-neighbor interactions[1], the triangular lattice antiferromagnet with multi spin exchange interactions[2], and the ferromagnetic and antiferromagnetic zigzag chain[3, 4]. The previous density matrix renormalization group (DMRG) analysis[5] indicated that the field-induced spin nematic liquid phase appears in the $S = 1$ antiferromagnetic chain with the biquadratic interaction. Thus it would be important to investigate this system using another method, in order to confirm the spin nematic liquid phase. We investigated the magnetization process of the $S = 1$ antiferromagnetic chain with the biquadratic interaction, using the numerical exact diagonalization of finite-size clusters[6]. The present analysis confirmed

the appearance of the field-induced spin nematic Tomonaga-Luttinger liquid phase and gives the ground state phase diagram which is qualitatively consistent with the previous DMRG study[5]

References

- [1] N. Shannon, T. Momoi and P. Sindzingre, *Phys. Rev. Lett.* 96 (2006) 027213.
- [2] T. Momoi, P. Sindzingre and N. Shannon, *Phys. Rev. Lett.* 97 (2006) 257204.
- [3] A. V. Chubukov, *Phys. Rev. B* 44 (1991) R4693.
- [4] T. Hikihara, I. Kecke, T. Momoi and A. Furusakai, *Phys. Rev. B* 78 (2008) 144404.
- [5] T. S. R. Manmana, A. M. Lauchli, F. H. L. Essler and F. Mila, *Phys. Rev. B* 83 (2011) 184433.
- [6] T. Sakai, *AIP Advances* 11 (2021) 015306.

Symmetry Protected Topological Phase of the $S=2$ Antiferromagnetic Chain

Tôru SAKAI^{1,2}, Hiroki NAKANO¹, Rito FURUCHI¹, and Tokuro SHIMOKAWA³,

¹*Graduate School of Material Science, University of Hyogo,
Kouto, Kamigori, Hyogo 678-1297, Japan*

²*Synchrotron Radiation Research Center, Kansai Photon Science Institute,
Quantum Beam Science Research Directorate,
National Institute for Quantum and Radiological Science and Technology (QST)
SPring-8, Kouto, Sayo, Hyogo 679-5148, Japan*

³*Okinawa Institute of Science and Technology Graduate University, Onna,
Okinawa 904-0945, Japan*

The spin gap of the integer-spin antiferromagnetic Heisenberg chain was proposed by Haldane[1, 2] many years ago. Recently it has been generalized as the symmetry protected topological phase[3, 4], which is the gapped phase of the odd-integer-spin antiferromagnetic chain. On the other hand, the numerical diagonalization and the level spectroscopy analyses on the $S = 2$ antiferromagnetic chain with the coupling anisotropy Δ and the single-ion anisotropy D , indicated that the symmetry protected topological phase appears at a small region in the $\Delta - D$ phase diagram[5, 6]. This phase corresponds to the intermediate D phase which had been predicted by Oshikawa[7]. In the present study, the $S = 2$ antiferromagnetic Heisenberg chain with the biquadratic interaction J_{BQ} and the single-ion anisotropy D is investigated using the numerical diagonalization and the level spectroscopy analyses. As a result, it is found that the intermediate D phase appears at a wide region in the $J_{BQ} - D$ phase diagram.

- [2] Phys. Rev. Lett. 50 (1983) 1153.
- [3] F. Pollmann, A. M. Turner, E. Berg and M. Oshikawa, Phys. Rev. B 81 (2010) 064439.
- [4] F. Pollmann, E. Berg, A. M. Turner and M. Oshikawa, Phys. Rev. B 85 (2012) 075125.
- [5] T. Tonegawa, K. Okamoto, H. Nakano, T. Sakai, K. Nomura and M. Kaburagi, J. Phys. Soc. Jpn. 80 (2011) 043001.
- [6] K. Okamoto, T. Tonegawa and T. Sakai, J. Phys. Soc. Jpn. 85 (2016) 063704.
- [7] M. Oshikawa, J. Phys.: Condens. Matter 4 (1992) 7469.

References

- [1] F. D. M. Haldane, Phys. Lett. 93A (1983) 464.

Ground-State Phase Diagram of the $S=1/2$ Heisenberg- Γ model on a Honeycomb Lattice

Takafumi SUZUKI

Graduate School of Engineering,

University of Hyogo, Shosha, Himeji, Hyogo 670-2280

In this study, we investigated the ground-state phase diagram of the $S=1/2$ Heisenberg- Γ model on a honeycomb lattice [1] by the numerical exact diagonalization method and cluster-series expansion method [2]. We focused on the effects of the anisotropic interaction; by tuning the coupling constants, the system changes between the spin-chain and isolated dimer models. We found that, in the spin-chain limit, there are three kinds of states, namely a Tomonaga-Luttinger liquid and two magnetically long-range-ordered states. All three states change two-dimensional long-range ordered states, when the interchain interaction is included infinitesimally except for the case where the Heisenberg interaction is much weaker than the off-diagonal symmetric interaction (Γ). When the antiferromagnetic Γ interaction is large enough and the system locates near the spin chain limit, we observe that there are no prominent peaks of the static structure factor and the feature of the low-energy excitation is quite similar to that in the spin chain limit. We consider that two-dimensional true-long-range-ordered state is suppressed in such parameter region. Starting

from the isolated dimer limit, we found that a triplet dimer phase can survive up to the isotropically interacting system in a large part of the phase diagram, where the Heisenberg and Γ interactions are ferromagnetic and antiferromagnetic, respectively. Otherwise, a phase transition to a magnetically ordered phase takes place before the interaction becomes isotropic. This means that the quantum spin liquid discussed in the Γ model [3] is unstable against the anisotropy of the interactions. The obtained results, namely the unitability of this spin liquid and the stable triplet dimer phase, are the same as those of the previous results for the Kitaev- Γ model on a honeycomb lattice [4].

References

- [1] T. Suzuki, T. Yamada, and S. Suga, in preparation.
- [2] J. Oitmaa, et al., *Series Expansion Methods for Strongly Interacting Lattice Models*, Cambridge University Press, 2006.
- [3] A. Catuneanu, et al., *npj. Quantum Materials*, **3** 23 (2018).
- [4] T. Yamada, T. Suzuki, and S. Suga, *Phys. Rev. B* **102**, 024415 (2020).

Numerical analysis for nonequilibrium dynamics in electronic systems on quasicrystals & Study of new ordered phase and nonequilibrium phenomena in quasicrystals

Akihisa Koga

Department of Physics, Tokyo Institute of Technology, Meguro, Tokyo 152-8551

Recently, quasicrystals, which have no translational symmetry but have ordered lattice structures, are attracting interests in the condensed matter physics. So far, their static properties such as resistivity and specific heats have been mainly focused on. Thus, it is important to reveal nonequilibrium features of quasicrystal systems and understand how special lattice structures affect the dynamics.

Motivated by this, we studied nonequilibrium dynamics of the excitonic insulating (EI) phase described by the two-band Hubbard model on the Penrose lattice. The EI phase is the condensation of the electron-hole pairs (excitons) in semiconductors or semimetals. The EI phase is analogous to superconductors and is attracting much interests in the context of nonequilibrium condensed matter physics. By means of the real-space time-dependent mean-field theory for large systems, we revealed qualitatively different behaviors in the BCS and BEC regimes, see Fig.1. Namely, in the BCS regime, the order parameter is suppressed after a single cycle pulse, while, in the BEC regime, it is increased by the pulse. Such a behavior has been reported in a previous work on the square lattice, and its origin was discussed in the momentum space. However, in quasicrystals, one cannot define the momentum space and such argument does not apply. Our results indicate existence of a more fundamental origin regardless of the momentum picture. In addition, we revealed a characteristic dynamics in the BCS regime using the perpendicular space analysis.

Another interesting topic is possible ordered

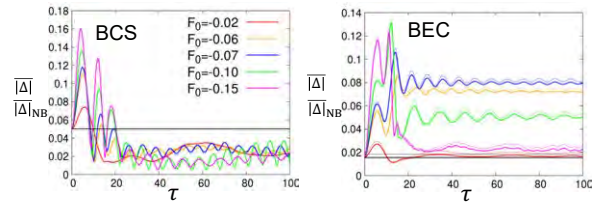


Figure 1: Dynamics of the EI order parameter for the two-band Hubbard model on the Penrose lattice. Horizontal lines indicate equilibrium values.

phases in quasicrystals. We have clarified the nature of magnetic orders in several types of quasi-periodic lattices [2].

Furthermore, we have also studied real-space dynamics and correlations in the Kitaev spin liquid states. We revealed peculiar spin transport mediated by itinerant Majorana fermions [3] and discuss how to modify the Majorana correlations using intrinsic degrees of freedom of the Kitaev model [4].

References

- [1] K. Inayoshi, Master thesis (2021); K. Inayoshi, Y. Murakami, A. Koga, in prep.
- [2] A. Koga, PRB **102**, 115125 (2020); Mater. Trans. **62**, 360-366 (2021).
- [3] T. Minakawa, Y. Murakami, A. Koga and J. Nasu, PRL **125**, 047204 (2020).
- [4] A. Koga, Y. Murakami and J. Nasu, submitted to PRB.

Rational computational design of proteins toward drug discovery and industrial applications

Nao SATO¹, Sairi MATSUMOTO¹, Mizuki TERANISHI¹, Katsuhisa IWAYA²,
Koji OOKA², Masataka YOSHIMURA¹, Shunji SUETAKA¹, Yoshiki OKA¹,
Yuuki HAYASHI¹, and Munehito ARAI^{1,2}

¹*Department of Life Sciences, Graduate School of Arts and Sciences, and*

²*Department of Physics, Graduate School of Science,*

The University of Tokyo, Komaba, Meguro, Tokyo 153-8902

Proteins have been extensively used in industrial and pharmaceutical applications; many protein-based drugs are among the top selling drugs. However, these proteins have been developed by experimental approaches that require a lot of time and cost. Therefore, theoretical approaches to efficiently design useful proteins are demanded. To solve this issue, we have been rationally designing various proteins, which are potentially applicable to industry and medicine, using the Rosetta 3.8 or 3.12 suite [1-3]. We have also performed experimental verification of the computational protein design.

Protein-protein interactions (PPIs) are related to many diseases, and thus designing PPI inhibitors is a promising way for drug discovery. We rationally designed inhibitors for the interactions between the KIX domain of a transcriptional coactivator CBP and transcriptional activators, which are involved in many diseases including leukemia [4]. The transactivation domain (TAD) of the

transcriptional activator mixed lineage leukemia protein (MLL) was used as a template. Theoretical design of the mutants of the MLL TAD fragment that may bind KIX more tightly than the wild type was performed using Rosetta. Among the designed mutants, we could obtain the mutant that binds KIX two-fold more tightly than the wild type, suggesting that our strategy is useful for designing PPI inhibitors.

Severe acute respiratory syndrome coronavirus 2 (SARS-CoV-2), which is responsible for coronavirus disease 2019 (COVID-19), infects human cells through the PPI between the receptor-binding domain (RBD) of the viral-surface Spike protein and the cell-surface receptor angiotensin-converting enzyme 2 (ACE2) [5]. To inhibit this PPI, we have computationally designed the antibodies that can bind the ACE2-binding region of the RBD of SARS-CoV-2. We are currently producing the antibodies and the RBD proteins, to experimentally verify the predictions.

Allergic asthma is known to occur through

the PPI between interleukin-33 (IL-33) released from damaged epithelial cells and the ST2 receptor of type 2 innate lymphoid cells [6]. To develop the IL-33–ST2 inhibitors, we rationally designed the IL-33 mutants that tightly bind to one of the two IL-33 binding sites on ST2 but does not to another site. The interaction of ST2 with one of the designed mutants of IL-33 was measured by fluorescence anisotropy. However, the experiment did not support the theoretical prediction, indicating the necessity of improving protein design methods.

Alkane biosynthesis has gained great attention as an alternative to fossil fuels and is expected as one of the promising ways to produce carbon-neutral renewable energy. Cyanobacterial alkane biosynthesis involves two enzymes, an acyl-ACP reductase (AAR) and an aldehyde deformylating oxygenase (ADO) [7]. Interaction between these proteins allows an efficient delivery of an aldehyde from AAR to ADO [8]. To improve bioalkane production, we rationally designed the mutants of ADO that have higher affinity with AAR. Our preliminary experimental results show that some of the designed mutants enhanced alkane production as predicted.

Finally, solving the protein folding problem is important in improving rational design of proteins. The WSME model can explain the folding pathways of small proteins and is considered to be a promising model to solve the

protein folding problem [9,10]. By extending this model, we have previously developed a statistical mechanical model of protein folding that can explain the folding pathways of multi-domain proteins having multiple disulfide bonds. To further extend this model for any types of proteins, here we applied this model to a protein that does not have disulfide bonds and succeeded in predicting its folding mechanism. Thus, our model may be useful for a unified theoretical description of protein folding mechanisms.

References

- [1] B.J. Bender, et al.: *Biochemistry*, **55** (2016) 4748-4763.
- [2] R. F. Alford, et al.: *J Chem Theory Comput.* **13** (2017) 3031-3048.
- [3] J. K. Leman, et al.: *Nat Methods*, **17** (2020) 665-680.
- [4] P. E. Wright, et al.: *Nat Rev Mol Cell Biol.* **16** (2015) 18-29.
- [5] J. Shang, et al.: *Nature*, **581** (2020) 221-224.
- [6] X. Liu, et al.: *Proc Natl Acad Sci USA.* **110** (2013) 14918-14923.
- [7] M. Arai, et al.: *Adv Exp Med Biol.* **1080** (2018) 119-154.
- [8] M. Chang, et al.: *Biosci Biotech Biochem.* **84** (2020) 228-237.
- [9] M. Sasai, et al.: *Biophys Physicobiol.* **13** (2016) 281-293.
- [10] M. Arai: *Biophys Rev.* **10** (2018) 163-181.

Development of Giant Thermal-property Databases for Amorphous Polymer Materials

Yuxuan Liao, Yoshihiro Hayashi

The Department of Mechanical Engineering

The University of Tokyo, Hongo 7-3-1, Bunkyo-ku, Tokyo, JAPAN

We intended to develop a giant thermal-property database for amorphous polymer materials. This year, we have established an automation framework for developing the giant databases, as shown in Figure 1. The automation framework allows us to generate amorphous polymer structures and calculate its thermal conductivity (TC) automatically. The steps are: 1) creation of polymer chain by random walk algorithm, 2) assignment of the force field and atomic charge into each atom, 3) generation of the amorphous polymer cell, 4) running the equilibration simulation by molecular dynamics (MD), 5) checking the convergence of total energy and density, etc. for the equilibration MD, 6) if not converged, restarting the equilibration MD, 7) running the non-equilibrium MD (NEMD) to compute the TC value, 8) collection of TC values for all polymers.

All MD calculations were performed using the corrected heat flux branch of LAMMPS package. We used an AMBER type GAFF2 forcefield. Atomic charges were derived by the Gasteiger method. The particle-particle particle-mesh (pppm) method was employed to

compute the long-range Coulombic interaction. In equilibration MD, NPT calculations using Nose-Hoover thermostat and the barostat were run for 5 ns annealing and 8 ns equilibration. All bonds and angles, including those of the hydrogen atoms, were constrained by the SHAKE algorithm, and the time step was set to 1 fs. The TC is calculated by performing the reverse NEMD (RNEMD) simulation proposed by Müller-Plathe, as shown in Figure 2.

We have calculated 500 amorphous polymer systems, with an experimental validation shown in Figure 2(B). The results are organized into a paper, which will be coming online soon.

Moreover, we also calculate the thermal transport properties of amorphous materials, which is published in Nano Energy 2021 [2].

References

- [1] **Yoshihiro Hayashi**, Ruimin Ma, **Yuxuan Liao**, et al, Automated calculation system of physical properties with molecular dynamics simulation for polymer informatics (Preparing for submitting)
- [2] **Yuxuan Liao** et al, Heat conduction below diffusive limit in amorphous superlattice structures, Nano Energy 84, 105903.

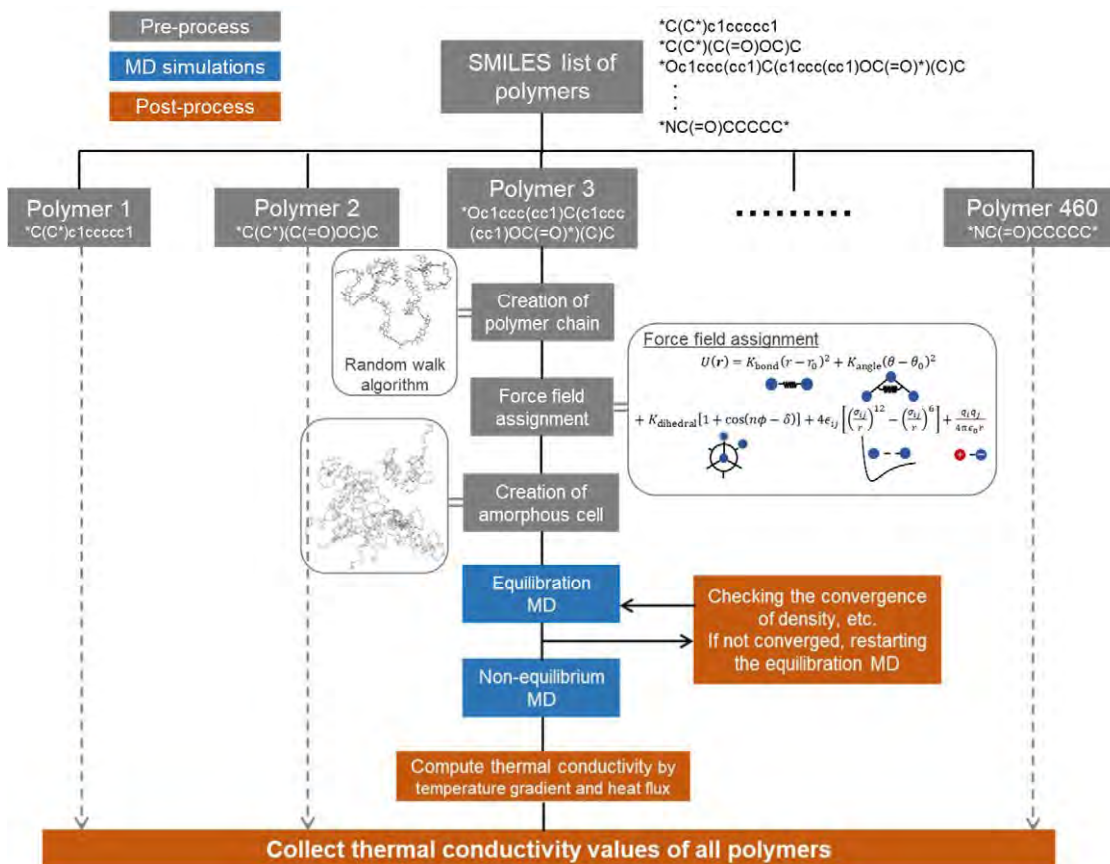


Figure 1 Automation framework for developing the giant thermal-property polymer databases

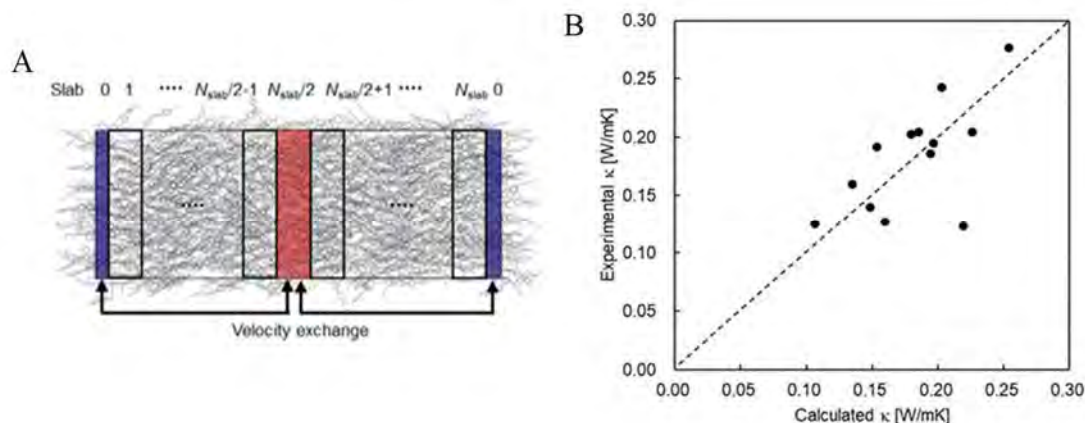


Figure 2. (a) Schematic representation of the simulation box for reverse nonequilibrium molecular dynamics (RNEMD). (b) Comparing the calculated thermal conductivity (κ) and experimental κ for 13 polymers. A dots line indicates calculated κ equal to experimental κ .

Development of Giant Thermal-property Databases for Amorphous Polymer Materials

Yuxuan Liao

The Department of Mechanical Engineering

The University of Tokyo, Hongo 7-3-1, Bunkyo-ku, Tokyo, JAPAN

We intended to develop a giant thermal-property database for amorphous polymer materials. This year, we have 1) optimized the thermal conductivity calculation method and 2) investigated the influence of the classical size effect and the chain length of polymers on the thermal conductivity of amorphous polymers.

The motivation is that 1) Since the calculation is computationally heavy, we need to find out the best NEMD method for our automation system. The Muller-Plathe (MP) method has the advantage of a rapidly converging quantity in temperature gradient rather than a slowly converging heat flux, thus, it can speed up the calculation speed. The results from the MP method are validated by comparing them with the results from the Langevin thermostat, as shown in Fig. 1. Here, a polymer with the ID of P010080 is used as an example. 2) Since the real polymer has extremely long chains consisting of over tens or hundreds of thousand atoms, which is challenging to be calculated with NEMD. The thermal conductivity of polymers typically increases with the chain length. Thus, we need to find out the converged thermal conductivity

in terms of the chain length.

Figure. 1 shows the thermal conductivity as a function of chain lengths, which is characterized by the number of atoms per chain. The results show that 20000 atoms per chain are needed to obtain a converged thermal conductivity. The results indicate that heat carriers with long mean free paths (propagons) play an important role in the heat conduction of amorphous polymers.

To give a deeper insight into the underlying physics, we have explored the relaxation process and mean free path of propagons in amorphous materials. Here, we have used amorphous silicon, amorphous silica, and amorphous silicon nitride as examples. We found that the Akhiezer mechanism dominates the relaxation process of propagons [1]. The next step is how to generalize the analysis into amorphous polymers, which is still under investigation.

References

- [1] **Yuxuan Liao** et al, Akhiezer Mechanism Dominates Relaxation of Propagons in Amorphous at Room Temperature, arXiv preprint [arXiv:2006.07773](https://arxiv.org/abs/2006.07773).

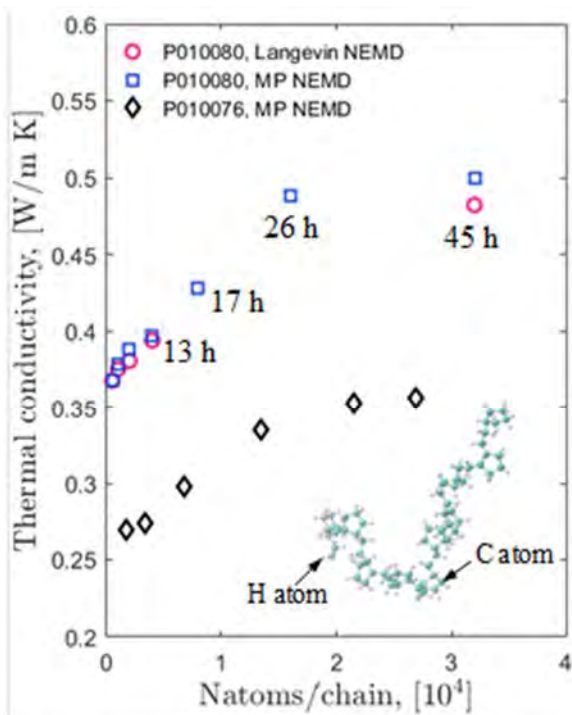


Fig. 1 Thermal conductivity as a function of chain length

Tensor renormalization-group study of spin glasses

Koji HUKUSHIMA

*Department of Basic Science, University of Tokyo
3-8-1 Komaba, Meguro-ku, Tokyo 153-8902*

One of the most important remaining problems in statistical physics is to clarify the low-temperature thermodynamic properties of Ising spin glasses in three dimensions. The search for the ground states is computationally intractable in the sense that it is one of the NP-hard problems in the theory of computation, and the Markov-chain Monte Carlo (MCMC) calculations at finite temperature have extremely slow relaxation phenomena, both of which make large size calculations difficult. Although many computational physical methods derived from spin-glass research, such as the extended ensemble method, have affected other research fields, they have not yet solved the spin-glass problem.

In this study, we aim to break the limit of computational size by applying the tensor renormalization group (TRG) method, which has attracted much attention in recent years, to the spin glass system instead of the MCMC method. We have previously applied TRG to a lattice glass model in two dimensions that exhibits a glass transition in the mean-field limit[1]. There have been a few previous studies that have applied the TRG to spin-glass systems, but they have not been studied extensively. One reason seems to be the problem of numerical accuracy. It has been pointed out that, as a result of frustration, a “negative partition function” appears even though it is originally positive definite, and there is another study showing that this can be solved by very high precision floating-point arithmetic. However, it has been suggested that the numerical accuracy is not realistic for such calculations at low temperature. We proposed a numerical method to detect the ordered phase in Ising spin glasses and explore the possibility of performing the calculation while avoiding the negative partition function problem in TRG.

We addressed two specific issues in Ising spin glasses.

(1) Vertically of ferromagnetic phase transition and ferromagnetic limit on the Nishimori line

It is rigorously known that the ferromagnetic transition on the Nishimori line is the ferromagnetic limit on disorder. MCMC calculations suggested that the phase boundary is somewhat reentrant, but this is not definite. The negative partition function problem is considered to appear at the point where the spin glassiness is strong. Therefore, it is expected to be reduced by getting closer to the ferromagnetic side. Here, we determined the ferromagnetic transition temperature on the Nishimori line with high accuracy by calculating the free energy difference under the twisted boundary condition using TRG.

(2) Development of an algorithm to evaluate the spin-glass order parameter by TRG

Here, we developed a method to calculate the spin-glass order parameter by TRG, and performed the calculation for the Ising spin glass model. The spin-glass order parameter is an overlap function, which is defined using two independent systems with the same interactions. There are two main ways to evaluate the expectation values of physical quantities using the TRG method. One is to use the numerical derivative of the free energy, and the other is to use the impurity tensor to construct the measurement tensor of the observables. In any case, it is necessary to devise a way to calculate the spin-glass order parameter using TRG. We constructed a tensor network for a replica coupled system that introduces an interaction between two systems, and succeeded in calculating the order parameter on the Nishimori line as its derivative with respect to the coupling.

[1] K. Yoshiyama and K. Hukushima: J. Phys. Soc. Jpn. **89**, (2020) 104003.

Parallel Bayesian computation in material science

Koji HUKUSHIMA

*Department of Basic Science, University of Tokyo
3-8-1 Komaba, Meguro-ku, Tokyo 153-8902*

Recent development of various experimental and measurement technologies has allowed us to obtain a large amount of high-precision data, but the methodologies for data analysis have not yet caught up with the improvement of experimental techniques. On the other hand, the development of machine learning, such as deep learning, has also been remarkable in recent years, and the practical application of machine learning to materials science has attracted much attention. However, the black-boxed application of deep learning to materials science is powerful for “prediction” but not necessarily suitable for “understanding”.

In this project, we attempted to apply and develop Bayesian inference based on statistical models that incorporate physical laws as much as possible, using data obtained from experiments as input. Since Bayesian statistical models using physical processes are nonlinear in general, they cannot be computed analytically. In the 1980s, the Markov-chain Monte Carlo (MCMC) method was found to be useful for Bayesian inference, and it started to be applied in large scale. In recent years, the amount of data to be analyzed has increased and the amount of computation per step has become large, and Markov chains which are bound by causality, are not necessarily easy to parallelize.

Therefore, we applied population annealing (PA), which is a population type Monte Carlo method, not based on Markov chains, to the problem of Bayesian statistics of materials science. PA, proposed by Hukushima-Iba(2003), has been introduced as a computational method for statistical mechanical models, and recently it has been working on large-scale parallel computations including GPGPU. This method has a large number of nearly independent computations and is compatible with parallel computation, which significantly re-

duces the computational time by parallel computation. In addition, an advantage of PA over MCMC methods is that the partition function in statistical mechanics, which is the normalization constant for the probability distribution, can be obtained as a by-product of the calculation. The partition function, which is called evidence in the context of Bayesian inference, is an important quantity that gives an indicator of model selection.

Furthermore, since the leave-one-out cross validation (LOOCV), which is one of the cross-validation methods, can be formulated by the reweighting method often used in statistical physics, its implementation is also carried out at the same time in PA. By systematically comparing the evidence and LOOCV, we developed a methodology for data analysis that integrates hyper-parameter estimation and model selection.

The proposed method has been implemented in linear regression models with noise. It has been pointed out that L_1 regularization-based methods such as LASSO lead to bias, and in order to avoid this, a direct method of analyzing sparsity as an L_0 regularization problem has been considered. However, the L_0 regularization problem is known to be NP hard, and no efficient algorithm is known. We successfully solved this problem in a realistic time using PA, and also succeeded in evaluating the magnitude of the noise by computing the evidence. This means that we have established a new data-analysis method for sparse modeling, including uncertainty evaluation. We believe that it can develop materials science through our sampling methods such as noise magnitude estimation and model selection, which are a step further than conventional Bayesian estimation usually attributed to optimization calculations.

Study on relaxations of fluctuation with the event-chain algorithm

Y. Ozeki and Y. Osada

Graduate School of Informatics and Engineering, The University of Electro-Communications

We investigate the applicability of the event chain algorithm [1, 2] to the relaxation of fluctuation for the nonequilibrium relaxation (NER) method, [3, 4] which has been an efficient numerical method to evaluate critical exponents. The event-chain algorithm has introduced for the Monte Carlo (MC) simulation with a multi-spin-flip algorithm, and shows estimation of the dynamical critical exponent $z \sim 1$ [1], which indicates a faster dynamics as compared with those with a single-spin-flip algorithm such as the the Metropolis one.

Previously, we investigated it for its applicability to the NER method and estimated the dynamical exponent z by means of the dynamical scaling analysis. The initial state of relaxation is prepared as an all-aligned state. As an example, we analyze the classical XY model in three dimensions; $\mathcal{H} = -J \sum_{\langle ij \rangle} \mathbf{S}_i \cdot \mathbf{S}_j$, where summation for $\langle ij \rangle$ is taken over all nearest-neighboring sites on a simple cubic lattice. Since the relaxation is much fast in the simulation with the event chain algorithm, we proposed the relaxation of the absolute value of the magnetization as the dynamical order parameter,

$$|m(t)| = \left\langle N^{-1} \left(\sum_i \mathbf{S}_i \right)^2 \right\rangle^{1/2} \quad (1)$$

and confirmed the efficiency of it.

Let us show the result of dynamical scaling analysis. The relaxation of the order parameter $|m(t)|$ are calculated for $2.182 \leq T \leq 2.222$ on a 300^3 simple cubic lattice up to an observation time of 100 MCSs. About 864 samples are taken for statistical averaging. The estimations are plotted in Fig. 1. Using the improved dynamical scaling analysis for the NER data [4], we analyze the dynamical scaling form,

$$|m(t, T)| = \tau^{-\lambda} Y[t/\tau], \quad (2)$$

where $\tau(T)$ is the relaxation time and λ is a dynamical critical exponent. The result is shown in Fig. 2 with $T_c = 2.202$ and $z = 1.47$.

The exponents estimated by dynamical scaling is used to deviate slightly because of corrections to scaling. To estimate the exponent more precisely,

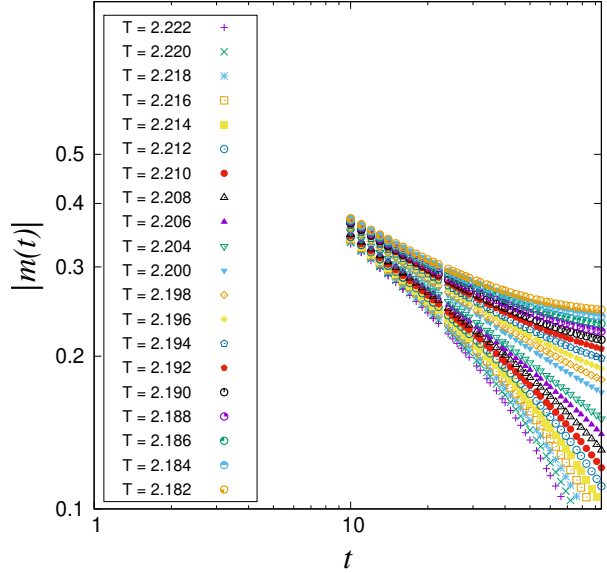


Figure 1: Relaxation of $|m(t)|$ for the 3D XY model in $2.182 \leq T \leq 2.222$ with the interval $\Delta T = 0.002$.

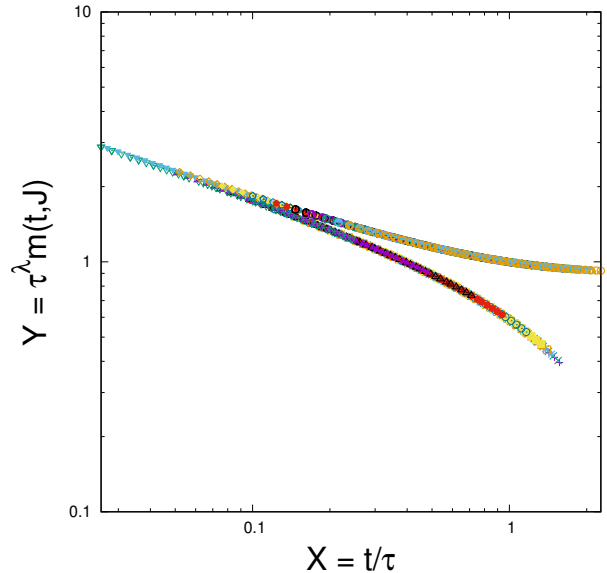


Figure 2: Scaling plot for the data in $2.182 \leq T \leq 2.222$ in Fig. 1

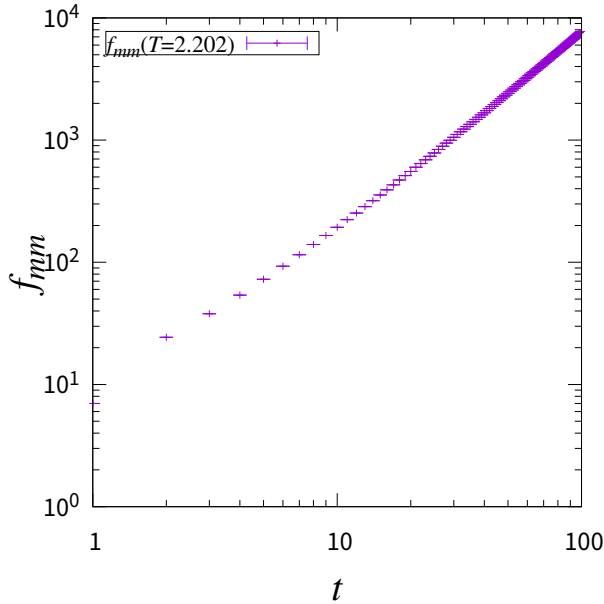


Figure 3: Relaxation of fluctuation f_{mm} calculated at $T = 2.202$

we analyze the relaxation of fluctuation,

$$f_{mm}(t) \equiv N \left[\frac{\langle |m(t)|^2 \rangle}{\langle |m(t)|^2 \rangle} - 1 \right], \quad (3)$$

at the transition temperature $T_c = 2.202$ estimated above. This function is expected to diverge as

$$f_{mm}(t) \sim t^{\lambda_{mm}}, \quad (4)$$

where $\lambda_{mm} = d/z$. Calculations are carried out on a 200^3 simple cubic lattice up to the observation time of 100 MCSs. About 645120 samples are taken for statistical averaging. The result is plotted in Fig. 3. We evaluate the numerical derivative

$$\lambda_{mm}(t) \equiv \frac{d \log f_{mm}(t)}{d \log t}, \quad (5)$$

and plot $d/\lambda_{mm}(t)$ in fig. 4, where the horizontal axis is modulated as $1/t^{0.704}$ to show a precise asymptotic value for $t \rightarrow \infty$. The result is $z = 1.67$, which is a little greater than the value obtained by the dynamical scaling. Consequently, the event-chain algorithm can be used in the NER analysis with an efficient relaxation performance, and would be applicable to various slowly relaxing problems such as frustrated and/or random systems.

References

- [1] Y. Nishikawa *et. al.*, *Phys. Rev.* **E92** 063306 (2015)

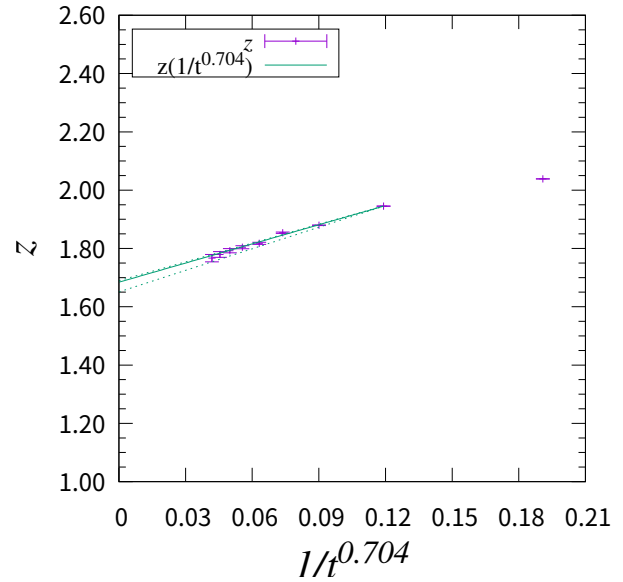


Figure 4: Critical exponent z is estimated as $t \rightarrow \infty$.

- [2] M. Michel *et. al.*, *Europhys. Lett.* **112** 20003 (2015)
- [3] Y. Ozeki and N. Ito, *J. Phys.: Math. Theor.* **40** R149 (2007).
- [4] Y. Echinaka and Y. Ozeki, *Phys. Rev.* **E94** 043312 (2016).
- [5] A. P. Aloysius and M. Harsenbusch, *Physica* **A201** 593 (1993)

Numerical study of bulk-edge correspondence and topological phases: From quantum to classical mechanics

Y. Hatsugai

*Department of Physics, University of Tsukuba
1-1-1 Tennodai, Tsukuba 305-8571, Ibaraki, Japan*

As for standard topological phenomena, non trivial topology of the bulk is reflected in the boundary physics which can be, in principle, easily accessible by experiments. This is the bulk-edge correspondence[1] that is widely used for various systems from quantum to classical ones. In this project, we have tried to extend the universal feature of the bulk-edge correspondence by using numerical methods. In this context, the adiabatic pump proposed by Thouless more than 30 years ago is quite special since the center of mass of the bulk, that has topological origin, is the physical observable although the edge physics is not directly observed by a realistic finite speed. Experimental realization the adiabatic limit including the gapless edge states is difficult although it is quite useful for clear understanding of topological character of the pumping[2]. We have extended the bulk-edge correspondence of the topological pumping for various systems with strong correlation[3, 4]. Another extension of the bulk-edge correspondence for the higher order topological phases is the bulk-corner correspondence. We demonstrated its validity for classical mechanical systems on a Kagome lattice[5]. We further applied numerical methods to various topological phenomena among quantum and classical ones. [6, 7, 8].

References

- [1] Y. Hatsugai, "Chern Number and Edge States in the Integer Quantum Hall effect", *Phys. Rev. Lett.* **71**, 3697 (1993).
- [2] Y. Hatsugai and T. Fukui, "Bulk-edge correspondence in topological pumping", *Phys. Rev. B* **94**, 041102(R) (2016).
- [3] Y. Kuno and Y. Hatsugai, "Interaction-induced topological charge pump", *Phys. Rev. Research* **2**, 042024 (2020)
- [4] K. Kudo and Y. Hatsugai, "Adiabatic heuristic principle on a torus and generalized Streda formula", *Phys. Rev. B* **102**, 125108 (2020). Also K. Kudo, Y. Kuno and Y. Hatsugai in preparation.
- [5] H. Wakao, T. Yoshida, H. Araki, T. Mizoguchi, and Y. Hatsugai, "Higher-order topological phases in a spring-mass model on a breathing kagome lattice", *Phys. Rev. B* **101**, 094107 (2020).
- [6] T. Mizoguchi, Y. Kuno, and Y. Hatsugai, "Detecting Bulk Topology of Quadrupolar Phase from Quench Dynamics", *Phys. Rev. Lett.* **126**, 016802 (2021).
- [7] T. Yoshida, K. Kudo, H. Katsura, and Y. Hatsugai, "Fate of fractional quantum Hall states in open quantum systems: Characterization of correlated topological states for the full Liouvillian", *Phys. Rev. Research* **2**, 033428 (2020).
- [8] T. Yoshida, T. Mizoguchi, and Y. Hatsugai, "Mirror skin effect and its electric circuit simulation", *Phys. Rev. Research* **2**, 022062(R) (2020).

Numerical study on low-energy states of quantum spin systems

Hiroki NAKANO

Graduate School of Material Science, University of Hyogo

In condensed matter physics, we often have to tackle many-body problems, in which it is difficult to estimate physical quantities precisely. Quantum spin systems are such typical cases. To examine the systems, under circumstances, numerical approaches have widely and effectively been employed in various studies. A lot of computational investigations have been carried out and gave us useful information of the target systems.

Within the field of quantum spin systems, three methods are effectively used. One is the numerical diagonalization method. The second is the quantum Monte Carlo (QMC) method. The third one is the density matrix renormalization group (DMRG) method. Each of the methods has advantages; at the same time, it also disadvantages. In the QMC simulations, large systems can be treated irrespective of the spatial dimensions of the systems although it is difficult to precisely evaluate physical quantities in frustrated systems due to the negative sign problem. When spatial dimension of a target system is one, on the other hand, the DMRG method is very useful irrespective of whether the target system includes frustration or not. For the cases when the spatial dimension is larger than one, however, this method is still under development. The numerical diagonalization method can be applied irrespective of the presence of frustrations and the spatial dimension. However, this method has a serious weak point that only very small system sizes can be treated. To overcome this disadvantage,

we developed a hybrid-type parallelized code of Lanczos diagonalization[1]. This Lanczos-diagonalization code enables us to treat various large systems that have not been previously treated yet within this method. We, thus, study various quantum spin systems by this method as a primary approach in this project.

In the project in 2020, we tackled the $S = 1/2$ Heisenberg antiferromagnet on the orthogonal-dimer lattice. This system was examined based on the calculations of 36- and 40-site systems of the same Lanczos diagonalization[2], which pointed out that the third characteristic ratio defined as J_2/J_1 appears between the edge of the exact-dimer phase and the edge of the Neel-ordered phase; here, J_1 is the amplitude of the exchange coupling on orthogonal-dimer bonds and J_2 is the amplitude of the exchange coupling forming the simple square lattice. In order to clarify whether or not the behavior showing the presence of the third characteristic ratio of J_2/J_1 survives when the system becomes larger, we additionally calculated the 44-site cluster of this system, which has not been treated before. As a result, our calculations for 44-site system show the behavior that is consistent with those for 40-site system. Our examination contributes to our deeper understandings of the quantum antiferromagnets with frustrations. Further investigations would clarify nontrivial effects of quantum nature and frustration.

References

- [1] H. Nakano and A. Terai: J. Phys. Soc. Jpn. **78** (2009) 014003.
- [2] H. Nakano and T. Sakai, J. Phys. Soc. Jpn. **87** (2018) 123702.

Thermal effects on quantum frustrated magnetisms

Tokuro SHIMOKAWA

*Theory of Quantum Matter Unit, Okinawa Institute of Science and Technology Graduate University
Onna-son, Okinawa 904-0412*

Quantum frustrated magnetism is well known as a source of exotic states of matter, but investigating the true nature, particularly at finite temperatures, is still a tough and challenging problem. In this fiscal year, we investigated both the ground state and finite-temperature properties of several two-dimensional frustrated magnetism by means of exact diagonalization (ED) and quantum typicality (QT) methods. We will here briefly report our numerical activities with the ISSP supercomputer.

1) $S=1/2$ breathing bilayer kagome (BBK) magnets for $\text{Ca}_{10}\text{Cr}_7\text{O}_{28}$ magnet

Motivated by recent experimental results on a new quantum spin liquid candidate, $\text{Ca}_{10}\text{Cr}_7\text{O}_{28}$, we investigated the ground state and finite- T properties of the $S=1/2$ BBK model. We developed a new ED code specialized for high fields [1], which enables us to treat much larger system sizes at most 2000 spin clusters and compute spin dynamics without any bias in our quantum Hamiltonian. We succeeded in reproducing bow-tie and ring-like features in quantum spin dynamics, which inelastic neutron scattering (INS) measurements reported as signatures of the quantum spin liquid state of this material. We also computed the temperature dependences of specific heat and equal-time spin structure factors by means of the QT method, and we found a realization of a spiral spin liquid state at moderate temperatures having a ring-like structure in equal-time spin structure factors. [2]

2) Signatures of finite- T phase transition in $S=1/2$ Shastry-Sutherland model

Recent experimental results under high pressures revealed the intermediate plaquette-singlet phase in $\text{SrCu}_2(\text{BO}_3)_2$ compound. In this intermediate phase, we naturally expect to have a spontaneous mirror symmetry breaking at a finite temperature; however, detecting the possible finite- T transition has been a challenging problem, such as in the traditional ED method because of the smallness of accessible system sizes. We used the quantum typicality (QT) method for this problem and succeeded in capturing some clear signatures of the finite- T phase transition. For example, the temperature dependence of the real-space spin-spin correlation is one of the valuable quantities to see the signatures: we could see two possible mirror symmetry broken correlation patterns at low temperatures depending on the random initial spin configurations used in QT method. We also discussed the relationship to the material $\text{SrCu}_2(\text{BO}_3)_2$. These results are published in Phys. Rev. B. [3]

References

- [1] H. Ueda, S. Yunoki, and T. Shimokawa, in preparation.
- [2] T. Shimokawa, R. Pohle, and N. Shannon, in preparation.
- [3] T. Shimokawa: Phys. Rev. B **103** (2021) 134419.

Global thermodynamic functions extended to nonequilibrium steady states

Naoko NAKAGAWA

*Department of Physics, Ibaraki University
2-1-1 Bunkyo, Mito, Ibaraki 310-8512*

We study spatially inhomogeneous systems, such as liquid-gas coexistence and multicomponent systems, from the viewpoint of global thermodynamics [1]. We conducted numerical research on the following two topics by utilizing the supercomputer at ISSP. In both topics, we performed molecular dynamics simulation using LAMMPS.

(1) Numerical experimental protocol to determine the standard entropy and free energy of two-component fluids:

The “standard” entropy or free energy plays a fundamental role to describe the thermodynamic properties of pure substances. This is also the case in mixtures to distinguish their variety and industrial applicability. We have developed a numerical protocol for determining the standard free energy of mixtures from thermodynamic measurements by using knowledge of fluctuating thermodynamics and information thermodynamics. The protocol is valid to numerical experiments, especially to molecular dynamics. In order to verify the validity of our protocol, we organized the molecular dynamics simulation taking a simple example on which we can make a theoretical prediction. We concluded the validity and the efficiency of our protocol as a method to determine the standard free energy, mixing entropy, solubility, and so on.

(2) Osmotic pressure in a binary mixture separated by a semipermeable membrane:

We have applied global thermodynamics to a binary mixture in thermal conduction, which

is separated by a semipermeable membrane. It predicts how the osmotic pressure changes from equilibrium. One of the point to be examined is whether the osmotic pressure is deviated from a conventional expectation, which corresponds to the balance of local chemical potential. To clarify this point, we start large-scale numerical experiments. The resources used were mainly the L9 CPU of System C (because LAMMPS has not been installed in the new System B). The simulation was run on 9 nodes in 360 parallel computation using MPI. This allowed us to perform long calculations on a system with up to 10^5 particles to measure the local and global thermodynamic quantities in the steady state with a sufficient relaxation time and a sufficiently large number of samples. We are now checking the effect of the finite system size.

References

- [1] N. Nakagawa and S.-i. Sasa: *J. Stat. Phys.* **177** (2019) 825.

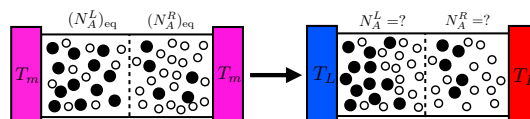


Figure 1: Configuration of the investigated system with two component fluid and a semipermeable membrane. The distribution of particles is modified by heat current.

Multiscale simulation of polymeric fluids and solids

Takahiro MURASHIMA

*Department of Physics, Graduate School of Science, Tohoku University,
6-3, Aramaki-aza-Aoba, Aoba-ku, Sendai, Miyagi 980-8578*

To develop multiscale simulation directly connecting macroscopic continuum system and microscopic molecular particle system, we need a suitable boundary condition for molecular dynamics simulation. For long years, extensional flows were difficult problems in molecular dynamics simulation. Recently, we have developed UEFEX algorithm [1] applicable for the Langevin thermostat. This new algorithm can solve the extensional flow

problems. In this algorithm, the flow frame and the simulation frame were separately treated. In the similar way, we have developed a QR-decomposition based deformation algorithm [2] and applied to a tensile deformation of polymeric solid. In this fiscal year, we extended this QR-decomposition based algorithm to be applicable for rotational flow, rotational shear flow, pure shear flow, and so on. Fig.1 shows the rotational shear flow.



Fig. 1: Snapshots of rotational shear flow. Non-symmetric deformation rate tensor applied. Simulation box (the flow frame) is rotating clockwise. Black frame represents “the MD frame”.

The rotational shear flow is typical in cavity flow and contraction and expansion flow. I would like to apply this technique to the ring-linear polymer blend [3], where the topological constraint of ring polymer causes unique phenomena; for example, the viscosity overshoot in a biaxial elongational flow.

References

- [1] T. Murashima, K. Hagita, T. Kawakatsu, J. Soc. Rheol. Jpn. 46 (2018) 207.
- [2] T. Murashima, S. Urata, S. Li, Euro. Phys. J. B, 92 (2019) 211.
- [3] T. Murashima, K. Hagita, T. Kawakatsu, arXiv:2102.02452.

Ground state and dynamical properties of the $J_1 J_2 K$ -Heisenberg model on the square lattice

Matthias GOHLKE, Tokuro SHIMOKAWA

*Theory of Quantum Matter Unit, Okinawa Institute of Science and Technology
1919-1 Tancha, Onna-son, Okinawa 904-0495*

In the absence of conventional magnetic order of spin-dipolar moments, ordering with higher-order moments like spin-quadrupoles may occur. Such spin-quadrupolar—or spin-nematic (SN)—order was found theoretically in spin-1 model with biquadratic spin-exchange [1].

Magnets with spin- $\frac{1}{2}$ degrees of freedom, however, can only exhibit a SN states if two spin- $\frac{1}{2}$ are combined into an effective spin-1 [2]. In fact, such SN states on bonds has theoretically been observed in frustrated ferromagnets on the square lattice with dominant ferromagnetic Heisenberg exchange, J_1 , antiferromagnetic next-nearest neighbor exchange, J_2 , and cyclic permutation, K . It was found that the condensation of a two-magnon bound state, at strong magnetic fields along the z -axis, can stabilize a phase with bond-nematic order [3].

Experimentally, the nature of such a ground state is intrinsically difficult to verify, due to the lack of probes that couple directly to the spin-quadrupole moments. Instead, it is necessary to examine the dynamics of a SN: A continuous symmetry for the director of a spin-quadrupole remains, that give rise to a gapless Goldstone mode [4, 5].

We started by studying the square-lattice frustrated J_1 - K model [2],

$$\begin{aligned} \mathcal{H} = & J_1 \sum_{\langle i,j \rangle} \mathbf{S} \cdot \mathbf{S} \\ & + K \sum_{(i,j,k,l)} \left(P_{ijkl} + P_{ijkl}^{-1} \right) + h_z \sum_i S_i^z, \end{aligned} \quad (1)$$

where J_1 represents dominant ferromagnetic

Heisenberg exchange between nearest neighbor spins, K the cyclic ring exchange around squares, and h_z the Zeeman coupling to a magnetic field along the z -axis.

Using iDMRG and the matrix product states (MPS) framework, we confirm the existence of the bond-nematic phase in an extended range of $K/|J_1|$ while being sandwiched between the fully-polarized phase at high fields and a long-range magnetically ordered phase at low fields. A recently developed exact diagonalization method near saturation [6], shows a good agreement with iDMRG on cylindrical geometries with circumference $L_{\text{circ}} \geq 6$ sites.

Given the ground state wave function as an MPS, dynamical properties can then be studied by applying a time-evolution unitary $U(dt)$ represented as a matrix product operator. In doing so, we observe the condensation of two-magnon bound state at the corresponding wave vector of the SN state. Within the SN phase, we observe a gapless mode with vanishing spectral weight in the $\mathbf{q} \rightarrow 0$ & $\omega \rightarrow 0$ limit as predicted by prior mean-field studies. We do, however, observe some relevant qualitative differences, whose origin we are currently investigating.

References

- [1] K. Harada and N. Kawashima, Phys. Rev. B **65** (2002) 052403.
- [2] A. Andreev and I. Grishchuk, Sov. Phys. JETP **60** (1984) 267.

- [3] N. Shannon, T. Momoi, and P. Sindzingre, *Phys. Rev. Lett.* **96** (2006) 027213.
- [4] R. Shindou, S. Yunoki, and T. Momoi, *Phys. Rev. B* **87**, (2013) 054429.
- [5] A. Smerald, H. T. Ueda, and N. Shannon, *Phys. Rev. B* **91** (2015) 174402.
- [6] H. Ueda, S. Yunoki, and T. Shimokawa, in preparation.

Development of entanglement optimization method

Kenji HARADA

Graduate School of Informatics, Kyoto University, Kyoto 606-8501, Japan

There are various interesting algorithms on tensor networks to calculate the free energy and critical properties of classical systems and the ground state of quantum systems. In these algorithms, we often need to control the entanglement structure in a tensor network. For example, we need to remove the short entanglement loop structure in grid tensor networks to calculate a critical fixed point tensor.

In this project, we try to optimize an entanglement structure in a local tensor network directly. In particular, we consider the development of a new optimization method for a branching operator[1]. To make a branching operator, we usually use the truncation optimization for a local tensor network. Instead, we directly reduce the entanglement after applying a branching operator. Combining automatic differentiation and manifold optimization techniques, we can construct an iteration method to reduce the entanglement by a branching operator.

Applying the new method to a tensor network representation of a Born machine[2, 3], we can directly transform a MPS into a MERA tensor network[4, 5]. In the case of the Born machine of the Ising model, we can construct a correct MERA tensor network from an exact MPS of the Born machine. In two-dimensional tensor networks, it is hard to transform the PEPS into a tree tensor network. We need to transform the PEPS into the MERA tensor network directly. It is also necessary to develop a similar optimization method of a branching operator for the two-dimensional network.

[1] K. Harada, “Entanglement branching operator,” *Phys. Rev. B* **97**,045124 (2018).

[2] Z.-Y. Han, J. Wang, H. Fan, L. Wang, and P. Zhang, “Unsupervised Generative Modeling Using Matrix Product States,” *Phys. Rev. X*, **8**, 031012 (2018).

[3] S. Cheng, L. Wang, T. Xiang, and P. Zhang, “Tree tensor networks for generative modeling,” *Phys. Rev. B*, **99**, 155131 (2019).

[4] G. Vidal, “Entanglement Renormalization,” *Phys. Rev. Lett.*, **99**, 220405 (2007).

[5] G. Vidal, “Algorithms for entanglement renormalization,” arXiv:0707.1454v1 (2007).

Kinetics of phase transition and polyamorphism

Kazuhiro Fuchizaki, Hiroki Naruta, and Katsumi Nakamura
Department of Physics, Ehime University, Matsuyama 790-8577

In FY2020, we mainly treated the structural variation during the amorphous–amorphous transition in SnI_4 . We conducted *in situ* synchrotron x-ray measurements along the isotherm at room temperature from 30 GPa down to 1.1 GPa, using a diamond anvil cell to obtain the structure factor required for the analysis. We also succeeded in applying an idea of nonequilibrium relaxation to machine learning (ML) for predicting the order-disorder transition temperature in a 2-dimensional (2D) Ising system. The last project was unscheduled at the outset. We exploited System B in the following scene.

Amorphous–amorphous transition in SnI_4 [1]

We decided to analyze the structure employing reverse Monte Carlo (RMC) simulation because it is much advantageous than a usual Fourier inversion in the following respect: we can extract 3D structural information, from which partial radial distribution functions are obtainable. Before conducting the RMC fit of the experimental structure factor $S(k)$, we had to determine the system’s density and initial configuration transferred to the fit as input. For this purpose, we prepared a system, which “mimics” the actual system at the measured thermodynamic conditions, using classical isothermal and isobaric molecular dynamics simulation for a system composed of 2744 rigid regular tetrahedral molecules confined in a cubic box with periodic boundary conditions. System B took care of this process.

We call the system, whose density is to be determined, a target system. Our model system [2] was known to capture the real system below 1 GPa. Hence, we first searched in a

trial-and-error manner thermodynamic conditions at which the model system “looks like” the real system, at least in the length scale k_m^{-1} , where k_m denotes the principal-peak position of $S(k)$. The conditions thus found were listed in Table 1 of Ref. [1]. The resultant model systems after equilibration were all metastable liquids.

Our method for density estimation from $S(k)$ presumes the existence of a reference state that has a similar structure on the length scale of k_m^{-1} . Let n_t be a trial number density. We redefine the system’s length by multiplying $n_t^{-1/3}$ and calculate the structure factor, $S_t(k)$, using the scaled length. If we denote the principal-peak position of $S_t(k)$ by k_t , we can define the difference, $\delta k = k_t - k_m$, as a function of n_t . The target’s number density, n , is then estimated by the condition, $\delta k / \delta n_t|_n = 0$. After finalizing the density, we resized the whole system uniformly so that not only the length of sides of the system but also the interatomic distances were updated. We transferred the configuration along with the density to the RMC program.

The RMC simulation (see Fig. 1 for an example) could reveal that the high-density amorphous (HDA) state is divided into two states: the high-pressure HDA state beyond 14 GPa containing isolated Sn atoms and the low-pressure HDA state below 14 GPa consisting of deformed molecules connected by metallic I_2 bonds. In the latter state, the molecular shape becomes C_{3v} -like just before the transition to the low-density amorphous (LDA) state, in which molecules recover the original T_d symmetry. This local symmetry change has been

detected on the liquid–liquid transition of SnI_4 , suggesting the strong coupling between the local symmetry and the global order parameter of density.

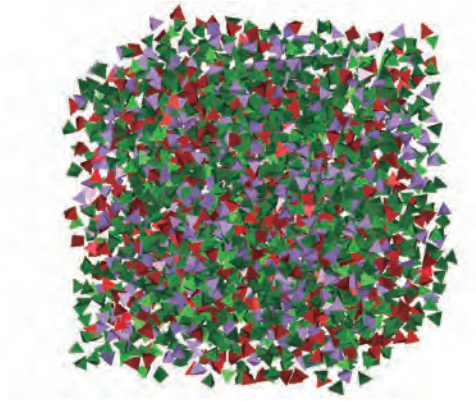


Figure 1: The RMC-simulation result obtained from $S(k)$ at 3.3 GPa, just before the transition to the LDA state on decompression, is visualized as an example. SnI_4 units (not necessarily molecules) are depicted in red, green, and purple when they are regularly tetrahedral shaped, severely deformed, and even dissociated, respectively.

Applying nonequilibrium-relaxation scheme to ML for detecting a phase transition [3]

There seems no need to explain the significance of applying the ML technique to problems across the various disciplines today. One example in physics problems is detecting the phase transition without any information about the “answers” *a priori*, as intelligibly illustrated for a 2D Ising model [4]. Tanaka and Tomiya identified that the weights, more strictly, their sum W_{sum} , in a convolutional neural network (CNN) can play a relevant order parameter [4]. The identification then readily prompted us to apply the idea of nonequilibrium relaxation [5] to the detection.

We employed the same CNN with one hidden layer besides the input and output layers. To investigate the learning processes in detail, we realized the CNN in-house. We used the same 2D Ising system on an $L \times L$ lattice with periodic boundary conditions imposed for the

examination, where $L = 32, 64, 128,$ and 256 . We used as training data the systems well equilibrated at the specified temperature. Here, the temperatures constituted the labels, which were one-hot encoded into the binary vector.

Initially, we set W_{sum} to zero, which corresponds to the completely “unlearned” state. W_{sum} soon evolved into one of the two states with learning, depending on the pattern’s temperature, leaving W_{sum} at the transition temperature T_c unlearned. We could thus identify T_c as the fixed point in the label space. Because W_{sum} with labels on both sides of the fixed point soon bifurcates with learning, a CNN with proper filters implemented can judge the location of a T_c at an early stage of learning. In this context, the existence of hidden layers is practically relevant to efficiency.

However, such a T_c irregularly depends on L ; T_c does not follow the relationship, $T_c(L) \sim L^{-1}$, expected from the finite-size scaling. The unusual L -dependence happened to make such an $L = 32$ system predict the transition temperature remarkably close to the exact one, and large systems used as training data do not necessarily bring about a better result for predicting T_c .

References

- [1] K. Fuchizaki, A. Ohmura, H. Naruta, and T. Nishioka, submitted to J. Phys.: Condens. Matter.
- [2] K. Fuchizaki and Y. Asano, J. Phys. Soc. Jpn. **84**, 064601 (2015).
- [3] K. Fuchizaki, K. Nakamura, and D. Hiroi, J. Phys. Soc. Jpn. **90** (2021), in press.
- [4] A. Tanaka and A. Tomiya, J. Phys. Soc. Jpn. **86**, 063001 (2017).
- [5] N. Ito, Physica A **192**, 604 (1993).

Investigation of the molecular origins of the mechanical and thermal properties of realistic bio-polymers using all-atomistic molecular dynamics

Okazaki Susumu

Department of Advanced Materials Science,

The University of Tokyo, Kashiwa-no-ha, Kashiwa, Chiba 277-8581

We have studied the impact fractures of amorphous glassy polymer materials using all-atomistic molecular dynamics (MD) simulations for the past few years [1, 2]. In the second half of the past year, we continued the pursuit of the molecular scale understanding of the yielding and the glass transition phenomena using the protocols employing large-scale parallel MD simulations and analyses established earlier, by utilizing the supercomputer resources at ISSP.

In the first half, we investigated the stress origins of the yielding process of the brittle material poly-(methyl methacrylate) (PMMA) using the stress decomposition method we developed previously, and found that 1) the brittle materials share the same stress origins as the ductile materials; 2) the dense and bulky sidechains of PMMA makes it a brittle material by lowering its flexibility and increasing the stress strength. [3]

In the second half, we thoroughly studied the glass transition phenomenon by analyzing the MD trajectories, and realized that various degrees of freedom, including the translation and rotation of polymer chains, the dihedral angle rotation, and some angle bending, defreeze

at different temperatures, within the observation time of current MD simulation time scale. This causes the volume, the order parameter usually used to define glass transition, to show a broad glass transition over decades of kelvins. The same phenomenon is believed to occur in experimental conditions, although the impact of the faster degrees of freedom are less.

References

- [1] K. Fujimoto, Z. Tang, W. Shinoda, S. Okazaki, All-atom molecular dynamics study of impact fracture of glassy polymers. I: Molecular mechanism of brittleness of pmma and ductility of pc, *Polymer* 178(12) (2019) 121570.
- [2] Z. Tang, K. Fujimoto, S. Okazaki, All-atom molecular dynamics study of impact fracture of glassy polymers. II: Microscopic origins of stresses in elasticity, yielding, and strain hardening, *Polymer* 207(20) (2020) 122908.
- [3] Z. Tang, K. Fujimoto, S. Okazaki, A comparison of the brittle PMMA with the ductile PC on the elasticity and yielding from a molecular dynamics perspective, *Polymer* (2021), in press.

Global Optimization of Tensor Renormalization Group using the Corner Transfer Matrix

Satoshi MORITA

*Institute for Solid State Physics, University of Tokyo
Kashiwa-no-ha, Kashiwa, Chiba 277-8581*

Tensor network methods attract much attention as powerful tools for computing strongly correlated many-body problems. The tensor renormalization group method (TRG) [1] and the higher-order TRG (HOTRG) [2] provide a way to calculate coarse-grained tensor based on the singular value decomposition. Both the methods do information compression by solving local optimization problems. Approximations in these methods are locally optimal but not so for contraction of the whole tensor network. The second renormalization group method (SRG) [3] and the higher-order SRG method (HOSRG) [2] introduce global optimization of tensor renormalization group. Although these methods drastically improve accuracy, calculation of the environment tensor requires performing the forward-backward iterations.

To resolve this problem, we propose another approximation for global optimization [5]. We replace the environment tensor with the corner transfer matrices (CTM) and the edge tensors, which can be updated by using the CTM renormalization group (CTMRG) [4]. Moreover, we introduce additional decomposition, which reduces computational cost of tensor contraction for the coarse-grained tensor. The computational time of our algorithm (CTM-TRG) in two dimensions scales as $O(\chi^6)$ against the bond dimension χ while the HOTRG and HOSRG have $O(\chi^7)$ scaling.

We perform benchmark calculations in the Ising model on the square lattice and show

that the time-to-solution of the proposed algorithm is faster than that of other methods. As shown in Fig. 1, our proposed method shows better accuracy than HOTRG and compatible to HOSRG.

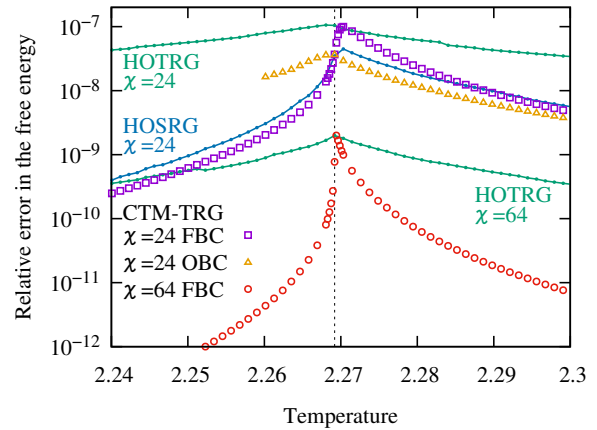


Figure 1: Relative errors in the free energy measured in the Ising model on the square lattice.

References

- [1] M. Levin and C. P. Nave, Phys. Rev. Lett. **99**, 120601 (2007).
- [2] Z. Y. Xie, J. Chen, M. P. Qin, J. W. Zhu, L. P. Yang, and T. Xiang, Phys. Rev. B **86**, 045139 (2012).
- [3] Z. Y. Xie, H. C. Jiang, Q. N. Chen, Z. Y. Weng, and T. Xiang, Phys. Rev. Lett. **103**, 160601 (2009).
- [4] T. Nishino and K. Okunishi, J. Phys. Soc. Jpn. **65**, 891 (1996).
- [5] S. Morita and N. Kawashima: Phys. Rev. B **103**, 045131 (2021).

Dynamics of Phonon Entanglement Creation between Remote Electron-phonon Systems

Kunio ISHIDA

School of Engineering and Center for Optics Research and Education

Utsunomiya University, Yoto, Utsunomiya, Tochigi 321-8585

Coherent control of quantum mechanical states is important to realize various states of quantum materials. In particular, quantum entanglement is a measure for quantum mechanical features, and thus we have focused on its control method by photoirradiation[1-3]. In the present study, we study the dynamics of entanglement generation between remote systems by irradiation of a quantized light pulse by employing a model of coupled electron-phonon-photon systems described by[2]

$$\mathcal{H} = \sum_{i=1}^3 \Omega_i c_i^\dagger c_i + \sum_{j=1}^2 \left[\omega a_j^\dagger a_j + \{ \mu (a_j^\dagger + a_j) + \varepsilon \} \frac{\sigma_z^{j+1}}{2} + \{ \sum_{i=1}^3 v_i (c_i^\dagger + c_i) + \lambda \} \sigma_x^j \right].$$

Solving the time-dependent Schrödinger equation by numerical calculation on the System B at ISSP, we found that the quantum mutual information for phonons reveals the dynamics of phonon entanglement generation[4].

In order to investigate the dynamical behavior of phonon states in both material systems, we performed a Schmidt decomposition on the electron-phonon-photon states in which the entire system is divided into the phonons and the

electrons and photons. In this case, the wavefunction $|\Phi\rangle$ is described by

$$|\Phi\rangle = \sum_n \sqrt{\lambda_n} |\eta_n\rangle |\theta_n\rangle,$$

where $|\eta_n\rangle$ and $|\theta_n\rangle$ denote the phonon states and the electron-photon states, respectively.

We calculated the dynamical behavior of λ_n and the entanglement entropy between phonons in $|\eta_n\rangle$ as functions of time, and found that the entanglement in the singular vector $|\eta_0\rangle$ for the largest singular value λ_0 is weak, while $|\eta_1\rangle$ and $|\eta_2\rangle$ for the second and the third largest singular values λ_1 and λ_2 are strongly entangled. The phonon entanglement is generated as λ_1 and λ_2 increase, i.e., the entanglement generation process corresponds to the conversion of the phonon states from a pure decomposable state to a mixed state of entangled states.

References

- [1] K. C. Lee, et al., Science **334**, 1253(2011).
- [2] F. Borjans, et al., Nature **577**, 195 (2020).
- [3] K. Ishida, Eur. Phys. J. **D73**, 117 (2019).
- [4] K. Ishida and H. Matsueda, arXiv: 2005.14615.

A Theoretical Study for Thermal Unfolding of Proteins with Quite Similar Native Structure

Takashi YOSHIDOME

*Department of Applied Physics, Graduate School of Engineering, Tohoku University,
6-6-05, Aoba, Aramaki, Aoba-ku, Sendai 980-8579*

Recently, drug design for inhibiting the folding of proteins has begun. This indicates the importance of the elucidation of the molecular mechanism of folding process of proteins for drug design.

In the present study, we focused on the two proteins that have quite similar native structures but different structures at the transition state [1]. They are goat alpha-lactalbumin and human lysozyme, respectively. To elucidate the molecular mechanism of the difference in the transition state structures among goat alpha-lactalbumin and human lysozyme, we performed molecular dynamics (MD) simulations for their unfolding processes at 400 K. We successfully reproduced the experimental results for the transition state structures. By carefully analyzing the simulation results, we elucidated that the difference in the transition state structures arose from the existence of the Ca^{2+} ion in the native structure of the goat alpha-lactalbumin, and

from difference in the length of the secondary structures among the two proteins.

The calculations were performed using the F4cpu and L4cpu in the system B, and L4cpu in the system C. We used Gromacs program suite [2] for the MD simulations. CHARMM22 force field [3] and TIP3P model [4] were used for the proteins and ions and for the water molecule, respectively.

References

- [1] T. Oroguchi, M. Ikeguchi, M. Ota, K. Kuwajima, and A. Kidera: *J. Mol. Biol.* **371** (2007) 1354.
- [2] H. J. C. Berendsen, D. Van der Spoel, R. van Drunen: *Comput. Phys. Commu.* **91** (1995) 43 (1995).
- [3] A. D. MacKerell, Jr. *et al.*: *J. Phys. Chem. B*, **102** (1998) 3586.
- [4] W. L. Jorgensen, J. Chandrasekhar, and J. D. Madura: *J. Chem. Phys.* **79** (1983) 926.

A Method for Analyzing Protein Dynamics: A Hybrid of Cryo-Electron Microscopy Experiment and Molecular Simulation

Takashi YOSHIDOME

*Department of Applied Physics, Graduate School of Engineering, Tohoku University,
6-6-05, Aoba, Aramaki, Aoba-ku, Sendai 980-8579*

Cryo-electron (Cryo-EM) microscopy is one of the methods for analyzing the three-dimensional structures of biomolecules like proteins. In this method, the three-dimensional electron density map of a protein is reconstructed using a lot of two-dimensional electron density maps of the protein projected from several projection angles. To reconstruct the three-dimensional electron density map, the projection angle for each map is necessary to estimate. A method is the “common-line method” [1], but verification method for the estimation using the common-line method has been lacking.

In the present study, we investigated whether generative topographic mapping (GTM) method [2] can be used for an estimating method. The method enables us to estimate the function describing the two-dimensional electron density maps as the function of the projection angle. Thus, the estimation of the projection angle can be possible with the GTM method. To demonstrate the possibility of the estimation, simulations for

cryo-EM microscopy experiments were performed. In computing the maps, the protein was rotated by assigning the polar coordinates $z=(\theta, \phi)$ as follows: the variable θ was fixed to 0° ; and the variable ϕ was randomly assigned in the range of $0^\circ \leq \phi \leq 360^\circ$. It was found that estimating the projection angle for each projection image was successful using the GTM method. In future, our method will be improved in order to apply to actual cryo-electron microscopy experimental data.

The calculations were performed using the F4cpu and L4cpu in the system B, and L4cpu in the system C. We used our custom-made programs for the calculations. The program of the GTM method was implemented using the Python3 program language.

References

- [1] S. J. Ludtke, P. R. Baldwin, and W. Chiu: *J. Struct. Biol.* **128** (1999) 82.
- [2] C. M. Bishop, M. Svensén and C. K. I. Williams: *Neural Comput.* **10** (1998) 215.

Large-Scale Metadynamics Simulations for Water and Aqueous Solutions

Hiroki NADA

*National Institute of Advanced Industrial Science and Technology (AIST),
16-1 Onogawa, Tsukuba, Ibaraki 305-8569*

Phase transitions in water and aqueous solutions, such as crystallization and amorphous formation, have been studied in fields of physics and chemistry from long ago. Nevertheless, there still exist a lot of unresolved issues concerning phase transitions of water and aqueous solutions. For example, some of metastable phase transitions that are postulated to occur in water at a large supercooling, such as liquid-liquid phase separation (LLPS), have not yet been demonstrated.

Molecular dynamics (MD) simulations have often been used to study the structure of water at a large supercooling. However, evidence for the occurrence of LLPS can hardly be obtained by standard MD simulations.

In this study, a metadynamics (MTD) method was introduced to search for metastable phases of water at a large supercooling. An MD simulation in which the MTD method was implemented (MTD-MD simulation) was performed for a liquid water phase

consisting of 2880 water molecules using ISSP system C with high efficiency. Following a previous study [1], two discrete oxygen-oxygen radial distribution functions represented by Gaussian window functions were used as collective variables.

A free energy landscape obtained by the MTD-MD simulation for the TIP4P/Ice model at 233 K indicated two local minima. One of the minima corresponded to a low-density water phase, and the other corresponded to a high-density water phase. The high density water phase had a structure resembling the structure of high-density ice VII. At present, it is difficult to judge whether the observed two different water phases corresponded to water phases formed by the postulated LLPS of supercooled water. More detailed studies are needed to elucidate it in the future.

References

[1] H. Nada: *Sci. Rep.* **10** (2020) 4708

Metadynamics Simulation Analysis of Various Cluster Structures Appearing in Calcium Carbonate Supersaturated Solution

Hiroki NADA

National Institute of Advanced Industrial Science and Technology (AIST),

16-1 Onogawa, Tsukuba, Ibaraki 305-8569

Terrestrial water on the Earth contains mineral components, such as calcium carbonate (CaCO_3), with a high concentration and, hence, the formation of CaCO_3 crystals occurs ubiquitously. Industrially, the control of CaCO_3 crystal nucleation is crucial in connection with issues concerning the formation of scales, causing blockage of drainage pipes and reduction of thermal efficiency of boilers. However, the control of it is quite difficult. This is because the mechanism of CaCO_3 crystal formation from a supersaturated solution still has remained unclear.

Atomistic simulations, such as molecular dynamics (MD) simulations, are helpful to elucidate the structure and thermodynamic stability of precursors. However, the timescale of phenomenon that can be analyzed by an MD simulation is normally on the order of microsecond or shorter. This timescale is too short to pursue all possible precursor

structures that may stably appear in a solution.

In this study, a metadynamics (MTD) method was introduced to overcome the timescale problem of MD simulation [1]. An MD simulation in which the MTD method was implemented (MTD-MD simulation) was performed for a supersaturated CaCO_3 aqueous solution. The simulation was performed efficiently by parallel computing with multiple nodes of ISSP system B.

A free energy landscape (FEL) obtained with the MTD-MD simulation indicated stable and metastable aggregates formed in the solution, each of which correspond to a local minimum on the FEL). The results are helpful to consider the mechanism of CaCO_3 crystal nucleation via precursors.

References

- [1] A. Laio and M. Parrinello: Proc. Natl. Acad. Sci. USA **99** (2002) 12562.

Transport properties of multiple- \mathbf{q} states in frustrated magnets

Kazushi AOYAMA

*Department of Earth and Space Science, Graduate School of Science, Osaka University
Machikaneyama-cho, Toyonaka-shi, Osaka 560-0043*

Transport phenomena in magnetic systems reflect dynamical properties of interacting spins, such as magnetic excitations and fluctuations. In this work, we theoretically investigate transport properties of two-dimensional antiferromagnetic insulators, putting emphasis on how nature of spin textures characterized by more than one ordering wave vectors \mathbf{Q} 's (multiple- \mathbf{Q} states) is reflected in spin transport. In the J_1 - J_3 classical Heisenberg model on the triangular lattice in a magnetic field, the Hamiltonian is given by

$$\mathcal{H} = \frac{1}{2} \sum_{i,j} J_{ij} \mathbf{S}_i \cdot \mathbf{S}_j - H \sum_i S_i^z \quad (1)$$

with $J_{ij} = J_1 \delta_{j \in N1(i)} + J_3 \delta_{j \in N3(i)}$, where $Nn(i)$ denotes the n th nearest neighbor sites of site i . For ferromagnetic J_1 and antiferromagnetic J_3 , it was shown by Okubo, Chung, and Kawamura [1] that single- \mathbf{Q} , double- \mathbf{Q} , and triple- \mathbf{Q} states are stabilized in the low, middle, and high field regions, respectively. In particular, the triple- \mathbf{Q} state is known to be the skyrmion lattice phase, and its higher-temperature region is another phase, the so-called Z phase, in which there are randomly distributed domains of the skyrmion and antiskyrmion lattices.

The spin current and the associated spin conductivity $\sigma_{\mu\nu}^s$ are respectively given by

$$\begin{aligned} \mathbf{J}_s^z(t) &= -\frac{1}{2} \sum_{i,j} J_{ij} \mathbf{r}_{ij} (\mathbf{S}_i \times \mathbf{S}_j)^z, \\ \sigma_{\mu\nu}^s &= \frac{1}{TL^2} \int_0^\infty dt \langle J_{s,\nu}^z(0) J_{s,\mu}^z(t) \rangle, \end{aligned} \quad (2)$$

where \mathbf{r}_{ij} and L denote a vector connecting two

sites i and j and the linear system size, respectively. We numerically integrate the semiclassical equation of motion with initial equilibrium spin configurations generated by Monte Carlo simulations and calculate the time correlations $\langle J_{s,\nu}^z(0) J_{s,\mu}^z(t) \rangle$ at each time step [2, 3].

It is found that the longitudinal spin-current conductivity σ_{xx}^s is significantly enhanced at the transition temperature between the triple- \mathbf{Q} and Z phases, whereas at the higher-temperature transition between the Z and paramagnetic phases, such an anomalous behavior is not obtained. This enhancement of σ_{xx}^s is quite similar to the divergent behavior of σ_{xx}^s at the Kosterlitz-Thouless-type topological transition [2, 3] in which long-lifetime vortex excitations play a crucial role. In the present case, the topological object of the skyrmion may be relevant to the spin transport, but further analysis is necessary to understand the origin of the significant enhancement of the spin-current conductivity at the transition into the skyrmion lattice phase.

References

- [1] T. Okubo, S. Chung, and H. Kawamura, Phys. Rev. Lett. **108**, 017206 (2012).
- [2] K. Aoyama and H. Kawamura, Phys. Rev. B **100**, 144416 (2019).
- [3] K. Aoyama and H. Kawamura, Phys. Rev. Lett. **124**, 047202 (2020).

1/N bias of the hump of Binder parameter for Potts Model

Hiroshi WATANABE

*Department of Applied Physics and Physico-Informatics, Keio University
Yokohama, Kanagawa 223-8522, Japan*

The Binder parameter has been widely used to analyze critical phenomena [1]. Since the parameter is the dimensionless, the parameters for different system sizes are collapsed into a single curve by scaling only horizontal axis. The Binder parameter is usually a monotonic function, but it sometimes peculiar behavior. A typical example of this is the Potts model. The Binder parameter of the Potts model is non-monotonic function and exhibits a hump near the criticality. Since the hump has the system-size dependence, the Binder parameter of Potts model cannot be collapsed into a single curve by scaling only horizontal axis. The humps become larger as the system size increases and these humps interfere with the finite-size scaling analysis especially for the high-temperature side of the critical point. We also found that the peak value of the hump strongly depends on the MCs as well as the system size. In order to identify the origin of the hump, we study the Binder parameter of $Q = 3$ Potts model. We found that the Binder parameter can be decomposed into a high- and a low-temperature components, and that the humps originate from the low-temperature one. The system size and MCs dependence of the peak value of the low-temperature component of the Binder parameter U_{low} is shown in Fig. 1. One can see that the MCs dependence becomes large as the system size increases. These MCs dependence are found to be almost independent of the relaxation time. The MCs dependence originate

from the strong $1/N$ bias of the Binder parameter as it is a function of the expected value. Therefore, this bias can be removed by the jackknife resampling method. However, since the $1/N$ bias is removed and the N -infinity limit still exhibit system-size-dependence, the finite size scaling function appears to be system size dependent. The size-dependence of the peak position is stronger for larger values of Q , and the peak value is expected to be infinite at N infinity for systems involving the first-order transition. The existence of the universal finite-size scaling function in the limit of infinite system size for systems involving the continuous transitions is still non-trivial, and therefore, the further study is required.

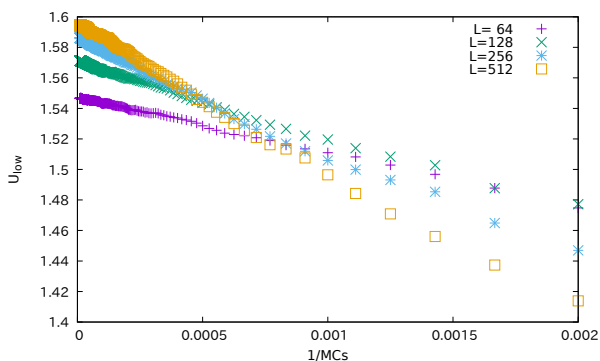


Figure 1: The system size and MCs dependence of the peak value.

References

- [1] K. Binder, Z. Phys. B Cond. Matt. , vol. 43, pp. 119-140 (1981).

Magnetism in the Multiple-Spin Exchange Model on the Honeycomb Lattice

Chitoshi YASUDA

*Department of Physics and Earth Sciences, Faculty of Science,
University of the Ryukyus, Okinawa 903-0213, Japan*

^3He atoms adsorbed on graphite form the commensurate solid layer regarded as the spin-1/2 quantum spin system on a triangular lattice at a certain density of ^3He . There are not only an exchange of ^3He atoms between two neighbor atoms but also that among three or more neighbor atoms. In relation to the solid ^3He , the multiple-spin exchange (MSE) model on the triangular lattice has been extensively studied. Ground states and thermodynamic properties of the model have been investigated using various methods [1,2,3]. In particular, the model has attracted attention owing to the existence of novel states such as the quantum spin liquid and the spin-nematic state, and owing to the effects of fluctuations on ordered phases with chirality. Recently, a new quantum spin liquid is experimentally observed in the solid ^3He layer. This layer is a monolayer ^3He adsorbed on graphite preplated with atomic layers of deuterium hydride. At low density of ^3He , it was suggested that there exists the quantum spin liquid with novel dependences of the heat capacity and the magnetic susceptibility on temperature. The details of this experimental work are not yet clear, however, it is suggested that the solid ^3He layer forms a honeycomb lattice.

In this project, we research the classical MSE model with the two-spin and six-body ring exchange interactions on the honeycomb lattice using numerical methods. The ground state is investigated using the conjugate gradient method. In this method, we need to prepare many random spin states as the initial states because of avoidance of the trap

to a metastable state. When the external magnetic field is zero, the ground state in the region where the contribution of the six-body exchange interaction is small becomes an antiferromagnetic state. This is the same ground state as the antiferromagnetic Heisenberg model on the honeycomb lattice. On the other hand, in the region where the contribution of the six-body exchange interaction is large, the eight-sublattice structure with a nearest-neighbor correlation function and a finite sublattice scalar chirality is stabilized as the ground state. When an external magnetic field is applied, the antiferromagnetic state becomes the canted state at very small fields, while the eight-sublattice structure can be maintained up to a certain finite field. When the applied magnetic field is increased, the eight-sublattice structure changes to the large sublattice structure, the four-sublattice structure, and the canted state, sequentially.

In this project, we also research thermodynamic properties of the classical MSE model using the Monte Carlo simulation with the exchange Monte Carlo method. We confirm its usefulness in the classical MSE model on the honeycomb lattice.

References

- [1] C. Yasuda, D. Kinouchi, K. Kubo: J. Phys. Soc. Jpn. **75** (2006) 104705.
- [2] C. Yasuda, Y. Uchihira, S. Taira, K. Kubo: J. Phys. Soc. Jpn. **87** (2018) 104704.
- [3] S. Taira, C. Yasuda, T. Momoi, K. Kubo: J. Phys. Soc. Jpn. **88** (2019) 014701.

Microwave transmission through a Josephson junction array

Tsuyoshi YAMAMOTO

*Institute for Solid State Physics, University of Tokyo
Kashiwa-no-ha, Kashiwa, Chiba 277-8581*

Recent technological development enables us to perform quantum simulation using artificial quantum systems. Its use for solving quantum many-body problems is one of hot topics in condensed matter physics. The superconducting circuits are one of promising platforms for such an attempt. However, background random charge in superconducting circuits hinders a “good” simulation. Our study facilitates the opposite view. Namely, randomness in a circuit provides to simulate quantum disordered systems [1].

In one-dimensional systems, localization occurs no matter how the disorder is weak. While disorder in the one-dimension system with long-range interactions induces a transition into an insulating phase, its properties is known little. In this study [2], we show microwave transmission through a Josephson junction array which represents one of the simplest one-dimension disordered systems with the Coulomb interaction.

A one-dimensional nature of the system allows for the most comprehensive analytical and numerical approaches. We find signatures of the insulating modes in the microwave transmission for a wide frequency range. At high frequencies, the high accurate numerics reveals that the localization property affects the microwave transmission, which has been missed in the previous work [3], by the detailed comparison with the analytics (Fig. 1). At low frequencies, by performing the parallel computation with respect to configurations to take a

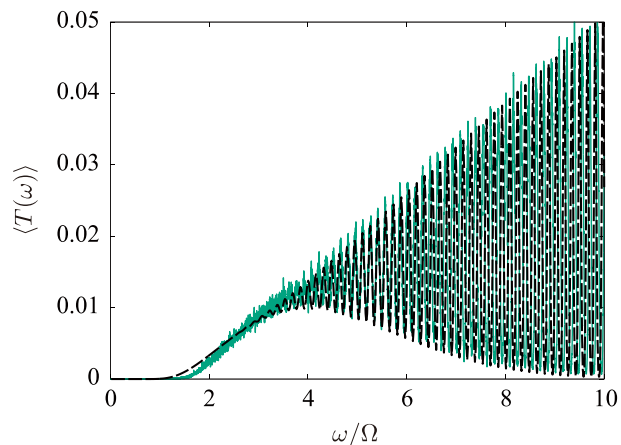


Figure 1: The frequency dependence of the transmission. The green line is the numerics and the black dashed line is the analytics.

disorder average, we gather several non-trivial pieces of information about statistics of the transmission.

The versatility of the design of Josephson-junction arrays motivates their further development for quantum simulation.

References

- [1] R. Kuzmin *et al.*, Nat. Phys. **15**, 930 (2019).
- [2] T. Yamamoto, L. I. Glazman, and M. Houzet, Phys. Rev. B **103**, 224211 (2021).
- [3] M. Houzet and L. I. Glazman, Phys. Rev. Lett. **122**, 237701 (2019).

Molecular dynamics simulation of liquid BaTiO₃

T. Hashimoto

*National Institute of Advanced Industrial Science and Technology (AIST),
Tsukuba Central 2, 1-1-1 Umezono, Tsukuba, Ibaraki 305-8568, Japan*

The structure of oxides in a liquid state at high temperature is being studied by the containerless method using a floating furnace. The field strength is expressed as $F = Z_M/(r_{MO} - r_O)^2$, where Z_M , r_{MO} , and r_O are the cation charge, the bond length of the cation and oxygen, and the ionic radius of oxygen. In SiO₂, which has a large F , the coordination number of oxygen around Si, whether solid or liquid, is 4, but in ZrO₂, Y₂O₃, etc., where F is small, the coordination number of oxygen around the cation drops significantly in the case of liquids[1]. Ti has an F value in the middle of them, but in the case of BaTi₂O₅, it has been reported that n_{TiO} drops significantly from the crystalline case to the liquid case[2]. Furthermore, it has been reported that the temperature dependence of r_{TiO} and n_{TiO} is $\partial r_{TiO}/\partial T < 0$ and $\partial n_{TiO}/\partial T < 0$. In the case of BaTiO₃, it was reported by X-ray scattering and neutron scattering by ⁴⁶Ti-rich and ⁴⁸Ti-rich samples that n_{TiO} is reduced from 6 for crystals to about 4.4 for liquids at 2073 K[4]. However, the temperature dependences of r_{TiO} and n_{TiO} are not known. In addition, the validity of the partial radial distribution function obtained by the empirical potential structure refinement (EPSR) method using experimental data has not been fully investigated. We calculated the structure of liquid BaTiO₃ by first-principles molecular dynamics simulations.

The calculations were performed using the plane wave pseudopotential method (QUANTUM-ESPRESSO), ultrasoft pseudopotential (GBRV), and GGA (PBE). The density data from Paradis *et al.*[4] was ex-

trapolated to the high temperature side and low temperature side. We calculated at 3500, 3000, 2500, 2000, 1500, 900 K using 135 atoms, using the (N, V, T) ensemble and the velocity scaling method.

The partial radial distribution functions of the liquid BaTiO₃ at 2000 K obtained by this study[5] were compared with those by the EPSR method at 2073 K[3]. The Ti-O results were in good agreement with each other, but Ba-Ba and Ti-Ti results were inconsistent. The reason for this is that the pair weighting factor contained in $S(Q)$ is small for both neutron scattering and X-ray scattering, especially for Ti-Ti, so there is a possibility that the interatomic interaction cannot be obtained correctly by the EPSR method. However, r_{TiO} and n_{TiO} were in good agreement with the experiment. Liquid BaTiO₃ had the same temperature dependence of r_{TiO} and n_{TiO} as liquid BaTi₂O₅.

- [1] L. Skinner *et al.*, Phys. Rev. Lett. **112**, 157801 (2014).
- [2] O. L. G. Alderman *et al.*, J. Phys. Chem. C **120**, 26974 (2016).
- [3] O. L. G. Alderman *et al.*, J. Phys.: Condens. Matter **31**, 20LT01 (2019).
- [4] P.-F. Paradis *et al.*, Appl. Phys. A **79**, 1965 (2004).
- [5] T. Hashimoto *et al.*, J. Phys. Soc. Jpn **90**, 044604 (2021).

Tensor-Network Renormalization Study of Finite-Size Conformal Spectrum

Atsushi Ueda and Masaki Oshikawa
Institute for Solid State Physics, University of Tokyo
Kashiwa-no-ha, Kashiwa, Chiba 277-8581

April 30, 2021

We have studied the finite-size effects of classical 2D systems, using Tensor Network Renormalization (TNR). Based on the finite-size scaling theory of conformal field theory (CFT) [1], we demonstrated that it is possible to reconstruct an effective quantum Hamiltonian from the spectrum of the renormalized tensors. Tracking the effective Hamiltonian at each scale allows to numerically construct the renormalization group (RG) flow. We performed it for the classical Ising and XY model as concrete examples, as shown in Figs. 1 and 2.

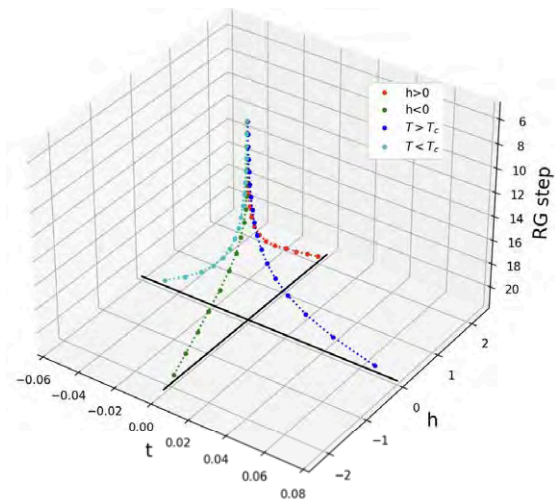


Figure 1: The numerically computed RG flow of the Ising model. t and h denote the deviations from the fixed point, corresponding to the reduced temperature $T - T_c$ and the magnetic field. The RG flows away from the fixed point induced by the relevant perturbations t and h are visualized.

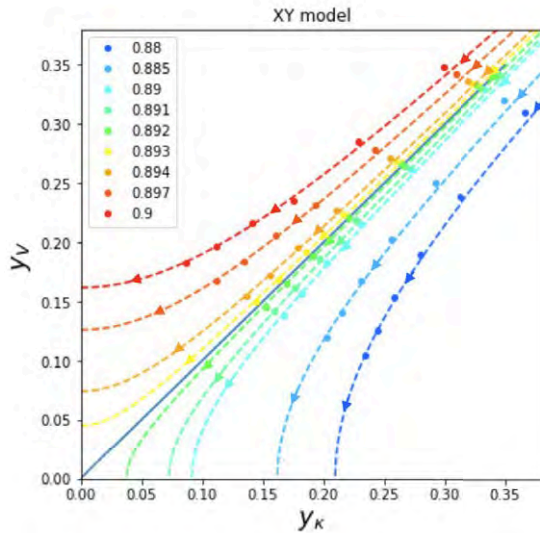


Figure 2: The numerically computed RG flow of the XY model. y_K and y_V are the perturbations corresponding to the spin-wave stiffness and the vortex fugacity, respectively. Our numerical construction gives a quantitative verification of the celebrated Kosterlitz RG flow [2].

Throughout the study above, we also investigated the effect of the finite bond cutoff, which had been often overlooked previously. We showed that there emerges an effective correlation length $\xi_D = D^\kappa$ that is observed for Matrix Product State(MPS) [3], by mapping renormalized tensors to a reduced density matrix. As the exponent κ becomes smaller when the central charge c is large, the focus of our study ($c = 2$) turns out to call for a massive calculation. Thus, we are in attempt to implement a parallel computation of TNR with the supercomputer. More details of our study will be reported elsewhere [4].

References

- [1] J. L. Cardy, *Conformal invariance and universality in finite-size scaling*, Journal of Physics A: Mathematical and General 17, L385 (1984).
- [2] J. M. Kosterlitz, *The critical properties of the two-dimensional xy model*, Journal

of Physics C: Solid State Physics 7, 1046 (1974).

- [3] Frank Pollmann, Subroto Mukerjee, Ari M Turner, and Joel E Moore, *Theory of finite-entanglement scaling at one-dimensional quantum critical points*, Physical Review Letters, 102(25):255701, (2009).
- [4] A. Ueda and M. Oshikawa, in preparation.

Magnetic field dependence of the thermal Hall effect based on the augmented quasiclassical equations

Takafumi KITA

*Department of Physics, Hokkaido University
Sapporo, 060-0810*

Charging of vortices in the equilibrium superconducting state was studied before calculating linear responses such as the thermal Hall effect. The results are reported below.

Vortices in type-II superconductors have not only a single magnetic flux quantum but also accumulated charge. It is known that the vortex-core charging is caused by three forces: (i) the Lorentz force [1], (ii) pair-potential-gradient (PPG) force [2], and (iii) the pressure difference arising from the slope in the density of states (SDOS) [3]. Recently, augmented quasiclassical (AQC) equations with these forces were derived by incorporating the next-to-leading-order contributions in the expansion of the Gor'kov equations in terms of the quasiclassical parameter $\delta \equiv 1/k_F\xi_0$ [4], where k_F is the Fermi wavenumber and ξ_0 is the coherence length. Numerous studies on the charging in an isolated vortex were performed [4], but the magnetic field dependence of the vortex-charging has not been fully calculated. To this end, we calculated the vortex-core charging in two-dimensional s -wave superconductors with the Abrikosov vortex lattice due to the Lorentz and PPG forces by using the AQC equations. The SDOS pressure is now absent for this case with the cylindrical Fermi surface. The fixed parameters are the magnetic penetration depth as $\lambda_0 = 5\xi_0$, Thomas-Fermi screening length as $\lambda_{TF} = 0.03\xi_0$, and quasiclassical parameter as $\delta = 0.03$.

Figure 1 plots the spatial variation of the charge density due to the Lorentz and PPG

forces at temperature $T = 0.2T_c$ and the average flux densities $\bar{B} = 0.15B_{c2}$, $0.42B_{c2}$, and $0.88B_{c2}$, respectively, where T_c is the transition temperature and B_{c2} is the upper critical field. Figure 2 shows the spatial variation of the charge density due to the PPG force at temperatures $T = 0.2T_c$ and $0.5T_c$, respectively. The charge caused by the Lorentz force has a strong field dependence with a peak and can be enhanced substantially from the value of an isolated vortex as shown in our previous work [5]. Moreover, we show in this report that the charge caused by the PPG force monotonically decreases as the magnetic field increases.

These calculations require a fine mesh of space and momenta when differentiating the Green's functions and self-energies numerically. Therefore, we performed parallel calculations using the ISSP supercomputer.

References

- [1] F. London, *Superfluids* (Dover, New York, 1961), Vol. 1, p. 56.
- [2] N. B. Kopnin, *J. Low Temp. Phys.* **97** (1994) 157.
- [3] D. I. Khomskii and A. Freimuth, *Phys. Rev. Lett.* **75** (1995) 1384.
- [4] H. Ueki, M. Ohuchi, and T. Kita, *J. Phys. Soc. Jpn.* **87** (2018) 044704.
- [5] W. Kohno, H. Ueki, and T. Kita, *J. Phys. Soc. Jpn.* **85** (2016) 083705.

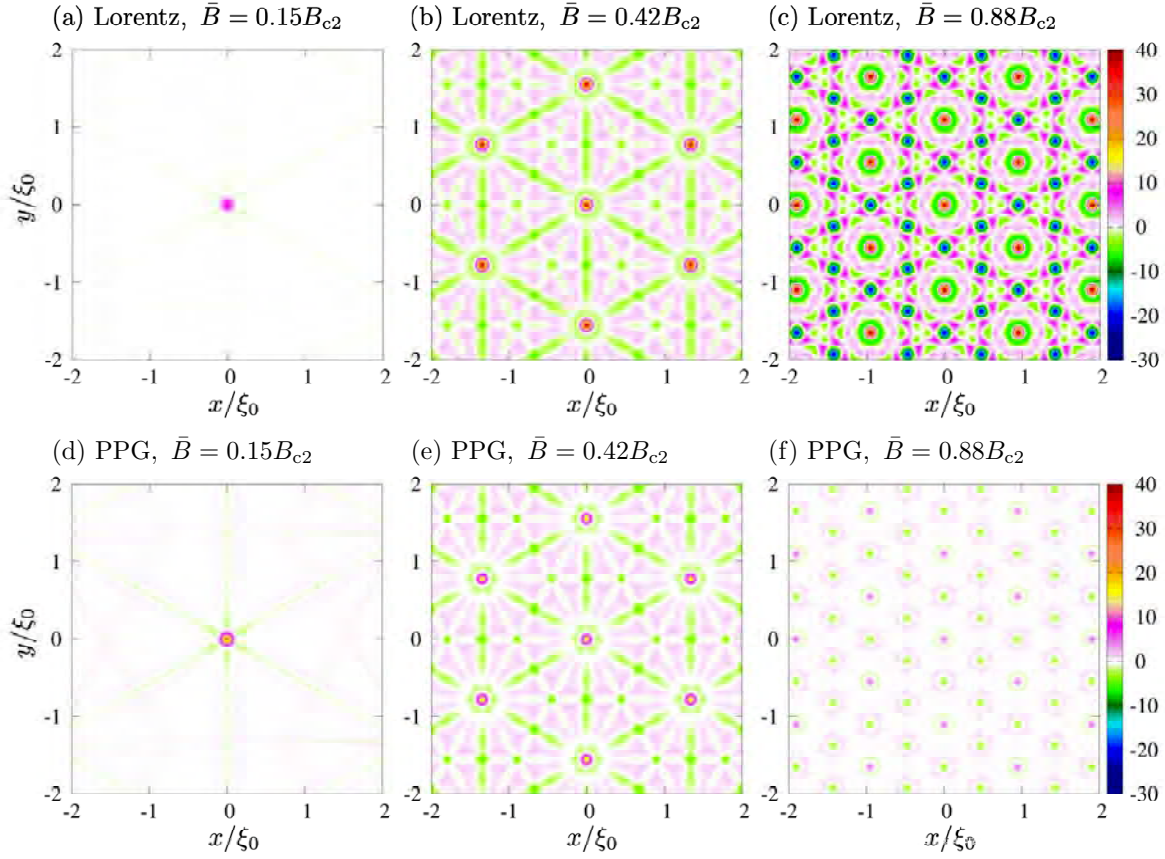


Figure 1: Spatial dependence of the charge density $\rho(\mathbf{r})$ due to the Lorentz force ((a), (b), and (c)), and the PPG force ((d), (e), and (f)) at temperature $T = 0.2T_c$ in units of $\rho_0 \equiv \Delta_0 \epsilon_0 d / |e| \xi_0^2$ on a square grid with x and y ranging from $[-2\xi_0, +2\xi_0]$ for the average flux densities $\bar{B} = 0.15B_{c2}$, $0.42B_{c2}$, and $0.88B_{c2}$ from left to right, respectively. Δ_0 is the energy gap at zero temperature. 0 is the electron

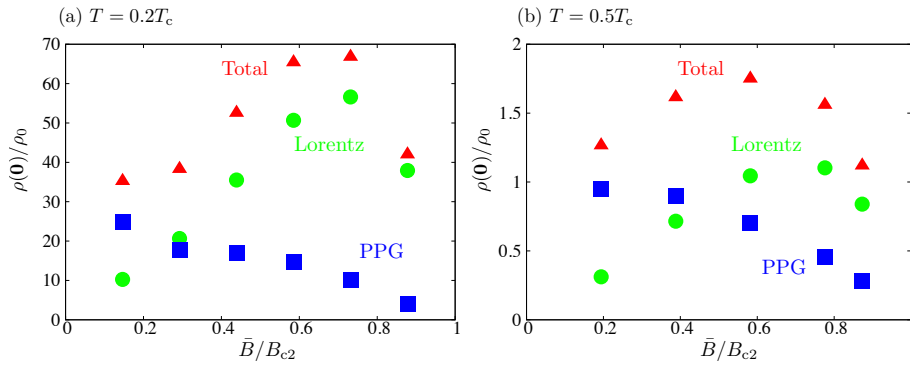


Figure 2: Magnetic field dependence of the charge density at the vortex center $\rho(0)$ due to the Lorentz force (green circular points), the PPG force (blue square points), and the total force (red triangular points), in units of $\rho_0 \equiv \Delta_0 \epsilon_0 d / |e| \xi_0^2$ as a function of the magnetic field, at temperatures (a) $T = 0.2T_c$ and (b) $0.5T_c$ from left to right.

Calculation of ordered structures, dynamics and optical properties of soft materials

Jun-ichi FUKUDA

Department of Physics, Kyushu University, Motoooka 744, Nishi-ku, Fukuoka 819-0395

We studied the structural properties of cholesteric blue phases, three dimensional ordered structures exhibited by a chiral liquid crystal. We particularly focused on how the cubic lattice of blue phases (BPI with O^8 symmetry and BPII with O^2 symmetry) is oriented when in contact with confining surface(s) that impose unidirectional surface alignment of the liquid crystal (unidirectional surface anchoring). Our study was motivated by a recent experimental study [1] that demonstrated specific lattice orientation of blue phases in contact with such surfaces.

Our study [2] was based on a continuum theory describing the orientational order of a liquid crystal by a second-rank tensor (Landau-de Gennes theory). The free energy of the liquid crystal was given as a functional of the tensor order parameter, and the profile of orientational order was obtained by minimizing the free energy numerically. The discretization of the liquid crystal system by a regular grid allows an efficient use of OpenMP (Our system was not large enough to require the use of MPI).

We carried out systematic evaluation of the

free energy with the variation of the direction of the alignment imposed by the surface. We considered two cases commonly observed experimentally: BPI with its (110) planes parallel to the surface(s) and BPII with its (100) planes parallel to the surface(s). In both cases, the blue phase lattice adopts one specific lattice orientation that minimizes the free energy. The surface anchoring strength of 10^{-5} Jm^{-2} , easily achievable experimentally, was shown to be sufficient to lock the lattice orientation. Our finding is consistent with some of the experimental observations, but unfortunately not all. Our study provides a starting point for the understanding of how the blue phase lattice is oriented in response to the surface anchoring, which is strongly desired for practical optical application of blue phases that requires the preparation of large-scale monodomain lattices.

References

- [1] M. Takahashi *et al.*: J. Phys. D: Appl. Phys. **51**, 104003 (2018).
- [2] J. Fukuda and S. Zumer: Phys. Rev. Res. **2**, 033407 (2020).

Molecular simulation of colloidal particles

Takamichi TERAO

*Department of Electrical, Electronic and Computer Engineering,
Gifu University, Yanagido 1-1, Gifu, 501-1132*

Structural formation of colloidal particles have been studied both theoretically and experimentally for many years. In previous studies, spherical colloidal particles with isotropic interparticle interaction were investigated. Recently, there has been a great deal of research on colloidal systems with anisotropic interactions. A typical example is the so-called patchy particle system, in which anisotropic interparticle interaction exists.

The aggregation phenomena of colloidal particles have been a long-standing interest [1]. In this study, we performed computer simulations of the aggregation phenomenon in patchy particles and clarified their structure formation. In Fig. 1, an example of the snapshot of patchy particles with four patches is shown. In particular, we have quantitatively clarified the sol-gel transition and the phase diagram of the system (Figure 2). In this figure, the abscissa and the ordinate denote the rescaled dimensionless temperature and the volume fraction of the system, respectively. In this figure, the red squares show that the patchy particles form a gel network with these sets volume fraction and temperatures. The cluster size distribution and the static structure factor

in aggregates were also quantitatively clarified. From these studies, we have been able to clarify the behavior of patchy particle systems with respect to the formation of various structures.

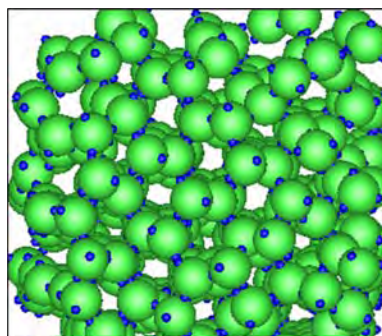


Fig. 1: Snapshot of patchy particles.

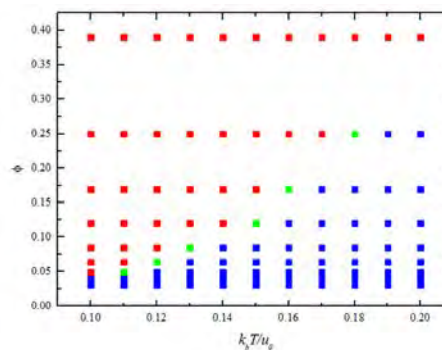


Fig. 2: Phase diagram of patchy particles.

References

- [1] N. E. Valadez-Pérez, Y. Liu, and R. Castañeda-Priego: *Phys. Rev. Lett.* **120** (2018) 248004.

Nematic Tomonaga-Luttinger Liquid Phase in an Anisotropic $S = 1/2$ Two-Leg Ladder System

Takashi Tonegawa

Professor Emeritus, Kobe Univ. and Visiting Professor, Osaka Prefecture Univ.

Recently, we [1] have explored the ground-state phase diagram of the $S=1/2$ two-leg ladder with different leg interactions, which is described by the Hamiltonian,

$$\mathcal{H} = \sum_{\ell=a,b} J_{1,\ell} \sum_{j=1}^L [\vec{S}_{j,\ell}, \vec{S}_{j+1,\ell}]_{\Delta_1} + J_r \sum_{j=1}^L [\vec{S}_{j,a}, \vec{S}_{j,b}]_{\Gamma_r},$$

where

$$[\vec{S}_{j,\ell}, \vec{S}_{j+1,\ell}]_{\Delta_1} = S_{j,\ell}^x S_{j+1,\ell}^x + S_{j,\ell}^y S_{j+1,\ell}^y + \Delta_1 S_{j,\ell}^z S_{j+1,\ell}^z,$$

$$[\vec{S}_{j,a}, \vec{S}_{j,b}]_{\Gamma_r} = \Gamma_r (S_{j,a}^x S_{j,b}^x + S_{j,a}^y S_{j,b}^y) + S_{j,\ell}^z S_{j+1,\ell}^z.$$

In these equations, $S_{j,\ell}^x$, $S_{j,\ell}^y$ and $S_{j,\ell}^z$ are, respectively, the x -, y - and z -components of the $S=1/2$ operator $\vec{S}_{j,\ell}$ at the (j, ℓ) site assigned by the j th rung and the ℓ ($= a$ or b) leg; $J_{1,a}$ and $J_{1,b}$ denote, respectively, the magnitudes of the a leg and b leg interactions, while J_r denotes that of the rung interaction; Δ_1 and Γ_r are, respectively, the parameters representing the XXZ -type anisotropies of the former and latter interactions; L is the total number of rungs, which is assumed to be even. It is emphasized that this system has a frustration when $J_{1,a}J_{1,b} < 0$ irrespective of the sign of J_r .

Using various numerical methods, we [1] have determined the phase diagram on the Δ_1 versus $J_{1,b}$ plane in the case where $J_{1,a} = 0.2$, $J_r = -1.0$, and $\Gamma_r = 0.5$. Interestingly enough, we have found that the nematic Tomonaga-Luttinger Liquid (nTLL) phase appears in the unfrustrated region ($J_{1,b} > 0$) as well as in the frustrated one ($J_{1,b} < 0$). The nTLL phase is characterized not only by the formation of two-magnon bound pairs but also by the dominant nematic four-spin correlation function $\omega^{++--}(j) = \langle S_{j_0,a}^+ S_{j_0,b}^+ S_{j_0+j,a}^- S_{j_0+j,b}^- \rangle$. It is noted that the asymptotic forms of $\omega^{++--}(j)$ are given, respectively, by $\omega^{++--}(j) \propto 1/j^{\eta^{++--}}$ in the former nTLL phase and by $\omega^{++--}(j) \propto (-1)^j/j^{\eta^{++--}}$ in the latter nTLL phase. Thus, both nTLL phases are different phases, and the latter nTLL phase may be called the staggered nTLL phase.

According to the above result, it is reasonably expected that the nTLL state appears as

the zero-field ground state in general $S=1/2$ unfrustrated one-dimensional systems in which pairs of $S=1/2$ spins coupled strongly with the Ising-type ferromagnetic interaction are connected by the weak XY -type antiferromagnetic interactions. Some examples of such systems are (A) the $S=1/2$ ferromagnetic-antiferromagnetic bond alternating chain, (B) the $S=1/2$ two-leg ladder with ferromagnetic rung and antiferromagnetic leg interactions, (C) the $S=1/2$ Kondo necklace chain with ferromagnetic rung and antiferromagnetic leg interactions, and so on.

This report aims at discussing the system (B) which is governed by the Hamiltonian \mathcal{H} with $J_{AF} = J_{1,a} = J_{1,b}$ and $J_F = -J_r$. We determine the following three ground-state phase diagrams, that is, (a) the phase diagram on the Δ_{AF} ($|\Delta_{AF}| \leq 1.0$) versus Γ_F ($0.0 \leq \Gamma_F \leq 1.0$) plane for $J_F = 1.0$ and $J_{AF} = 0.1$, (b) the phase diagram on the Δ_{AF} ($-0.7 \leq \Delta_{AF} \leq 0.6$) versus J_{AF} ($0.0 \leq J_{AF} \leq 0.3$) for $J_F = 1.0$ and $\Gamma_F = 0.7$, and (c) the phase diagram on the Γ_F ($0.0 \leq \Gamma_F \leq 1.0$) versus J_{AF} ($0.0 \leq J_{AF} \leq 1.0$) for $J_F = 1.0$ and $\Delta_{AF} = -0.12$.

The obtained results for the ground-state phase diagrams (a), (b), and (c) are presented in Fig. 1, Fig. 2, and Fig. 3, respectively. In these phase diagrams, there appear the Haldane (H), stripe Néel (sN), $XY1$ ($XY1$), and ferromagnetic (F) phases in addition to the nTLL phase. It is expected that, at least for $J_F = 1.0$, $\Delta_{AF} = -0.12$ and $0.0 \leq \Gamma_F \ll 1.0$, the nTLL phase survives even when the antiferromagnetic leg interactions are stronger than the ferromagnetic rung interaction (see Fig. 3).

Finally, we discuss how to obtain the phase boundary lines in these phase diagrams. All of the phase transition between the $XY1$ and H phases, that between the nTLL and H phases, and that between the nTLL and sN phases are the Berezinskii-Kosterlitz-Thouless transition [2]. As has been rigorously shown by Kitazawa *et al.* [3], the phase boundary lines for these transitions are given by $\Delta_{AF} = 0.0$. The other phase boundary lines have been numerically determined. We denote, respectively, by $E_0^P(L, M)$ and $E_1^P(L, M)$, the lowest and second-lowest energy eigenvalues of the Hamiltonian \mathcal{H} under the periodic bound-

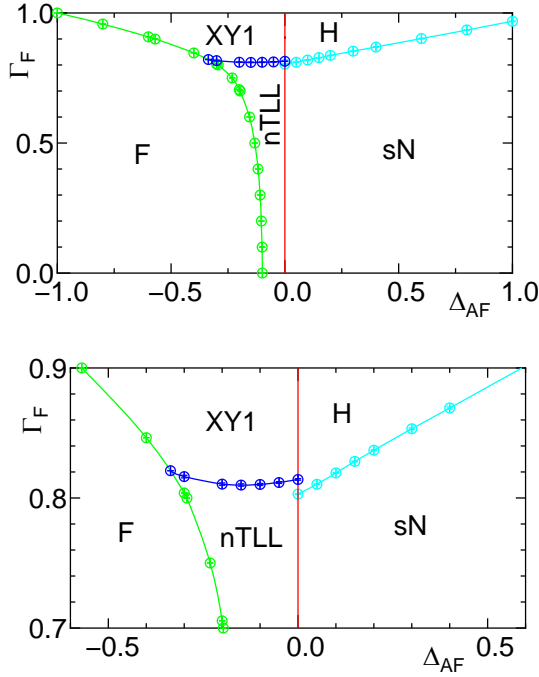


Figure 1: Ground-state phase diagram for $J_F=1.0$ and $J_{AF}=0.1$. A part of the upper figure is enlarged in the lower one.

ary condition within the subspace of L and M , where M is the total magnetization ($M=0, \pm 1, \dots, \pm L$). We have numerically calculated these energies for finite-size systems with up to $L=12$ rungs by means of the exact-diagonalization method. The ground-state energy of the finite- L system is given by $E_0^P(L, L)$ in the F region and by $E_0^P(L, 0)$ in the other regions. In the following way, we have estimated the finite-size critical values of the interaction parameters for each phase transition. Then, the phase boundary line for the transition has been obtained by connecting the results for the $L \rightarrow \infty$ extrapolation of the finite-size critical values. First, the phase transition between the H and sN phases is the 2D Ising-type transition. Then, it is well known that the phase transition line is determined by the phenomenological renormalization-group (PRG) method [4]. Then, to estimate the finite-size critical values, we solve the PRG equation, $L \Delta_{00}(L) = (L+2) \Delta_{00}(L+2)$, where $\Delta_{00}(L) = E_1^P(L, 0) - E_0^P(L, 0)$. Secondly, the nTLL state accompanies two-magnon bound-states, while the XY1 state does not. Then, in the ground-state magnetization curve for the finite-size system, the magnetization increases from $M=0$ to $M=2$ in the former state and from $M=0$ to $M=1$ in the latter state. Thus, the finite-size critical values are estimated from $\Delta_{10}(L) = \Delta_{20}(L)/2$, where $\Delta_{M0}(L) = E_0^P(L, M) - E_0^P(L, 0)$. Lastly, it is apparent that the finite-size critical values for

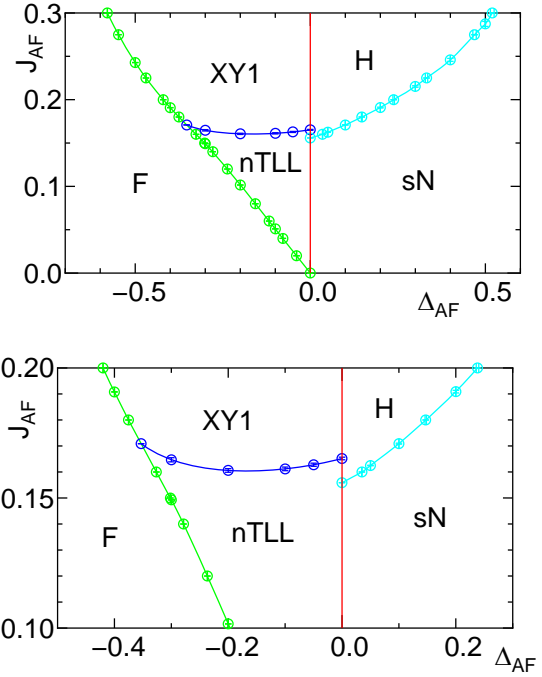


Figure 2: Ground-state phase diagram for $J_F=1.0$ and $\Gamma_F=0.7$. A part of the upper figure is enlarged in the lower one.

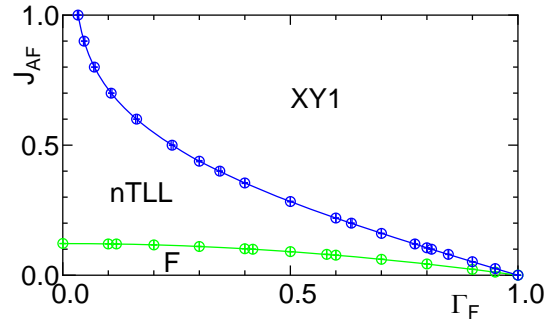


Figure 3: Ground-state phase diagram for $J_F=1.0$ and $\Delta_{AF}=-0.12$.

the phase transitions between the F phase and one of the nTLL and XY1 phases are estimated from $E_0^P(L, L) = E_0^P(L, 0)$.

Invaluable discussions with K. Okamoto, K. Nomura, and T. Sakai are gratefully acknowledged.

[1] T. Tonegawa, T. Hikihara, K. Okamoto, S. C. Furuya, and T. Sakai, *J. Phys. Soc. Jpn.* **87**, 104002 (2018).

[2] Z. L. Berezinskii, *Sov. Phys. JETP* **34**, 610 (1971); J. M. Kosterlitz and D. J. Thouless, *J. Phys. C* **6**, 1181 (1973).

[3] A. Kitazawa, K. Hijii, and K. Nomura, *J. Phys. A: Math. Gen.* **36**, L351 (2003).

[4] M. P. Nightingale, *Physica A* **83**, 561 (1976).

Coarsening mechanism in mass-conserved reaction-diffusion systems

Michio Tateno and Shuji Ishihara

Graduate School of Arts and Sciences, The University of Tokyo

Universal Biology Institute, The University of Tokyo

Komaba 3-8-1, Meguro-ku, Tokyo 153-8902

Reaction-diffusion systems (RDs) are central mathematical scheme that comprehensively describe molecular assemblies driven by chemical reactions, and have tremendously contributed to our understanding of pattern formation observed in nature, particularly those in biological systems. Nearly 14 years ago, it was reported that in RDs satisfying the mass conservation law (MCRDs), patterns exhibit coarsening and result in formation of single isolated domain, unlike usual behavior of RDs [1]. MCRDs were originally introduced and have been discussed as models for molecular localization such as membrane-bounded GTPases which are responsible for the formation of cell polarity [1]. Recently the relevance of MCRDs has been recognized in a broad range of biological phenomena such as oscillatory motion in min-Protein and chemical turbulence (see, e.g., [2]). Despite its uniqueness and fundamental importance, the physical mechanism underlying coarsening behavior in MCRDs remains elusive. This is partially because most of earlier studies only investigated one-dimensional systems. Considering the fact that morphology of the patterns is strongly influenced by spatial dimensions, an intensive study in high dimension is highly desirable.

In this project, we realize a large-scale MCRD simulation in both two and three dimensions using multiple GPUs, and successfully capture coarsening dynamics of MCRDs in high dimension with statistical significance

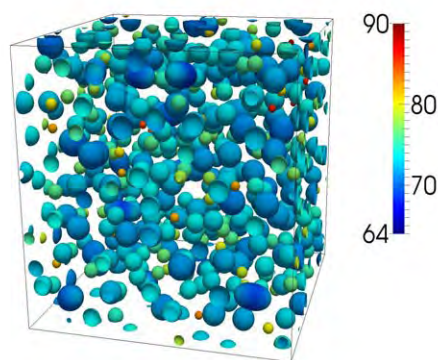


Figure 1: A spatial pattern obtained from a three-dimensional simulation. A contour surface indicates the interface between bistable states. The color is labeled according to the value of chemical-potential-like quantity in MCRDs. The numerical simulation was performed in a cubic lattice of 1024^3 .

for the first time (see Fig. 1). We have an eye on similarity between coarsening dynamics in MCRDs and classical phase separation systems, and apply analysis methods established in thermodynamic phase transition (dynamic scaling law, nucleation-growth process, etc.) to the simulation results. We reveal that droplets forming in MCRDs obey the Young-Laplace law and coarsen following the evaporation-condensation (Lifshitz-Slyosov-Wagner) mechanism (see Fig. 2). These outcomes indicate that in the presence of conserved variable, a physical quantity similar to surface tension is relevant to RDs,

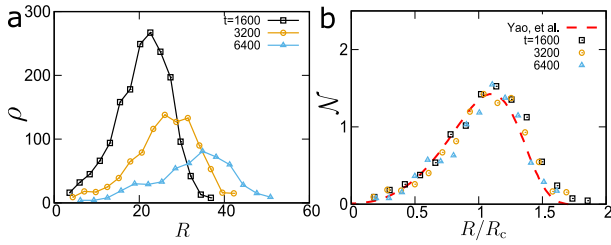


Figure 2: **a** Droplet-radius distribution $\rho(R)$ for various time t . **b**. Dynamic scaling of ρ based on Lifshitz–Slyozov–Wagner theory. The symbol shows the same simulation results as in panel a. The red dashed lines represent theoretical predictions for the scaled distribution $\mathcal{N}(R/R_c)$ [4], where R_c is critical radius.

which provides new insight into molecular self-assembly driven by chemical reactions. The result is now under review in an international peer reviewed journal, and the preprint is uploaded in an online paper repository [3].

References

- [1] M. Otsuji, S. Ishihara, et al.: PLOS Comput. Biol. **3**, (2007) 1.; S. Ishihara, M. Otsuji and A. Mochizuki: Phys. Rev. E **75**, (2007) 015203.
- [2] E. Frey, J. Halatek, et al.: *Physics of Biological Membranes*, Springer International Publishing, pp.229-260 ; J. Halatek and E. Frey: Nat. Phys. **14**, (2018) 507.
- [3] <http://arxiv.org/abs/2010.03900>
- [4] J. H. Yao, K. R. Elder, et al.: Phys. Rev. B **47**, (1993) 14110.

Multicellular simulation by phase field method

Michio Tateno and Shuji Ishihara

Graduate School of Arts and Sciences, The University of Tokyo

Universal Biology Institute, The University of Tokyo

Komaba 3-8-1, Meguro-ku, Tokyo 153-8902

The central aim of this project is to establish a multicellular simulation method that can capture multiscale dynamics, ranging from intracellular chemical concentration, shape changes of cells, to their collective motions in a tissue scale. To realize this, we adopted the phase field (PF) model, which can express cells with arbitrary shape. In this method, an auxiliary field (phase field) which obeys a bistable energy functional is introduced to distinguish the inside and outside of a cell. This procedure allows us to describe the time evolution of cell shape via interfacial dynamics without suffering from moving boundary problems.

One of the authors (SI) and coworkers combined PF model with a reaction-diffusion system, in which a bistable and excitable chemical network is incorporated to model cell migration driven by F-actin. They demonstrated that this model can precisely reproduce complex motion of amoebic cells (*Dictyostelium* at early starvation stage) as well as intracellular chemical waves related to actin polymerization [1]. In this term, we have made an attempt to extend this PF model to multicellular systems.

In PF model for a single cell, a square moving frame with lattice size L^2 is provided to compute the phase field. Here L should be sufficiently larger than the cell size (typically L being hundreds of order) to capture the complex morphology of a cell and avoid the cell from overhanging the frame. When increase the cells, of course, the computational cost is not simply scaled by the number of cells N ; one need to deal with overlap regions among

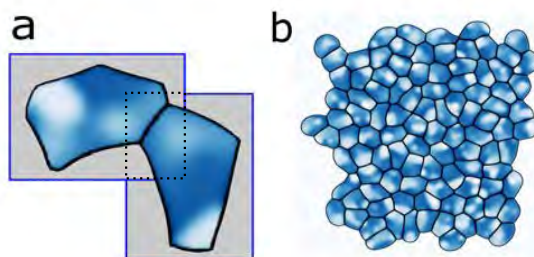


Figure 1: **a.** Adaptive moving frame (gray areas) is used in our PF model. This largely reduces the computational cost for intercellular interactions (the region surrounded by a dotted line). The white and blue regions represent the distributions of PIP3 and PTEN, respectively. **b.** A snapshot of multicellular simulation with 100 cells.

the frames for different cells, to compute intercellular interactions such as steric effect or cell adhesion, which is a computation bottleneck. The resulting computational cost was roughly the order of $10 \times NL^2$.

To overcome this problem, we improve the computational efficiency by updating the moving frames to adapt to the shape of cells. Figure 1a show the computational regions for two cells (gray rectangle areas). The area surrounded by a dotted line represent the region required to compute the intercellular interaction between the cells. Using this algorithm and GPU, we have speeded up the computation by four times and realized simulation with order of 100 cells as shown in Fig. 1b. In the further, we plan to apply our program to specific problems such fluidity transition or cell

sorting of a epithelial tissue.

References

- [1] D. Taniguchi, Ishihara, et al.: Proc. Natl. Acad. Sci. USA **110**, (2013) 5016.

Universal properties of dissipated many-body quantum systems

Tatsuhiko Shirai

*Department of Computer Science and Communications Engineering, Waseda University
Ookubo, Shinjuku-ku, Tokyo 169-8555*

We have studied two different types of non-equilibrium quantum systems: bulk-dissipated systems and boundary-dissipated systems.

1 Bulk-dissipated systems

In the bulk-dissipated systems, the dissipative environments are uniformly coupled to the system of interest. We consider that the system-environment coupling is weak and the environment is nonequilibrium (i.e., the detailed balance condition is broken). The reference [1] has argued that the Gibbs state at an effective temperature gives a good description of the nonequilibrium steady state provided that the system Hamiltonian obeys the eigenstate thermalization hypothesis and the perturbation theory in the weak system-environment coupling is valid in the thermodynamic limit. The numerics are based on the exact diagonalization method, which restricts the system size studied. We have developed a tensor-network approach that directly studies not only the steady states but also the relaxation dynamics in the thermodynamic limit [2]. The study reveals that when an initial state is given by a thermal Gibbs state, the states during the relaxation dynamics are well described by Gibbs states with a time-dependent effective temperature.

2 Boundary-dissipated systems

We discussed the relaxation time of the boundary-dissipated systems, where the environments with different thermodynamic potentials (e.g., temperature and chemical potential) are coupled to the edges of the non-integrable systems. The presence of the diffusive transport indicates that the relaxation time τ is proportional to the square of the system size L (i.e., $\tau \sim L^2$). The relaxation time is naively related to the gap of the time-evolution operator called the Liouvillian, but the previous studies have shown that the gap closing is slower than L^{-2} [3]. We have solved this discrepancy by numerically showing that the relaxation time is not determined by the lower-lying eigenvalues of the Liouvillian but by superexponentially large expansion coefficients for Liouvillian eigenvector with non-small eigenvalues at an initial state [4].

References

- [1] T. Shirai, and T. Mori: Phys. Rev. E **101** (2020) 042116.
- [2] H. Nakano, T. Shirai, and T. Mori: arXiv:2012.12274.
- [3] M. Žnidarič, Phys. Rev. E **92** (2015) 042143.
- [4] T. Mori, and T. Shirai: Phys. Rev. Lett. **125** (2020) 230604.

Quantum annealing in transverse-field Ising chains with a correlated disorder

Tatsuhiko Shirai

*Department of Computer Science and Communications Engineering, Waseda University
Ookubo, Shinjuku-ku, Tokyo 169-8555*

We have studied disordered Ising chains under transverse fields to examine the effects of a correlated disorder on quantum phase transitions. The Hamiltonian is given by

$$H = - \sum_{i=1}^{N-1} J_i \sigma_i^z \sigma_{i+1}^z - \sum_{i=1}^N \Gamma_i \sigma_i^x, \quad (1)$$

where $\vec{\sigma}_i = (\sigma_i^x, \sigma_i^y, \sigma_i^z)$ are Pauli spin matrices, and J_i and Γ_i denote nearest-neighbor coupling strength and transverse-field strength, respectively. J_i is chosen from two different types of distribution: weak disorder and strong disorder. The distribution in the weak disorder case is uniform over $(J^{(0)}, 1]$ and gapped (i.e., $J^{(0)} > 0$), and thus given as

$$\pi_w(J_i) = \begin{cases} (1 - J^{(0)})^{-1} & \text{for } J^{(0)} < J_i \leq 1, \\ 0 & \text{otherwise.} \end{cases} \quad (2)$$

On the other hand, the distribution in the strong disorder case is a gapless power-law distribution over $(0, 1]$ given as

$$\pi_s(J_i) = \begin{cases} \frac{1}{D} J_i^{-1+\frac{1}{D}} & \text{for } 0 < J_i \leq 1, \\ 0 & \text{otherwise,} \end{cases} \quad (3)$$

where $D > 0$ denotes the disorder strength. In the correlated disorder case, the transverse-fields are given by

$$\begin{cases} \ln \frac{\Gamma_1}{\Gamma} = (1 - s) \ln J_1, \\ \ln \frac{\Gamma_i}{\Gamma} = s \ln J_{i-1} + (1 - s) \ln J_i \\ \quad \text{for } 2 \leq i \leq N - 1, \\ \ln \frac{\Gamma_N}{\Gamma} = s \ln J_{N-1}, \end{cases} \quad (4)$$

where $s \in [0, 1]$ is a parameter for tuning the transverse fields.

In [1], we analytically show that the dynamical critical exponents z in the system with the correlated disorder are finite: $z = 1$ in the weak disorder case and $\max(D(1/2 + |s - 1/2| + 1/2), 1) \leq z \leq D + 1$ in the strong-disorder case. We numerically estimate z in the strong disorder case. The numerics is based on the Jordan–Wigner transformation and an exact diagonalization method [2]. The finite z is in contrast to infinite z obtained in the uncorrelated disordered Ising chains (i.e., no correlation between the transverse fields and nearest-neighbor couplings) [2, 3]. The suppression of z is useful to enhance the performance of adiabatic quantum computations including quantum annealing with an argument based on the Kibble–Zurek mechanism.

References

- [1] T. Shirai, and S. Tanaka: arXiv:2007.07439 (2020).
- [2] A. P. Young and H. Rieger: Phys. Rev. B **53** (1996) 8486.
- [3] D. S. Fisher: Phys. Rev. Lett. **69** (1992) 534.

Study of superstructure induced novel phenomena: stacking of atomically thin materials

Toshikaze KARIYADO

International Center for Materials Nanoarchitectonics,

National Institute for Materials Science, Namiki, Tsukuba, Ibaraki 305-0044

The purpose of this study is to propose a new design for van der Waals heterostructures of atomically thin materials to realize novel phases or phenomena. Particularly, we focus on twisted bilayers, where two layers are stacked with angle mismatch. When the relative angle is small, the system shows a long-range structure called moiré pattern that can induce novel physics. With the small relative angle, a twisted bilayer system locally resembles to a bilayer system without twist, but globally, the relative in-plane shift between two layers depends on position due to the twist. Then, it is a powerful scheme to analyze crystalline and electronic structures for untwisted bilayers and scan over the possible relative in-plane shift.

In this project, we have applied the above procedure on several candidate materials, including graphene relatives and group-IV monocalcogenide monolayers. For the analysis of crystalline and electronic structures, we have used the first-principles density functional theory method implemented in Quantum Espresso package. One of the key quantities in crystalline structure analysis is relative in-plane

shift dependence of layer-layer distance, which is derived by computing the binding energy as a function of layer-layer distance with rev-vdW-DF2 type functional to take account of the van der Waal force. Once the layer-layer distance is fixed, the electronic structure is computed using PBE-GGA type functional.

Overall, we have to scan over the possible relative in-plane shift, and therefore, it is important to make a calculation for each parameter as light as possible. In that perspective, MPI parallelization implemented in Quantum Espresso package helps us a lot if it is used on a massively parallel computational system.

In addition to the above project, we have analyzed diamagnetic responses in an antiperovskite type Dirac electron system [1]. The numerically obtained susceptibility compares well with the experimental result.

References

- [1] S. Suetsugu, K. Kitagawa, T. Kariyado, A. W. Rost, J. Nuss, C. Mühle, M. Ogata, and H. Takagi: *Phys. Rev. B* **103** (2021) 115117.

Numerical Study of One Dimensional Frustrated Quantum Spin Systems

Kazuo HIDA

*Professor Emeritus, Division of Material Science,
Graduate School of Science and Engineering,
Saitama University, Saitama, Saitama 338-8570*

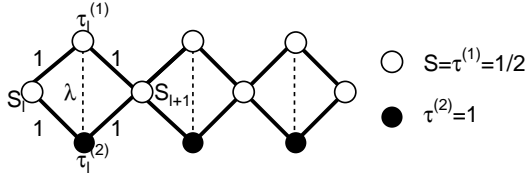


Figure 1: Structure of the diamond chain investigated in this work.

We investigate the ground-state phases of mixed diamond chains described by the following Hamiltonian [1]:

$$\mathcal{H} = \sum_{l=1}^L \left[S_l (\tau_l^{(1)} + \tau_l^{(2)}) + (\tau_l^{(1)} + \tau_l^{(2)}) S_{l+1} + \lambda \tau_l^{(1)} \tau_l^{(2)} \right], \quad (1)$$

where $S_l, \tau_l^{(1)}$ and $\tau_l^{(2)}$ are spin operators with magnitudes $S_l = \tau_l^{(1)} = 1/2$ and $\tau_l^{(2)} = 1$. The number of the unit cells is denoted by L . Here, the parameter λ controls the frustration as depicted in Fig. 1. Defining the composite spin operators \mathbf{T}_l as $\mathbf{T}_l \equiv \tau_l^{(1)} + \tau_l^{(2)}$, it is evident that $\forall l [\mathbf{T}_l^2, \mathcal{H}] = 0$. Thus, we have L good quantum numbers $\mathbf{T}_l^2 \equiv (T_l + 1)T_l$ where $T_l = 1/2$ and $3/2$. The total Hilbert space of the Hamiltonian (1) consists of separated subspaces, each of which is specified by a definite set of $\{T_l\}$. For large λ , $\forall l T_l = 1/2$. Hence, the ground state is equivalent to that of the uniform spin 1/2 chain, namely a gapless spin liquid. For $\lambda \leq 0$, $\forall l T_l = 3/2$. Hence, the ground state is a Lieb-Mattis ferrimagnetic phase with spontaneous magnetiza-

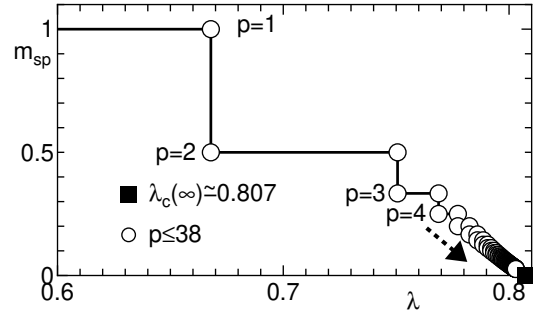


Figure 2: λ -dependence of m_{sp} calculated by the infinite size DMRG method.

tion $m_{\text{sp}} = 1$ per unit cell. For intermediate λ , we find a series of ferrimagnetic phases with $m_{\text{sp}} = 1/p$ where p takes positive integer values as shown in Fig. 2 based on the infinite-size DMRG calculations for various configurations of $\{T_l\}$. The calculations for many different $\{T_l\}$ are independent from each other. Hence, they are suitable for the massively parallel system of the ISSP supercomputer center. The phases with $p \geq 2$ are accompanied by the spontaneous breakdown of the p -fold translational symmetry. It is suggested that the phase with arbitrarily large p , namely infinitesimal spontaneous magnetization, is allowed as λ approaches the transition point to the gapless spin liquid phase.

References

- [1] K. Hida, arXiv:2102.02116, to be published in J. Phys. Soc. Jpn.

Development of observation-noise estimation method by machine learning

Ryo TAMURA

*International Center for Materials Nanoarchitectonics,
National Institute for Materials Science,
1-1 Namiki, Tsukuba, Ibaraki, 305-0044*

To know the Hamiltonian of target materials, a data-driven approach is useful, in which model parameters of Hamiltonian are determined so as to fit the experimentally measured data[1, 2, 3, 4]. In a data-driven approach, the posterior distribution is defined, and the appropriate parameters are searched by a maximum a posteriori (MAP) estimation. Thus, the Hamiltonian, which can well explain the experimental results, is obtained by the framework of MAP estimation. However, by MAP estimation, observation noise cannot be evaluated. The Hamiltonian estimation method based on Bayesian inference is formulated under the assumption of finite observation noise. Then, there must be errors in the estimated parameters. Therefore, we proposed a method to evaluate the error of the parameters by estimating the observation noise[5].

In our framework, the noise amplitude σ is considered to be a hyperparameter, and a plausible value is determined by minimizing the Bayes free energy $F(\sigma)$, defined as

$$F(\sigma) = -\log Z(\sigma), \quad (1)$$

where $Z(\sigma)$ is the normalization of the posterior distribution given by

$$Z(\sigma) = \left(\frac{1}{2\pi\sigma^2}\right)^{\frac{L}{2}} \int_{\Omega_x} d\mathbf{x} \exp[-E(\mathbf{x}, \sigma)]. \quad (2)$$

Here, Ω_x is the support of the posterior distribution determined by the prior distribution. In addition, \mathbf{x} is the model parameters in the

Hamiltonian and $E(\mathbf{x}, \sigma)$ is the energy function to be minimized in our model estimation. To evaluate $F(\sigma)$, it is convenient to extend the normalization factor with a “finite temperature”, which is defined as

$$Z_\beta(\sigma) = \left(\frac{1}{2\pi\sigma^2}\right)^{\frac{L}{2}} \int_{\Omega_x} d\mathbf{x} \exp[-\beta E(\mathbf{x}, \sigma)], \quad (3)$$

where β is the inverse temperature. By using $Z_\beta(\sigma)$, the Bayesian free-energy is defined as

$$\begin{aligned} F(\sigma) &= -\int_0^1 d\beta \left(\frac{d}{d\beta} \log Z_\beta(\sigma)\right) - \log Z_0(\sigma) \\ &= \int_0^1 d\beta \langle E(\mathbf{x}, \sigma) \rangle_\beta + \frac{L}{2} \log(2\pi\sigma^2) \\ &\quad - \log \int_{\Omega_x} d\mathbf{x}, \end{aligned} \quad (4)$$

where the ensemble average $\langle E(\mathbf{x}, \sigma) \rangle_\beta$ can be obtained by the MCMC method. Here, the third term on the right-hand side does not depend on σ and can be omitted. The noise amplitude of the experimental data σ^* is evaluated as the value where $F(\sigma)$ is minimized.

This noise estimation method is applied for the effective model estimation of $\text{KCu}_4\text{P}_3\text{O}_{12}$. As a result, we obtained the noise amplitude, and the magnetic interactions with error bars can be estimated as $J_1 = -8.54 \pm 0.51$ meV, $J_2 = -2.67 \pm 1.13$ meV, $J_3 = -3.90 \pm 0.15$ meV, and $J_4 = 6.24 \pm 0.95$ meV, by using our noise estimation method.

This work is the collaboration work with Koji Hukushima, Akira Matsuo, Koichi Kindo, and Masashi Hase.

References

- [1] R. Tamura and K. Hukushima, PLoS ONE **13**, e0193785 (2018).
- [2] H. Takenaka, K. Nagata, T. Mizokawa, and M. Okada, J. Phys. Soc. Jpn. **83**, 124706 (2014).
- [3] R. Tamura and K. Hukushima, Phys. Rev. B **95**, 064407 (2017).
- [4] H. Fujita, Y. O. Nakagawa, S. Sugiura, and M. Oshikawa, Phys. Rev. B **97**, 075114 (2018).
- [5] R. Tamura, K. Hukushima, A. Matsuo, K. Kindo, and M. Hase, Phys. Rev. B **101**, 224435 (2020).

Systematic Investigation on Phonon Transport at Nanoscale Interfaces

Susumu FUJII

*Nanostructures Research Laboratory, Japan Fine Ceramics Center
Mutsuno, Atsuta, Nagoya 456-8587*

Grain boundaries and hetero interfaces are known to suppress lattice thermal conductivity of a material dramatically, because of their disordered structures different from the corresponding crystal structure(s). Recently, there is an increasing demand for revealing the mechanisms of interfacial thermal conduction at the nanoscale, as electronic devices have become miniaturized and nanostructuring techniques have been extensively developed. However, there is a few studies that investigate the impact of interface atomic structures or interfacial scattering mechanisms of phonons that are defined in the reciprocal space, making it difficult to obtain a guideline for controlling thermal conductivity on the basis of interfaces.

In the present study, we have mainly investigated the interfacial thermal conduction across silicon grain boundaries (Fig. 1). We chose silicon as a model material because it has many technologically important applications such as electronic devices and thermoelectrics. We performed two types of molecular dynamics simulations: (1) perturbed molecular dynamics and (2) phonon wave packet. The former adds a small magnitude of perturbation to atoms and calculate thermal conductivity from the average of heat flux of the system. The latter introduces an phonon wave packet generated from a single phonon mode from phonon dispersions and simulate its scattering process at the interface. The necessary codes were developed by the author and implemented to the Large-scale Atomic/Molecular Massively

Parallel Simulator (LAMMPS) [1]. In addition, we used a machine learning potential for Si distributed in MACHINE LEARNING POTENTIAL REPOSITORY [2], which are much less computationally demanding compared with density functional theory calculations but more demanding than the empirical interatomic potentials such as Stillinger-Weber and Tersoff potentials.

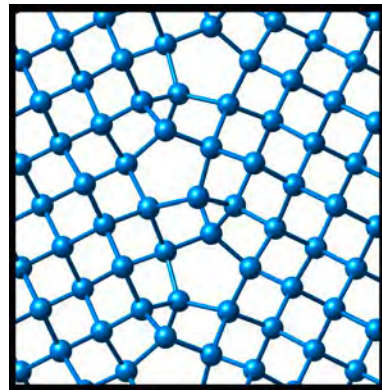


Figure 1: An example of silicon grain boundary structure derived from the machine learning potential.

The perturbed molecular dynamics simulations require a large number of timesteps more than one million and large computational cells with a few thousands of atoms. On the other hand, phonon wave packet simulations require a smaller number of timesteps less than 100000 but the computational cells must be very long for the direction perpendicular to the grain boundary plane and thus contain tens of thousands of atoms. The former were per-

formed with five different magnitudes of perturbations, and the latter were performed for 40 - 60 different phonon modes for each grain boundary. Each of these calculations was performed in a single node.

The results perturbed molecular dynamics simulations show that thermal conductivity of Si grain boundaries significantly correlates with their microscopic atomic structures rather than their energies. On the other hand, our phonon wave packet simulations reveal that the phonon transmission (or reflection) at the grain boundaries does not depend on the grain boundary structures much, especially for the acoustic phonons that transfer most of heat. This contradicting trends obtained from two kind of molecular dynamics simulations suggest that anharmonic effect of atomic vibrations at the grain boundaries, which is naturally included in the perturbed molecular dynamics while is intentionally neglected in the phonon wave packet simulations, is one of the dominant factors for determining interfacial thermal conduction.

In addition, comparisons of grain boundary structures, phonon properties and thermal conductivity between the machine learning potential and a classical interatomic potential (Tersoff potential) demonstrate the high predictive power of the machine learning potential. By combining machine learning potentials with supercomputers and advanced computational programs, it is becoming possible to quantitatively analyze interfacial thermal conduction.

References

- [1] S. Plimpton, *J. Comput. Phys.* **117** (1995) 1.
- [2] A. Seko, arXiv:2007.14206.

Developing numerical tool for open quantum dynamics based on neural networks

Nobuyuki YOSHIOKA

Department of Applied Physics,

The University of Tokyo, 7-3-1 Hongo, Bunkyo-ku, Tokyo, Japan, 113-8656.

In this project, we have planned to use neural networks to study the property of open quantum many-body systems which are subject to dissipations that give rise to competition similar to “frustration” in closed quantum many-body systems. While the proposed project is currently on-going, we have achieved some other works regarding scalable simulations using neural networks. In the following, we report the results in such two works [1, 2].

In the first work, we have successfully demonstrated a novel simulation algorithm that perform first-principles calculation of solid-state systems. Namely, we have shown that the expressive power of neural networks are sufficiently high so that the essential properties of solids, the ground state and the quasiparticle band spectra, can be simulated both efficiently and accurately. The ground states are computed by the standard variational Monte Carlo manner, such that the imaginary-time evolution is realized approximately. This enables us to simulate the potential curve of various real solids including polymers, non-organic crystals, or strongly correlated systems. In particular, we

have shown that, the thermodynamic limit of the strongly correlated hydrogen chain can be computed within chemical accuracy.

In the second work, we have developed two algorithms that simulates the thermal equilibrium of an isolated quantum many-body system using deep neural networks. In one method, we exploit the quantum-to-classical correspondence to construct the exact representation of Gibbs state using the deep Boltzmann machine (DBM). This demonstrates the expressibility of the DBM. In the other method, we approximate the imaginary-time evolution to generate finite-temperature density matrix starting from the infinite-temperature Gibbs state. We have numerically demonstrated that the second approach opens a door to scalable simulation even in frustrated systems where the thermal property is still under debate.

References

- [1] N. Yoshioka, W. Mizukami, and F. Nori, arXiv:2010.01358 (2020).
- [2] Y. Nomura, N. Yoshioka, and F. Nori, arXiv:2103.04791 (2021).

Quantum Monte Carlo study of the antiferromagnetic Ising model on a square lattice with longitudinal and transverse magnetic fields

Ryui KANEKO

*Department of Physics, Kindai University
Higashi-Osaka, Osaka 577-8502, Japan*

Analog quantum simulations have attracted much interest recently. Ground-state properties and nonequilibrium dynamics of quantum spin, SU(N) Heisenberg, and SU(N) Hubbard systems have been extensively studied. It is important to verify how far the simulation of the experiment is correct by comparing numerical simulations on classical computers. It is an interesting challenge to investigate the properties of complex models in static systems and those in nonequilibrium systems using numerical methods such as tensor network algorithms. On the other hand, it is also indispensable to study static properties in simple systems because it is much easier to compare the experiments and numerical simulations.

The Rydberg-atom systems are suitable for realizing the fundamental spin models. The quantum Ising models are frequently experimented with. The Hamiltonian is given as

$$H = \sum_{i,j} J_{ij} S_i^z S_j^z - h \sum_i S_i^z - \Gamma \sum_i S_i^x. \quad (1)$$

The longitudinal (transverse) field h (Γ) can be controlled by the frequency detuning (the Rabi frequency) of the laser [1]. The Ising interaction is given as van der Waals interaction, whose long-range part is often ignored for simplicity [2].

Although the ground-state phase diagram of the quantum Ising models on complex lattices have been extensively investigated, the simple model on a square lattice has yet to be ex-

plored. The ground-state phase diagram was obtained only for few dozen sites using the exact diagonalization method [3]. We investigate the ground-state phase diagram of the model on the square lattice using the quantum Monte Carlo method with the DSQSS library [4]. We typically choose 10^5 Monte Carlo steps for calculation of physical quantities and for thermalization. We use the system sizes $N_s = L^2$ with $L \leq 32$ and consider the periodic-periodic boundary condition.

To determine the phase boundary, we calculate the staggered susceptibility defined as

$$\chi_{\text{stag}}^{zz} = \frac{\langle \hat{M}^z(\mathbf{Q})^2 \rangle}{\beta L^d}, \quad \mathbf{Q} = (\pi, \pi), \quad (2)$$

$$\text{and } \hat{M}^z(\mathbf{q}) = \int_0^\beta d\tau \sum_j \hat{S}_j^z(\tau) e^{-i\mathbf{q}\cdot\mathbf{r}_j}, \quad (3)$$

where \mathbf{r}_j is the real space coordinate at site j , $d(= 2)$ is the spatial dimension, and β is the inverse temperature.

We perform the finite-size scaling analysis to determine the phase boundary between the antiferromagnetic and disordered phases. The scaling form of χ_{stag}^{zz} is given as

$$\chi_{\text{stag}}^{zz} \sim L^{2-\eta} \mathcal{F}(\delta L^{1/\nu}), \quad (4)$$

where \mathcal{F} is a scaling function, η is the anomalous dimension, and ν is the correlation length exponent. The difference between the field and the critical point is given as δ . Since the dynamical exponent would satisfy $z = 1$ for the

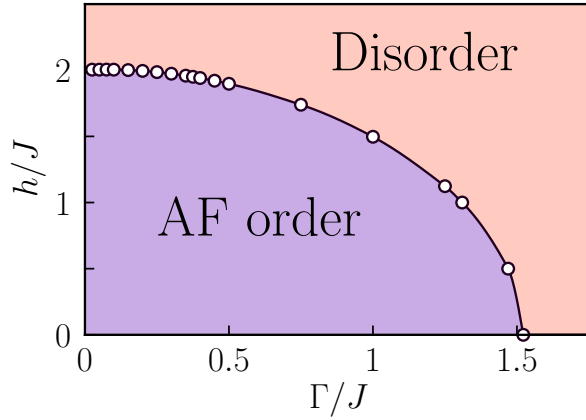


Figure 1: Phase diagram of the antiferromagnetic Ising model on a square lattice with longitudinal and transverse magnetic fields.

Ising universality class, we choose the inverse temperature β to be proportional to L during the simulation.

Figure 1 shows the ground-state phase diagram of the mixed-field Ising model on the square lattice. When the transverse field $\Gamma \sim 0$, the transition longitudinal field h_c is nearly intact as a function of Γ . On the other hand, when $h \sim 0$, h_c drops nearly vertically as a function of Γ . The latter behavior is consis-

tent with the phase boundary obtained by the mean-field approximation [5].

By scrutinizing the phase diagram near $\Gamma \sim 0$, we have also uncovered the narrow region where the disordered phase exhibits reentrance. Our phase diagram [6] would be useful for examining the accuracy of the analog quantum simulation in the Rydberg-atom systems.

References

- [1] F. Robicheaux and J. V. Hernández, Phys. Rev. A **72**, 063403 (2005).
- [2] A. Browaeys and T. Lahaye, Nat. Phys. **16**, 132 (2020).
- [3] V. Lienhard et al., Phys. Rev. X **8**, 021070 (2018).
- [4] Y. Motoyama et al., Comput. Phys. Commun. **264**, 107944 (2021).
- [5] A. A. Ovchinnikov et al., Phys. Rev. B **68**, 214406 (2003).
- [6] R. Kaneko et al., arXiv:2103.12364

Theoretical study for caged compound and its conjugate acid/bases

Miyabi HIYAMA

*Graduate School of Science and Technology, Gunma University,
Tenjin-cho, Kiryu, Gunma 376-8515*

Caged luciferins, which can generate luciferin by UV photolytic reaction, would be useful to understand the firefly bioluminescence. We synthesized the new caged luciferin named coumarin caged luciferin and obtained its absorption spectra [1]. When we use this caged-luciferin for spectroscopic studies, we need the detail of electronic states of this molecule in aqueous solutions.

The optimization structure of ground state for coumarin caged-luciferin anion expected to be main component in the pH 8 aqueous solutions was obtained from the density functional theory. The time dependent DFT (TDDFT) calculations were carried out to estimate the theoretical absorption spectra for this structure. These theoretical spectra were used to assign the experimental spectra measured at pH 8 [2]. However, these theoretical results cannot explain the difference between the shape of absorption spectra of coumarin caged luciferin at pH 3 and those at pH 8. We expect that the main chemical species in the acidic experimental condition would be neutral coumarin caged luciferin molecule of which total charge is 0.

In this year, we performed the DFT calculations for the neutral coumarin caged luciferin molecule. The excitation energies and the oscillator strengths at the ground state were obtained using TDDFT calculations for the optimization structure of the neutral coumarin caged luciferin molecule. The polarized continuum model was used for the description

of water solute molecules. We found that the absorption energy for neutral coumarin caged luciferin is larger than that for coumarin caged luciferin anion. It was also found that the shape of absorption spectra for neutral coumarin caged luciferin has a large main peak, while that for coumarin caged luciferin anion has a double peak.

All calculations were performed using the GAUSSIAN09 program [3] on system B and C of Super Computer Center in ISSP.

References

- [1] Kurata et al. , J. Photochem. Photobiol. B, **189** (2018) 81.
- [2] Usukura et al. Photochem. Photobiol. (2020) Photochem. Photobiol. (2020) 96, 805.
- [3] Gaussian 09, Revision D.01, M. J. Frisch et al.

Exact diagonalization calculations of density of states and dynamical structure factor for the spherical-kagome spin-system $\{W_{72}V_{30}\}$

Yoshiyuki Fukumoto

*Department of Physics, Faculty of Science and Technology, Tokyo University of Science
2641 Yamazaki, Noda, Chiba 278-8510*

For the spherical-kagome cluster with thirty spin-1/2s, as well as for the 2D kagome lattice, many low-energy singlet excitations have been expected to exist in the energy region below spin gap [1], which has been actually confirmed by Kihara *et al.* in their specific heat measurements at low temperature in $\{W_{72}V_{30}\}$ [2]. However, the experimental curve of the specific heat can not be reproduced by the theoretical curve in the Heisenberg model $\mathcal{H} = J \sum_{\langle i,j \rangle} \mathbf{S}_i \cdot \mathbf{S}_j$, where $\langle i,j \rangle$ denote nearest neighbors and the exchange parameter was estimated as $J = 115\text{K}$ [1]. The experimental curve does not have the peak around 2K, although the theoretical one has the 2K peak [1,2].

In last year, incorporating Dzyaloshinskii-Moriya (DM) interactions and bond randomness into our model Hamiltonian, both of which were originally proposed to explain the luck of the step-wise behaviour in the low-temperature magnetization curve of $\{W_{72}V_{30}\}$ [3,4], we used the method of thermal pure quantum (TPQ) state [5] to calculate the specific heat. Then, we found that 10% of randomness collapse the 2K peak.

In this year, we calculate density of states, entropy, and specific heat at low temperatures by using the Lanczos method [6]. In particular, we aim to understand low-temperature specific heat qualitatively via observation of the density of states. We find that DM interactions do not significantly affect the energy distribution

of a dozen or so singlet states above the ground state, which are involved in the peak structure of the specific heat around 2K. On the other hand, we find that 10% randomness disperses this distribution to collapse the 2K peak, which is consistent with the above-mentioned TPQ result.

In conclusion, we have clarified the similarities and differences between the effects of the DM interaction and bond randomness: the DM interaction breaks the conservation of the total spin and cause magnetic components to mix dense singlet states at low energies, while the bond randomness disperses the energy distribution of singlets and triplets without breaking the conservation of the total spin, which leads to similar effects on the magnetization process but does to different effects on the specific heat.

References

- [1] N. Kunisada *et al.*, PTEP 2014, 41I01 (2014).
- [2] T. Kihara *et al.*, PRB 99, 064430 (2019).
- [3] Y. Fukumoto *et al.*, J. Phys. Soc. Jpn. 87, 124710, 2018.
- [4] J. Schnack *et al.*, arXiv:cond-mat/1304.2603v1.
- [5] S. Sugiura and A. Shimizu, Phys. Rev. Lett. 108, 240401(2012).
- [6] H. Otsuka, Phys. Rev. B 51, 305 (1995).

Building Algorithms for Ising Machines

Shu TANAKA

*Department of Applied Physics and Physico-Informatics, Keio University
Hiyoshi, Yokohama, Kanagawa, 223-8522*

We have constructed an algorithm for the Ising machines. Ising machines are expected to be highly efficient solution machines for combinatorial optimization problems, but a significant challenge is to develop an algorithm that can exploit its potential and expand its range of applications. With this background, we have studied the following three topics.

(I) Minor-embedding algorithm for simulated-annealing-based Ising machines

To input the Ising model, which represents the objective function and constraints, into the actual Ising machine to solve the combinatorial optimization problem using the Ising machine, an operation called embedding is required. The accuracy of the solution depends on the value of the hyperparameters in embedding algorithms. Therefore, appropriate hyperparameter tuning is necessary to obtain a highly accurate solution using the Ising machine. We have proposed an appropriate method for adjusting this hyperparameter based on the viewpoint of statistical mechanics. We also verified the properties of the proposed method by simulation. The results suggest that the proposed method is superior to the commonly used hyperparameter adjustment method for embedding algorithms [1]. The work was done in collaboration with Tatsuhiko Shirai (Waseda Univ.) and Nozomu Togawa (Waseda Univ.).

(II) Quantum annealing with correlated disorder transverse fields

When solving a combinatorial optimization problem in conventional quantum annealing, a uniform transverse magnetic fields are applied

to all spins, and the transverse fields are gradually weakened on the same schedule. It was recently reported that the solution accuracy is improved by introducing inhomogeneity in the transverse fields. We have succeeded in obtaining rigorous inequalities for the upper and lower bounds of the dynamical critical exponents for the disordered one-dimensional transverse field Ising model, which can be analyzed rigorously through the free-fermion representation [2]. In addition, the dynamic critical exponents are confirmed by numerical calculations to see the finite size effect. The work was done in collaboration with Tatsuhiko Shirai (Waseda Univ.).

(III) Development of black-box optimization using Ising machines

We have previously proposed a method for black-box optimization using Ising machines and demonstrated it for automated metamaterial design [3]. We are currently working on expanding the scope of this method and are preparing a paper on it. The work was done in collaboration with Ryo Tamura (NIMS/Univ. of Tokyo).

References

- [1] T. Shirai, S. Tanaka, and N. Togawa: IEEE Access **8** (2020) 210490.
- [2] T. Shirai and S. Tanaka: Annals of Physics, Accepted.
- [3] K. Kitai, J. Guo, S. Ju, S. Tanaka, K. Tsuda, J. Shiomi, and R. Tamura: Physical Review Research **2** (2020) 013319.

Diversity in memory effects of flow in paste

Akio NAKAHARA

College of Science and Technology, Nihon University

7-24-1 Narashino-dai, Funabashi, Chiba 274-8501

A dense packed colloidal suspension, called a paste, remembers the direction of its motion, and its memory is visualized as a morphology of desiccation crack patterns. When a paste remembers the direction of its vibrational motion, desiccation cracks propagate in the direction perpendicular to the direction of the vibration, while, when a paste remembers its flow motion, cracks propagate along the flow direction, as are shown in Fig. 1 [1].

Here, CaCO_3 paste remembers the direction of vibrational motion but cannot remember flow direction. Note that CaCO_3 particles are charged in water. Numerical simulations of shear motion of colloidal suspension using LAMMPS show that, for the emergence of memory of flow, the attractive interaction should be dominant in short range interaction between colloidal particles. In numerical simulations, colloidal particles attract each other via Lennard-Jones potential and receives Stokes's drag force from surrounding fluid. Elongated clusters are formed along flow direction, but when attractive interaction is eliminated in the model, colloidal particles could not form any elongated clusters along flow direction and that is why CaCO_3 paste cannot remember flow direction.

When NaCl is added to CaCO_3 paste, the paste gets the ability of remembering flow direction due to the screening effect by Cl^- ions. Recently it is experimentally found that by adding filtered starch solution into CaCO_3 paste, the paste also gets the ability of remembering flow direction. However, if we add more filtered starch solution into the paste, the paste loses the ability of remembering flow direction. To explain this phenomenon, the adsorption of starch polymer onto colloidal particles should be included into the model, and numerical simulations based on the model are in preparation.

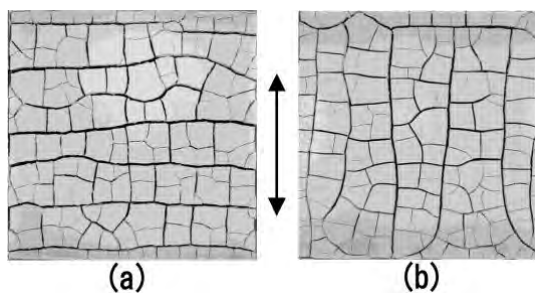


Fig. 1: Desiccation crack patterns induced by memory effect of vibration in (a) and flow in (b).

References

- [1] A. Nakahara, T. Hiraoka, R. Hayashi, Y. Matsuo, S. Kitsunozaki, *Phil. Trans. R. Soc. A377:20170395* (2018).

Magnetic structures under the non-equilibrium state of the magnetic thin films with the dipolar interaction

Hisato KOMATSU, Yoshihiko NONOMURA, and Masamichi NISHINO
National Institute for Materials Science, Namiki, Tsukuba, Ibaraki 305-0044

Magnetic structure of spin systems is an important subject of solid-state physics and statistical mechanics, which affects the various behaviors of systems. In particular, magnetic friction, the frictional force caused by the magnetic interaction between spins, is an example of non-equilibrium phenomena that the magnetic structure have an important role[1, 2].

We already introduced the model of magnetic friction which shows the crossover or transition from the Dieterich-Ruina law to the Stokes law in our previous study [3]. Spins of this model interact with each other by the short-range interaction, and we have not considered whether the behavior of the friction changes in the case of the long-range interaction system. However, consideration on general long-range interaction systems, including the dipolar interaction system, is difficult, because they make complicated magnetic structures depending on the condition[4] and need $O(N^2)$ computational complexity. Hence, we should first consider a relatively simple example of the long-range interaction system.

In this study, we introduce a model where the spins interact with each other by the infinite-range interaction. This model resembles that of our previous study, except for the interaction range. The reason why we choose the infinite-range interaction systems is the points that the computational complexity of the numerical simulation is $O(N)$, and the behavior at the thermodynamic limit can be investigated by mean field analysis.

According to the numerical and theoretical study, this model always obeys the Stokes law when the temperature is higher than the critical value, T_c , whereas the short-range model shows a crossover or transition from the Dieterich-Ruina law to the Stokes law even when the temperature is higher than the equilibrium transition temperature. This is because the frictional force of the present model depends directly on the long-range order and disappears when the order becomes zero. It is the large difference between two models. In the case that the temperature is lower than T_c , the model shows a crossover or transition similar to that of the short-range model when $N < \infty$, whereas it shows hysteresis dependence when $N \rightarrow \infty$. This seemingly contradictory behavior is caused by the divergence of the relaxation time in the large- N limit.

Result of this study is published as Ref. [5]. Systems with realistic long-range interaction such as the dipolar interaction should be studied in future works.

The numerical calculations of this study were mainly performed on the Numerical Materials Simulator at National Institute for Materials Science. We applied for the usage of the ISSP Supercomputer in preparation for transfer of affiliation. However, we have ended without any transfer, and have not used the ISSP Supercomputer.

References

- [1] D. Kadau, A. Hucht, and D. E. Wolf:
Phys. Rev. Lett. **101** (2008) 137205.
- [2] M. P. Magiera, L. Brendel, D. E. Wolf,
and U. Nowak: Europhys. Lett. **87** (2009)
26002.
- [3] H. Komatsu: Phys. Rev. E. **100** (2019)
052130.
- [4] K. De'Bell, A. B. MacIsaac, and J. P.
Whitehead: Rev. Mod. Phys **72** (2000)
225.
- [5] H. Komatsu: Phys. Rev. E. **102** (2020)
062131.

Establishment of new analysis method for extend X-ray absorption fine structure with sparse modeling

Hiroyuki KUMAZOE

*Institute of Industrial Nanomaterials, Kumamoto University
Kurokami, Chuo-ku, Kumamoto, 860-8555*

Measurement of extended X-ray absorption fine structure (EXAFS) is one of the primary methods to obtain local structure information around a specific element with atomic scale. We are building a new method for the analysis of EXAFS by the sparse modeling [1]. This year, we focused on using new basis function based on the multiple scattering theory.

To perform the sparse modeling on the EXAFS signals, we employed a new model of the EXAFS formalism based on the multiple scattering theory [3]. we consider two-body terms which are the main contribution of the EXAFS:

$$\chi(k) = \int_0^\infty \gamma^2(r, k)n(r) dr, \quad (1)$$

where, $\chi(k)$ is the EXAFS signal as a function of the photoelectron wavenumber; $n(r)$ is the coordination number of the distance r and $\gamma^2(r, k)$ contains the two-body scattering term corresponding to the same geometrical configuration. We use a complex Hedin–Lundqvist potential for inelastic loss effects in the framework of the multiple scattering theory. To obtain the local structure information, we solve Eq. (1) with L_1 regularization.

$$\hat{\mathbf{w}} = \arg \min_{\mathbf{w}} \left[\frac{1}{2} \|\mathbf{y} - \mathbf{X}\mathbf{w}\|_2^2 + \lambda \|\mathbf{w}\|_1 \right], \quad (2)$$

where the regression coefficient is \mathbf{w} . The response vector, \mathbf{y} comes from the target data and the predictor matrix, \mathbf{X} incorporates other

terms in Eq. (1). In this method, some elements of the coefficient, \mathbf{w} is are suppressed to exactly zero with the moderate value of λ .

Let us consider the sparse regression problem for the LASSO estimations within Bayesian inference to choose the regression parameter, λ . In Bayesian inference, this linear regression problem is optimized by maximizing the posterior probability. Here, we introduce the Bayesian free energy [2] as an information criterion to optimize a regularization parameter and to extract the physical model appropriately. As a result, we estimated the radial distribution function with fewer bases than in previous studies [1].

This work was supported by JST CREST Grant Number JPMJCR 1861, Japan.

References

- [1] I. Akai, K. Iwamitsu, Y. Igarashi, M. Okada, H. Setoyama, T. Okajima, and Y. Hirai, *J. Phys. Soc. Jpn.* **87**, 074003 (2018).
- [2] Y. Igarashi, H. Takenaka, Y. Nakanishi-Ohno, M. Uemura, S. Ikeda, and M. Okada, *J. Phys. Soc. Jpn.* **87**, 044802 (2018).
- [3] F. Iesari, H. Setoyama, Y. Igarashi, M. Okada, H. Kumazoe, K. Iwamitsu, I. Akai, Y. Seno, and T. Okajima, arXiv:2104.01805 [physics.data-an].

Nonequilibrium phase transition and slow dynamics in the dense hard sphere systems

Masaharu ISOBE

Nagoya Institute of Technology
Gokiso-cho, Showa-ku, Nagoya, 466-8555

As one of the simplest models, the hard disk/sphere systems have been investigated in the field of both equilibrium and non-equilibrium statistical physics. In this project, we investigated non-equilibrium phenomena in the hard disk/sphere model system with modern algorithms, especially for Event-Chain Monte Carlo (ECMC) [1] and Event-Driven Molecular Dynamics (EDMD) [2], where we propose the “Hybrid Scheme”, namely, ECMC for equilibration and EDMD for calculation of dynamical properties [3].

Direct Evidence of Void-Induced Structural Relaxations in Colloidal Glass Formers:

The mystery of the microscopic origin of kinetic arrest and slow relaxation mechanisms of glass-forming materials has puzzled scientists for decades in condensed and statistical physics. In general, when a liquid is rapidly cooled (compressed), its molecular arrangement remains disordered, and its motion becomes frozen, resulting in a glassy state. This causes “slow relaxation” due to the increase in viscosity. Most of the particles are frozen and do not move. Still, in rare cases, it is known that “active particles” that cause large displacements are generated in a spatially heterogeneous manner and move cooperatively. The cooperative motions of these “active particles” are roughly classified into two types: cooperative motions as a core-like domain region and string-like hopping chain motions, which have been observed in simulations at first. In the latter type of hopping chain motion, a void

with a size of diameter is required for the initial hopping. However, in high densities, such a void does not exist, which is a paradox. One of the crucial issues is understanding whether the essential properties of glass forming materials are fundamentally thermodynamic or dynamic in origin. One perspective that favors a dynamic origin is called Dynamic Facilitation (DF) theory [4, 5]. However, the microscopic origin of structural (so-called α) slow relaxation in deeply supercooled liquids at an atomic scale has remained elusive due to the limitation of electron microscopy experiments and computer simulation.

Recently, we devoted to investigating the applicability of DF theory to athermal systems, i.e., systems of hard particles where the relevant control parameter is pressure, under “super-compressed” conditions, using “Hybrid Scheme” [6]. Besides, the optical microscopy experiments on colloidal glass former system play an important role because detailed motions of individual particles can be accessible. International collaboration project with Hong Kong, we precisely traced the movement of individual colloidal particles for a long time in experiments. As a result, (A) the colloidal particles undergo a transition from collective “creeping” to the string-like “hopping” motion on approaching the glass transition, and the structural relaxation of the supercooled glass is just caused by string-like escape hopping motion. (B) In the supercooled glassy states, small fragmented voids distributed over a few

particle distances, called quasi-voids, cooperatively promote the formation of large voids. (C) The voids are transported like particles, which drive a string-like hopping chain motion. In addition, we found (a) the cooperative motion of the core-like domain regions of the “active particles” observed in previous studies can be decomposed into a hopping chain motion with a higher temporal resolution, and (b) the hopping chain motion is reversed with high probability and causes a string-repetition motion, which is proved to be the leading contribution to the kinetic arrest for slow relaxation. These new findings provide fundamental insights into the structural relaxation of glass-forming materials and may pave the way for a full understanding of the microscopic mechanism [7].

Non-equilibrium response and slow equilibration in hard disk systems

The “equilibration” (relaxation toward equilibrium states) from initial non-equilibrium states in the molecular simulations is one of the crucial preliminary tasks to obtain the physical properties in “true” equilibrium. The issue such as crystallization and glass/jamming transition have been actively studied recently. It often requires a large-scale simulation in dense molecular systems, which needs a long computational cost for equilibration. In general, the equilibration of particle positions in dense systems is much difficult due to the excluded volume effect being dominant. To obtain the equilibrium states, it is a reasonable choice to use ECMC for positional relaxation at first, which is the central idea of a hybrid scheme [3]. To elucidate the microscopic origin of equilibration in a hard disk system, we investigate the relaxing process toward the liquid states as a non-equilibrium response induced by the disturbance of the homogeneous expansion. After such disturbance around the Alder transition is induced, we performed EDMD and estimated the relaxation time of four physical properties. As the preliminary results, we

do not expect, an anomalous slow equilibration toward the liquid states to emerge when starting from the co-existence phase in large-scale EDMD. To identify the physical mechanism of anomalous slow equilibration, we found that the spatial inhomogeneity of the initial equilibrated phases would contribute to the relaxation time, which was confirmed by the probability distribution of local density and orientational order parameter[8]. We plan to investigate further by changing methodologies systematically.

References

- [1] E. P. Bernard, W. Krauth, and D. B. Wilson: Phys. Rev. E **80** (2009) 056704.
- [2] M. Isobe: Int. J. Mod. Phys. C **10** (1999) 1281.
- [3] M. Isobe: Mol. Sim. **42** (2016) 1317.
- [4] D. Chandler and J. P. Garrahan: Annu. Rev. Phys. Chem. **61** (2010) 191.
- [5] A. S. Keys, L. O. Hedges, J. P. Garrahan, S. C. Glotzer, and D. Chandler, Phys. Rev. X, **1** (2011) 021013.
- [6] M. Isobe, A. S. Keys, D. Chandler, and J. P. Garrahan: Phys. Rev. Lett. **117** (2016) 145701.
- [7] C.-T. Yip, M. Isobe, C.-H. Chan, S. Ren, K.-P. Wong, Q. Huo, C.-S. Lee, Y.-H. Tsang, Y. Han, and C.-H. Lam: Phys. Rev. Lett. **125** (2020) 258001.
- [8] D. Mugita and M. Isobe: EPJ Web Conferences, in press.

Quantum liquid crystals in the finite-field $K\Gamma$ model for α - RuCl_3

Masahiko G. YAMADA and Satoshi FUJIMOTO

*Department of Materials Engineering Science, Osaka University
Toyonaka, 560-8531, Japan*

We study the extended Kitaev model called the $K\Gamma$ model, using a perturbative expansion. From the Kitaev limit $K = 0$, the third-order perturbation in Γ leads to interacting Majorana models, which are solved by a well-controlled mean-field approximation and a cutting-edge exact diagonalization. In the exact diagonalization we use a thread parallelization up to 112 threads. By this large-scale calculation, the exact diagonalization up to 54 sites of Majorana fermions in the symmetric honeycomb geometry is possible, while usually the exact diagonalization has been done in the small system size up to 24 or 32 sites.

From the exact diagonalization combined with the mean-field theory, we found the following phases [1].

1. a Kekulé Kitaev spin liquid.
2. a non-Abelian chiral spin liquid.
3. an Abelian chiral spin liquid.
4. a nematic Kitaev spin liquid.
5. a Vijay-Hsieh-Fu surface code [2].

Especially, a Kekulé Kitaev spin liquid with a Chern number 0 and a Vijay-Hsieh-Fu surface code are new phases discovered in this large-scale calculation.

The results imply the existence of a vast region of quantum liquid crystal states (a nematic Kitaev spin liquid and a Kekulé Kitaev spin liquid). Both phases break the three-fold rotation symmetry of the system, and potentially explains the experimentally observed

high-field state with zero Chern number in α - RuCl_3 [3]. This observation leads to a potential control of quantum states by a domain wall motion in quantum liquid crystals.

References

- [1] M. G. Yamada, and S. Fujimoto: in preparation.
- [2] S. Vijay, T. H. Hsieh, and L. Fu: Phys. Rev. X **5** (2020) 041038.
- [3] O. Tanaka *et al.*: arXiv:2007.06757 (2020).

Crowding Movement of Cells

Katsuyoshi Matsushita

*Department of Biological Science, Graduate School of Science, Osaka University
Machikaneyama, Toyonaka, Osaka 560-0043*

Cells are indispensable constituents of the organism's body. Cells are distributed to proper positions to function in the various organs in the developmental processes of organisms [1]. In this distribution, cells sometimes take a crowding state and move spontaneously. This crowding movement is expected to finally lead to a jamming state of cells through their steric interactions [2, 3]. In contrast to this expectation, cells smoothly move, similarly to fluid, and, further, enhances their motility as shown in the observations of *Dictyostelium discoideum*, neuron, and blood cells [4]. The understanding of this crowding movement is a basic common issue in the fields of soft matter physics and developmental biology.

Some of the eukaryote cells including *Dictyostelium discoideum* use the persistent memory of cell trajectory to stabilize their movements [5]. We additionally showed that the memory induces the collective movement of cells [6, 7]. The formation of collective movements is expected to have the same origin of the self-propelled disks [8]. To get hints to clarify the mechanism of the crowding movement, the comparison to the self-propelled disks is effective. The self-propelled disks have been well confirmed to stabilize collective movement in the sparse condition through the inelastic multiple collisions. In this case, the memory of trajectories aligns movement directions of disks in the collisions. In contrast, the investigation of the crowding self-propelled disks so far has clarified the destabilization of the crowding movements and take a disordered state [9]. This result is contradictory to the crowding

movement of cells and implies that the crowding movements have an uncovered necessary condition.

To clarify the condition of the cellular crowding movement, we investigate the crowding movement on the basis of the cellular Potts model [10]. At the first step of this investigation, we attempt to confirm that the crowding model cells can stabilize their collective movements. To this end, we develop the model extension for dealing with the general polarity of cells [11, 12] and by using this extension remodels the memory of cell trajectory [13, 14]. By using Monte Carlo simulation based on our model, we successfully reproduced the collective movements even in crowding cells [15]. Further, the models show that the crowding state rather stabilizes the collective movement of cells. More concretely, we show that the threshold propulsion of the collective movement is reduced as the concentration of cells increases. This result at least shows that the crowding movement is possible for cells and clearly indicates that the model cells satisfies the aforementioned necessary condition of the crowding movements.

The key to clarify the condition is the origin of ordering, namely the memory of trajectories. To deeply examine effects of the memory, we try to evaluate the relation between the memory and the stability of collective movement in the crowding cells [15]. In a case, the crowding cells with movement show a solid to fluid transition, and then their configurations highly fluctuate. By using this transition, we confirm the stability in the order of movement in the

crowding model cells. We can show that even at the transition point, the cells exhibit the ordering of the movement under the high fluctuation of cell configurations. To further approach the origin of this stability [16], we consider memory time dependence of this movement order. We show that the stability depends highly on the memory time. Namely, the long memory time is the origin of the stability of movements in the crowding cells.

Based on the comparison of this result and that of the self-propelled disks, we attempt to shed light on the uncovered necessary condition. For the case of the self-propelled disks, the movement has an intrinsic fluctuation. In contrast to these disks, the model cells reduce the intrinsic fluctuation in their setting to resemble the cells with the memory of cell trajectory. In the disks, the intrinsic fluctuation shortens the memory time of the disk trajectory. Thus, the disks have a possibility that the disks lose the stabilization property of the collective movements. This difference in the intrinsic fluctuation of movements reflects the difference in the stability in crowding movements between the model cells and self-propelled disks. Thus, we speculate that the reduction of intrinsic fluctuation is the necessary condition of crowding movements.

These successes of the works are attributed to kind cooperation with Prof. H. Kuwayama, Prof. S. Yabunaka, Prof. K. Fujimoto, Dr. H. Hashimura, Prof. H. Yoshino, and Prof. M. Kikuchi. The author deeply thank them.

References

- [1] C. J. Weijer, *J. Cell Sci.* **122**, 3215 (2009).
- [2] S. Henkes, Y. Fily and M. C. Marchetti, *Phys. Rev. E* **84**, 040301(R) (2011).
- [3] L. Berthier *Phys. Rev. Lett.* **112**, 220602 (2014)
- [4] P. Rørth, *Ann. Rev. Cell Develop. Biol.* **25**, 407 (2009).
- [5] H. Takagi, *PLoS ONE* **3** e2648 (2008).
- [6] K. Matsushita, *et al.*, *Proc. Sympo. Traffic Flow Self-driven Parti.* **24**, 5 (2018a).
- [7] K. Matsushita, *et al.*, *J. Phys. Soc. Jpn* **88**, 103801 (2019).
- [8] C. A. Weber, *et al.*, *Phys. Rev. Lett.* **110**, 208001 (2013).
- [9] T. Hanke, C. A. Weber, and E. Frey *Phys. Rev. E* **88**, 052309 (2013).
- [10] F. Graner and J. Glazier, *Phys. Rev. Lett.* **69**, 2013 (1992).
- [11] K Matsushita, *Phys. Rev. E* **95**, 032415 (2017).
- [12] K Matsushita, *Phys. Rev. E* **97**, 042413 (2018).
- [13] B. Szabó, *et al.*, *Phys. Rev. E*, **74**, 061908 (2006).
- [14] A. J. Kabla *J. Royal Soc. Interface* **9**, 3268 (2012).
- [15] K. Matsushita, *et al.*, *Proc. Sympo. Traffic Flow Self-driven Parti.* **25** 5 (2019).
- [16] K. Matsushita, S. Yabunaka, K. Fujimoto *J. Phys. Soc. Jpn* **90**, 054801 (2021).

Multiple helical spin density waves in inversion-symmetric itinerant magnets

Takashi UCHIDA

Hokkaido University of Science

4-1, 7-15, Maeda, Teine-ku, Sapporo 006-8585

Since the discovery of magnetic skyrmions in B20 transition metal compounds, multiple helical spin density waves have attracted attention because the magnetic skyrmions emerge as 3Q multiple helical spin density waves in these materials. Typically, the magnetic skyrmions are realized in the Dzyaloshinskii-Moriya (DM) interaction driven systems under magnetic field. Recently, frustrated systems without the DM interaction have been found to reveal magnetic skyrmions [1, 2]. In order to explore theoretically the possibility of vortex-type multiple helical spin density waves such as magnetic skyrmions in the inversion-symmetric itinerant systems, we have applied the molecular spin dynamics (MSD) method [3] to the triangular-lattice single-band Hubbard model.

The MSD method is based on the functional integral method for the spin fluctuation theories and the isothermal molecular dynamics method. The method allows us to find automatically the magnetic structure of a large system with thousands of atoms in a unit cell at finite temperatures. Starting from the Hamiltonian expressed in terms of the locally rotated coordinates and by adopting the static approximation to the functional integral technique, the MSD method reduces to the generalized Hartree-Fock approximation at the ground state.

In the numerical calculations the most time-consuming process is the magnetic force calculation at each time step, where the lo-

cal electronic structures are calculated in real space by means of the recursion method. We have adopted the automatic parallel calculation scheme and found it to be effective in saving both computing time and CPU resources.

We have performed the magnetic structure calculations on the supercell with 20×20 triangular lattice, which is embedded in a large cluster consisting of 3×3 supercells, each of which are connected by the periodic boundary condition. Under zero magnetic field and the fixed value of the temperature $T/t = 0.0005$, we have explored the magnetic structures changing the Coulomb interaction strength U/t and the electron number n along the antiferromagnetic (AF)-ferromagnetic (F) boundary ($n = 1.3 \sim 1.4$). We have performed rather long-step MSD calculations (more than 15000 steps) to find the thermodynamically stable states among the various metastable multiple-Q states and have found that for $U/t = 5.0 \sim 8.0$ the 1Q helical spin density waves are stabilized in the vicinity of the AF-F boundary. To explore the possibility of 3Q multiple helical spin density waves, the MSD calculations for $U/t < 5.0$ are now in progress.

References

- [1] T. Okubo, S. Chung, and H. Kawamura: Phys. Rev. Lett. **108** (2012) 017206
- [2] Y. Kakehashi: J. Phys. Soc. Jpn. **89** (2020) 094710.
- [3] Y. Kakehashi, S. Akbar, and N. Kimura: Phys. Rev. **B57** (1998) 8354.

Robustness of cluster states and stabilizer states for surface codes against random local fields

Tetsufumi Tanamoto

*Department of Information and Electronic Engineering, Teikyo University
Utsunomiya 320-8511, Japan.*

By using the ISSP supercomputer, we numerically solve a time-dependent Schrödinger equation of a many-qubit system and theoretically describe how random local fields affect cluster states and stabilizer states for surface codes [1]. While there are already several known sources of decoherence in gate operation and measurement processes, we here focus on a new source of decoherence due to effects of field fluctuations on idling qubits which should become increasingly more serious as quantum computers scale up. We find similar temporal fidelity degradation for both cluster states and stabilizer states of surface codes for up to ten qubits. We also find that the effect of local-field fluctuations is greatly mitigated if the magnitude of the fluctuations can be suppressed to below 10% of the energy gap Δ for both cluster states and stabilizer states of the surface codes. If the magnitude of the fluctuations exceeds $\Delta/2$, the state fidelities for both states deteriorate dramatically. A simple estimate based on the average fidelity up to time $t \sim 2\hbar/\Delta$ shows that the maximum number of qubits that can suppress the system infidelity below the 1% is less than 28 for the surface code stabilizer states and 21 for the cluster states when the initial states are ground states (Fig.1).

We have also used the ISSP supercomputer to calculate the success probability of our proposed pulse sequence in the quantum annealing mechanism [2].

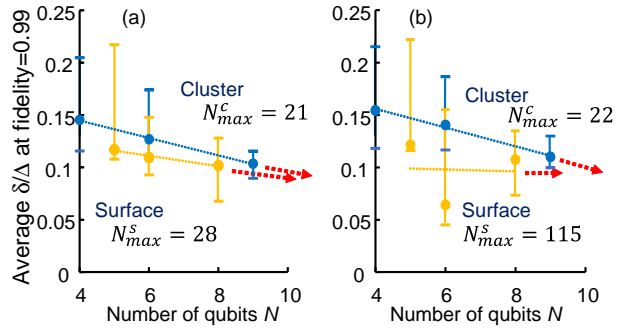


Figure 1: Average variation δ/Δ at which the fidelity is 0.99 for the cluster states and the surface-code states. The error bars are calculated from the standard deviation of δ/Δ . The extrapolation equations for the cluster states and surface-code states in (a) are given by $\delta/\Delta = -0.0053N + 0.1079$ and $\delta/\Delta = -0.0033N + 0.0924$, respectively. Those in (b) are given by $\delta/\Delta = -0.0004N + 0.0567$ and $\delta/\Delta = -0.0014N + 0.0732$, respectively. The extrapolation of these data points to the horizontal axis gives a rough estimate for the maximum number of qubits N_{max}^s and N_{max}^c , for which the errors can be corrected.

References

- [1] T. Tanamoto and M. Ueda: ArXiv:1910.05649
- [2] T. Tanamoto: J. Appl. Phys. **84** (2015) 31415.

Development of integrated interface of eigensolvers Rokko and application to quantum spin systems

Tatsuya Sakashita

*Center for Quantum Information and Quantum Biology, Osaka University
1-2 Machikaneyamachō, Toyonaka, Osaka 560-0043*

To establish universal exact diagonalization package for quantum lattice models including the Heisenberg-Kitaev model, we focused on developing integrated interfaces for eigensolvers, “Rokko”[1].

In Rokko, we implemented the integrated interfaces for the following types:

- Serial solvers for dense matrices (Eigen3, LAPACK)
- MPI parallelized solvers for dense matrices (EigenExa[2], ELPA[3], Elemental[4], ScaLAPACK)
- MPI parallelized solvers for sparse matrices (Anasazi in Trilinos[5], SLEPc[6]) to cover matrix representations below:
 - CRS (Compressed Row Storage)
 - Matrix-free method (the method to give matrix-vector product routines to solvers)

Rokko has the following features:

- Integrated interfaces for eigensolvers and matrices, independent of individual eigensolver libraries
- Rokko’s interfaces are implemented by utilizing factory. It enables the user to dynamically select a solver.
- C, Fortran, and Python bindings of Rokko
- Automatically detecting libraries by using CMake in building Rokko

- Unit and integrated test programs by GoogleTest
- Install scripts of eigensolvers for various architectures

We prepare a paper to report design policy, software structure, and usage examples of Rokko.

References

- [1] T. Sakashita, R. Igarashi, Y. Motoyama, T. Okubo, and S. Todo. Repository of Rokko. <https://github.com/t-sakashita/rokko.git>, 2012.
- [2] T. Imamura, T. Hirota, and T. Fukaya. EigenExa web page. <https://www.r-ccs.riken.jp/labs/lpnctrtr/projects/eigenexa/>, 2021.
- [3] ELPA Consortium. ELPA (Eigenvalue solvers for Petaflop Applications web page). <http://elpa.rzg.mpg.de>, 2013.
- [4] J. Poulson. Distributed-memory dense linear algebra Elemental web page. <https://github.com/elemental/Elemental>, 2013.
- [5] M. A. Heroux, R. A. Bartlett, and V. E. Howle. Trilinos Project web page. <https://trilinos.github.io>, 2003.
- [6] V. Hernandez, J. E. Roman, and V. Vidal. SLEPc web page. <http://slepc.upv.es>, 2002.

Comparison of rocking curves of 4 2 2 Bragg-reflected X-rays from thin silicon crystals calculated based on the conventional method and by solving the eigenvalue problem

Kouhei OKITSU

Institute of Engineering Innovation, School of Engineering,

The University of Tokyo, 2-11-16 Yayoi Bunkyo-ku Tokyo 113-8656

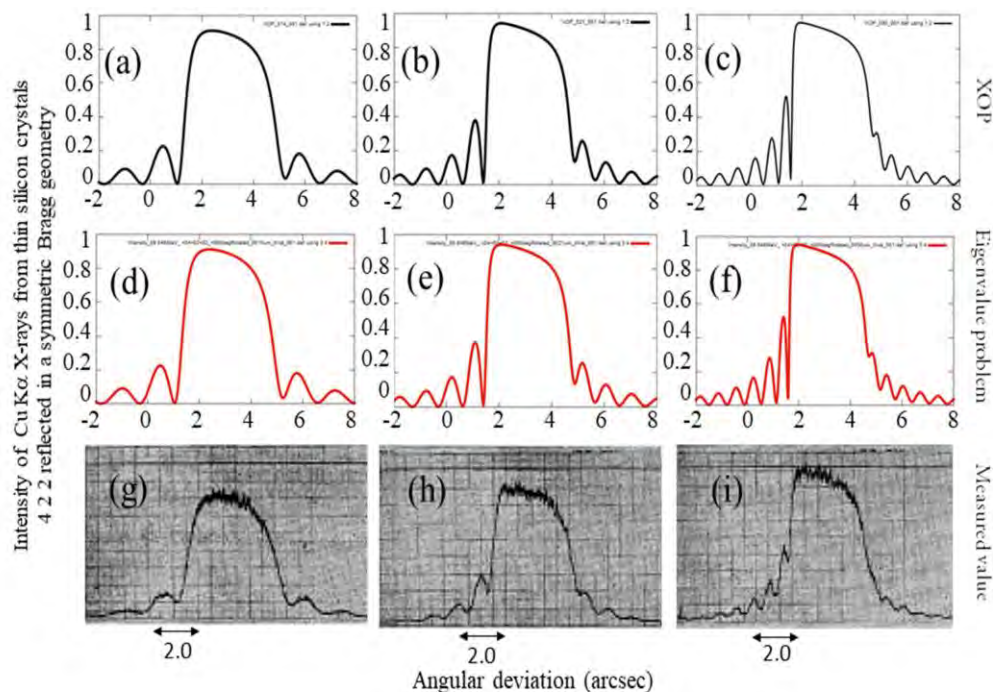


Fig. 1 Rocking curves of 4 2 2 Bragg-reflected X-rays from thin (14, 21 and 30 mm thick) silicon crystals. (a), (b) and (c) were calculated based on the conventional method. (d), (e) and (f) were obtained by solving the eigenvalue problem. (g), (h) and (i) were experimentally obtained [1]. The experiments were performed with the temperature carefully stabilized with the incidence of highly collimated and monochromatized X-rays generated from a Cu $K\alpha$ source.

The present author has worked on the n -beam Ewald-Laue (E-L) and Takagi (T-T) X-ray dynamical diffraction theories and numerical method to solve them for over twenty years [2,3]. However, this report describes two-beam rocking curves calculated based on the E-L theory and experimentally obtained over fifty years ago.

Professor H. Hashizume kindly taught the present author the existence of rocking curves experimentally obtained in 1970 [1]. He is one of the ranking authorities of the dynamical diffraction theory of X-rays. He also taught the present author that the description of the dynamical theory as the eigenvalue problem is not

general and is not widely recognized.

The E-L theory was developed by Ewald (1917) and Laue (1931). The fundamental equation given by Laue is described as follows:

$$\frac{\mathbf{k}_i^2 - \mathbf{K}^2}{\mathbf{k}_i^2} \mathbf{D}_i = \sum_j \chi_{\mathbf{h}_i - \mathbf{h}_j} [\mathbf{D}_j]_{\perp \mathbf{k}_i} \quad (1)$$

Here, \mathbf{K} is the wave vector of the incident X-rays, \mathbf{k}_i and \mathbf{k}_j are the wave vectors of the Bloch wave, \mathbf{D}_i and \mathbf{D}_j are amplitude vectors of the i th and j th numbered Bloch wave, $\chi_{\mathbf{h}_i - \mathbf{h}_j}$ is the $\mathbf{h}_i - \mathbf{h}_j$ order Fourier coefficient of the electric susceptibility. $[\mathbf{D}_j]_{\perp \mathbf{k}_i}$ is the vector component of \mathbf{D}_j perpendicular to \mathbf{k}_i .

By applying an approximation that $k_i + K \approx 2k_i$, the following equation is obtained [2,3]:

$$\xi_i D_i^{(l)} = \frac{K}{2} \sum_{j=0}^{n-1} \chi_{\mathbf{h}_i - \mathbf{h}_j} \sum_{m=0}^1 C_{i,j}^{(l,m)} D_j^{(m)}. \quad (2)$$

Here, $\xi_i = k_i - K$ (the eigenvalue), $D_i^{(l)}$ is the scalar amplitude of Bloch wave and $C_{i,j}^{(l,m)}$ is the polarization factor. The scalar amplitudes $D_i^{(l)}$ and $D_j^{(m)}$ of Bloch wave are defined as follows:

$$\mathbf{D}_i = D_i^{(0)} \mathbf{e}_i^{(0)} + D_i^{(1)} \mathbf{e}_i^{(1)}, \quad (3a)$$

$$\mathbf{D}_j = D_j^{(0)} \mathbf{e}_j^{(0)} + D_j^{(1)} \mathbf{e}_j^{(1)}. \quad (3b)$$

$\mathbf{e}_i^{(0)}$ and $\mathbf{e}_i^{(1)}$ are unit vectors defined such that they are perpendicular to \mathbf{k}_i and mutually perpendicular to each other.

Joko and Fukuhara pointed out [4], for the first time, that eq. (2) can be described as an eigenvalue problem of a matrix for an n -beam dynamical theory. When n is 2, eq.(2) is nothing but the E-L two-beam dynamical theory that is the most widespread X-ray dynamical theory. This fact has been almost completely overlooked even by Ewald, Laue and many other authorities of the X-ray

dynamical diffraction theory.

The conventional method to solve the X-ray two-beam dynamical theory has two steps. At first, the dispersion surfaces are calculated to give the condition that the amplitudes of Bloch wave has nonzero values. Next, for cross points (tie points) of the dispersion surfaces and the downward surface normal of the crystal, the amplitudes of Bloch wave are calculated to obtain the rocking curves.

However, eq.(2) for $n=2$ (two-beam case) can be solved directly without calculating the dispersion surfaces. The eigenvalue problem can be solved e.g. by using the LAPACK to calculate the rocking curves of Bragg-reflected X-rays as found in Figs. 1 (d), (e) and (f). They are in excellent agreement with those experimentally obtained [Figs. 1 (g), (h) and (i)] and calculated by the conventional way [Figs. 1 (a), (b) and (c)].

The present author is indebted to Mr. T. Sasaki who graduated from Tokyo Gakugei University in 2021 for his assistance when coding the program.

References

- [1] H. Hashizume, K. Nakayama, T. Matsushita and K. Kohra: *J. Phys. Soc. Jpn.* (1970) **29** 806-807.
- [2] K. Okitsu, Y. Imai, and Y. Yoda: *Recent Advances in Crystallography*, (2012) pp. 67-86. InTech Open. <http://dx.doi.org/10.5772/47846>.
- [3] K. Okitsu: *J. Jpn. Soc. Synchrotron Rad. Res.* **33** (2020) 61-80 [Invited].
- [4] T. Joko and A. Fukuhara: *J. Phys.Soc. Jpn.* (1967) **22** 597-604.

Non-uniform thermal transport properties in proteins

Takahisa YAMATO

Graduate School of Science,

Nagoya University, Furo-cho, Chikusa-ku, Nagoya 464-8602

We have studied thermal transport properties in proteins using molecular simulations [1-5]. Within protein molecules, tightly packed amino acid residues interact with each other through heat and energy exchanges. We illustrate non-uniform heat flow with our own model based on “local heat/energy conductivity” between each residue pair.

Native contacts in proteins are classified into nonpolar, polar, and charged types. Harmonic spring picture applies to energy transfer (ET) through nonpolar and polar contacts, and ET rates vary inversely with the variance of the contact length: whereas diffusion picture is relevant to ET through charged contacts and ET rates correlate inversely with the mean-square-distance between charged atoms of a residue pair.

The *CURP* program permits to compute inter-residue flow or energy/heat and atomic stress tensor in a protein, given atomic coordinates and velocity trajectories obtained through molecular dynamics (MD). Energy flow data permit to picture an inter-residue Energy Exchange Network (EEN) as a graph. For interactive analysis of EEN graphs using pointing devices, a new visualization tool, *EEN VIEWER*, with JavaScript and Python codes

(<https://youtu.be/zCXmIXskBFE>) is under development.

We implemented an accelerated *CURP* code via GPU computing with the OpenACC library. As a test calculation, this program was applied to a sensory domain of an oxygen sensor protein, FixL. As a result, the computation time of the auto-correlation function of heat currents in FixL was accelerated by 98.4%.

Human superoxide dismutase (SOD1) is known to bind metal ions for its function. To study the selective binding metal binding mechanism of SOD1, QM/MM molecular dynamics simulation using *Gromacs/DFTB* is under progress. We plan to analyze the fluctuations the metal binding sites using the *CURP* program.

References

- [1] P. Humanath, K. M. Reid, T. Yamato, D. M. Leitner: *J. Phys. Chem. B* **124** (2020) 9852.
- [2] K. M. Reid, T. Yamato, D. M. Leitner: *J. Phys. B.* **124** (2020) 1148.
- [3] T. Yamato: *Seibutsu Butsuri* **60** (2020) 94.
- [4] D. M. Leitner, T. Yamato: *Biophys. Rev.* **12** (2020) 317.
- [5] T. Yamato: *Biophys. Rev.* **12** (2020) 291